Institut für Hydrologie

der Albert-Ludwigs-Universität Freiburg i. Br.

Hannes Leistert

Modelling transmission losses; Applications in the Wadi Kuiseb and the Nahal Zin

Referent: Prof. Dr. Ch. Leibundgut

Koreferent: Dr. J. Lange

Diplomarbeit unter Leitung von Prof. Dr. Ch. Leibundgut
Freiburg i. Br., November 2005

Institut für Hydrologie

der Albert-Ludwigs-Universität Freiburg i. Br.

Hannes Leistert

Modelling transmission losses; Applications in the Wadi Kuiseb and the Nahal Zin

Referent: Prof. Dr. Ch. Leibundgut

Koreferent: Dr. J. Lange

Diplomarbeit unter Leitung von Prof. Dr. Ch. Leibundgut
Freiburg i. Br., November 2000

Danksagung

An erster Stelle gebührt mein herzlicher Dank meinem Professor Dr. Leibundgut für die Bereitstellung des Themas der vorliegenden Diplomarbeit.

An Dr. Lange für die Übernahme des Koreferrats und die Unterstützung und Beratung bei der Erstellung dieser Arbeit.

An meine Familie die mich während meines Studiums stets unterstützt hat.

An das gesamte Team des IHF, das jederzeit zur Lösung programmtechnischer Probleme beitrug und insbesondere an Dr. Külls für die Weitergabe seiner Erfahrungswerte aus Israel.

An die \`Mitdiplomanten\` die immer offen für Fragen und Anregungen waren und zu einer lustigen Arbeitsatmosphäre beitrugen.

Und last but not least an Elke für die seelische Unterstützung.

Content

List of Figures

List of Tables

Contents of the Annex

Notation

Notation	unit	symbol
Transmission losses	[m³]	TL
Volume upstream inflow	[m³]	V_u
Volume tributary inflow	[m³]	V_a
Volume downstream outflow	[m³]	V_d
Threshold volume	[ac ft]	P_o
Function of channel and flood characteristics		d
Function of channel and flood characteristics		e
Inflow	[m³/s]	Q_i
Outflow	[m³/s]	Q_0
Discharge	[m³/s]	Q
hydraulic conductivity	[mm/h]	k
Cross sectional area	[m²]	A
Height (chapter 2.4)	[m]	H
Length	[m]	L
Specific discharge	[m/s]	q
Depth	[m]	z
Specific moisture capacity	[h^{-1}]	C
Infiltration rate	[mm/h]	f
Constant	[mm/h]	k_k
Final infiltration rate	[mm/h]	f_∞
Potential	[mm]	Ψ
Saturated soil moisture content		θ_s
Initial soil moisture content		θ_i
Coefficient		α
Effective suction head	[mm]	h_e
Hydraulic conductivity (harmonic mean	[mm/h]	k_h
Hydraulic conductivity (layer one)	[mm/h]	k_1
Hydraulic conductivity (Layer two)	[mm/h]	k_2
Effective hydraulic conductivity	[mm/h]	k_{eff}
Macro pore hydraulic conductivity	[mm/h]	k_{nm}
Macro pore porosity		n_{mp}
Function (decomposition series)		ai
Function (decomposition series)		NF
Polynomials (decomposition series)		A_i
Function (decomposition series)		F_i
Function (decomposition series)		m_1
Function (decomposition series)		m_2
Storage volume	[m³]	S

Storage constant	[m³]	c
Input (chapter 3.4)	[m³]	x
Integration constant	[m³/s]	b
Hydraulic conductivity (underlying strata)	[mm/h]	k_f
Initial infiltration rate (bars, banks and floodplain)	[mm/h]	k_b
Time period	[h]	T1, T2
Mass	[kg]	m
Velocity	[m/s]	v
Shear stress	[N/m²]	τ
Density	[kg/m³]	ρ
Acceleration due gravity	[m/s²]	g
Hydraulic radius	[m]	R_h
Energy slope		I_e
Wetted perimeter	[m]	U
Water slope		I_w
Froude velocity	[m/s]	u
Reynolds number	[m/kg]	R_e
Grain size	[mm]	d
Density of the fluid	[kg/m³]	ρ_s
Froude number		F_r
Viscosity	[Ns/m²]	ν
Antecedent moisture index		Antec
Flooded width	[m]	bv
Flooded width (inner channel, bars and banks)	[m]	bv_1
Flooded width (inner channel, bars, banks and floodplains)	[m]	bv_2
Segment width	[m]	bc
Proportion of inner channel		v
Coefficient		x
Water depth (chapter 3.7)	[m]	H
Coefficient		d
Function (flooded width)		f_a
Function (flooded width)		f_b
Water depth when segment width is fully flooded	[m]	Hf
Proportion of bars and banks of inner channel		y
Brooks-Corey bubbling pressure head	[mm]	h_b
Brooks-Corey pore size distribution index		λ
Model efficiency		R_{eff}
Measured values (chapter 6.1)	[l/s]	x_i
Modelled values	[l/s]	y_i
Average measured value	[l/s]	x_{me}

Extended Summary

In arid regions, ephemeral rivers can stay dry for long periods depending on the meteorological conditions. Nevertheless, the rare high intense rainfalls can generate overland flow, which converges to the river channel network to create flood events. These runoff events are often characterized by a drop off in the flood hydrograph and flood volume when moving downstream, the so-called transmission losses. These losses can be accounted for by different processes such as artificial withdrawal, evaporation, bank storage, depression storage and infiltration. This thesis, however, focuses on infiltration as the main cause for the transmission losses.

This study deals with the modelling of transmission losses of ephemeral rivers in arid regions. Therefore, an existing rainfall-runoff model for large arid catchments, in particular the ZIN-model (Lange, 1999) was extended in different ways and has been tested in two different catchments as well as in two different scales.

As infiltration is considered the main reason for transmission losses, the modelling approach concentrated on the infiltration of floodwater into the riverbed and into the floodplains. Infiltration is a temporally and spatially varying process that is influenced by various processes as well as initial and boundary conditions.

The modified ZIN-model simulates infiltration into the inner channel using the Green-Ampt infiltration model. This approach has been chosen because it has a physical basis considering flood and channel characteristics such as the influence of the surface water depth, the effective suction head at the wetting front or the porosity. For calculating the infiltration rate with the Green-Ampt equation, it is necessary to compute, in a first step, the cumulative infiltration. Two approaches to determining the cumulative infiltration are presented, in particular an iteration method and a decomposition series. Irrespective of the method, these two ways of calculating the cumulative infiltration are only used for an incipient infiltration of a few millimetres. After that, the Green-Ampt equation is solved by adding up the actual amounts of infiltrated water of the previous time step to compute the cumulative infiltration. With that, the temporal varying conditions, such as a varying surface water depths or a blocked infiltration due to clogging of the riverbed surface are considered.

Infiltration into the floodplains is not modelled with the Green-Ampt equation. In this section an empirical approach was preferred because here different processes can occur such as losses through depression storage and through evaporation. The Green-Ampt approach thus loses its physical basis. The empirical approach is based on a single linear storage approach. Here, the loss rate depends on the storage content. More precisely the infiltration rate decreases with increasing storage content. To consider a varying flooded width and therefore additional areas with higher infiltration capacities, the storage volume is regarded as temporally variable depending on the flooded width. This was realized by incorporating the variable flooded

width into the calculation of the infiltration rate in such a way that the decline of the infiltration capacity slows down or that the infiltration rate even increases when additional areas are flooded.

To gain a better spatial resolution, the cross sectional profile, in particular the floodplains were subdivided into two sections representing two individual storages. One section comprises the bars and banks that form the transition from the inner channel to the second section, the floodplains. This is reasonable as banks and bars are flooded at least partly right from the beginning of the runoff event. Consequently, this storage starts to fill from the outset of the event. On the other hand, the floodplains are not flooded until the water depth has reached a certain level so that the flood overflows the bars. As a result, this storage only fills (and the infiltration capacity in this section decreases) when a certain water depth is surpassed.

An important precondition that strongly influences the infiltration process is the initial soil moisture content. To take this into account, an antecedent moisture index is build into the ZIN-model. This index is a simple empirical power function that depends on the time interval between two succeeding events. The infiltration rate as well as the possible total volume that can be adsorbed by the alluvium depend on the initial soil moisture content. The Green-Ampt equation includes and is therefore directly affected by the initial soil moisture content. The influence of the initial soil moisture content on bars, banks and floodplains is simulated by multiplying the infiltration rate with the antecedent moisture index.

Another process that strongly influences the total volume and the temporal behaviour of transmission losses is the process of scour and fill. The clogging of the alluvial surface happens due to fine grained material. Whether deposition or erosion occurs, depends on the balance of forces affecting the particles. Two different attempts to model the complex processes of sedimentation and erosion were accomplished and compared. One approach considers the shear stress and the other considers the flow velocity as criterion for the occurrence of erosion or sedimentation and therefore whether infiltration is obstructed or free.

The subdivision of the floodplains into two sections (bars plus banks and floodplains) was also considered when a new cross sectional geometry was developed. The ZIN-model approximated the flooded width linearly, starting from the inner channel up to a maximum channel width, depending on the water depth. The new approximation differs between the section bars plus banks and the section floodplain. The sections are described by composited power functions with adjustable inclinations. In this thesis, a steep convex form was chosen as inclination for the bars and banks and in a smooth concave form for the floodplains.

The different modifications require several site-specific parameters. Due to the lack of field data, some parameters were obtained from literature references (porosities, effective hydraulic suction head and to some extent the hydraulic conductivity). When field data were available they were used to calculate the missing parameter (to some extent the hydraulic conductivity) or they were plugged in directly (initial infiltration rates and to some extent the channel geometry properties). Further, some channel properties were obtained by analyzing aerial photographs with geographical information systems.

The different versions of the modified model were tested in several model runs and evaluated with measured runoff data. The two test areas were the hyperarid watershed of the Kuiseb River in Namibia and the hyperarid watershed of the Nahal Zin in Israel. In addition, the modified model was tested on two different scales, in particular on a meso- and a macro scale in the Nahal Zin catchment, Israel.

The results of the runoff simulations show that, despite of the uncertainties of the chosen parameters, the modifications influence the modelled hydrographs. Due to the process of scour and fill and the new methods to calculate the infiltration rates, the temporal variability of the transmission losses in the modified model are now associated with flood characteristics. Furthermore, preconditions and boundary conditions such as the initial soil moisture content or the description of the cross sectional geometry noticeably influence the total amount and spatial variability of the transmission losses.

Keywords:

Arid, Transmission losses, Infiltration, Green-Ampt model, Linear storage model, Antecedent moisture, Scour and fill, ZIN-Model, Kuiseb River, Nahal Zin

Zusammenfassung - Deutsch

In Trockengebieten können ephemere Flüsse, in Abhängigkeit von meteorologischen Bedingungen, lange Zeit trocken liegen. Die jedoch selten auftretenden Starkregenereignisse können Oberflächenabfluss bilden, welcher sich in den Flussläufen sammelt und Abflussereignissen zur Folge haben kann. Ein Merkmal dieser Ereignisse sind die so genannten Transmission Losses, welche sich, entlang des Fließweges, durch eine abnehmende Abflussganglinie und ein zunehmend vermindertes Abflussvolumen auszeichnen.

Transmission Losses haben eine Vielzahl von Ursachen, wie künstliche Entnahmen, Verdunstung, Muldenspeicher, Ufer- und Gerinnebettinfiltration, wobei in der vorliegenden Arbeit die Infiltration als Hauptgrund der Verluste angesehen wird.

Diese Studie beschäftigt sich mit der Modellierung von Transmission Losses ephemerer Flüsse in Trockengebieten. Das für große aride Einzugsgebiete entwickelte Niederschlag-Abfluss ZIN-Modell (Lange 1999) wurde hinsichtlich dessen auf mehrere Arten verändert und sowohl in zwei verschiedenen Einzugsgebieten, als auch mittels zweier unterschiedlicher Skalen getestet.

Da die Infiltration als Hauptursache der Verluste angesehen wird, konzentrierte sich die Modellierung auf die Versickerung des Abflusses in das Gerinnebett und in die Überschwemmungsflächen. Dies ist ein zeitlich variabler Vorgang, der durch viele Prozesse, sowie durch Anfangs- und Rahmenbedingungen beeinflusst wird. Diesbezüglich wurde das ZIN-Modell verändert.

Die Versickerung in das Hauptgerinne wird in dem umgestalteten ZIN-Modell mit Hilfe des Green-Ampt Infiltrations-Modells simuliert. Dieser Ansatz wurde ausgewählt, da er sowohl physikalisch basiert ist, als auch die Abfluss- und Gerinneigenschaften, wie der Einfluss des Wasserstandes, die Saugspannung an der Feuchtefront und die Porosität berücksichtigt. Um die Infiltrationsrate mit Hilfe der Green Ampt Gleichung berechnen zu können, ist es nötig, zuerst die kumulative Infiltration zu bestimmen. Hierzu werden zwei Ansätze vorgestellt, zum einen ein Annäherungs- und zum anderen ein Zerlegungsverfahren. Beide Berechnungsansätze werden nur für eine anfängliche Infiltrationsrate von wenigen Millimetern angewandt. Anschließend wird die kumulative Infiltration durch das Aufaddieren der infiltrierten Wassermengen vorangegangener Zeitschritte berechnet. Dadurch wird sichergestellt, dass die Bedingungen vorheriger Zeitschritte, wie die Veränderung der Wasserstandshöhe oder die Verschlämmung des Porenraumes der Flussbettoberfläche, miteinbezogen werden.

Die Infiltration in die Überschwemmungsflächen wird nicht mit der Green-Ampt Gleichung berechnet. In diesem Bereich wurde ein empirischer Ansatz bevorzugt, da zusätzlich zur Infiltration, Prozesse, wie beispielsweise Verluste durch Muldenspeicher und durch

Verdunstung, auftreten können und infolgedessen die Green-Ampt Methode hier ihren physikalische Hintergrund verliert. Der empirische Ansatz basiert auf der Beschreibung eines Einzellinearspeichers , bei welchem die Verlustrate von dem Speicherinhalt abhängig ist. Genauer gesagt verringert sich die Infiltrationsrate mit zunehmender Speicherfüllung. Da eine räumlich variierende Überflutungsfläche und demzufolge zusätzliche Areale mit höherer Infiltrationskapazität in die Berechnung mit einbezogen werden müssen, wird das Speichervolumen, in Abhängigkeit von der Überflutungsfläche, als zeitlich variabel beschrieben. Realisiert wurde dies unter Einbeziehung der variablen überschwemmten Flussbreite in die Berechnung der Infiltrationsrate. Wenn zusätzliche Areale überflutet werden, verringert sich die Abnahme der Infiltrationskapazität oder es hat sogar eine Erhöhung der Infiltrationsrate zur Folge.

Um eine verbesserte räumliche Auflösung zu erreichen, wurden innerhalb des Flussquerschnitts die Überflutungsflächen in zwei Abschnitte unterteilt, welche jeweils eigene Speicher darstellen. Der erste Abschnitt umfasst die Ufer und die Sandbänke, die den Übergang vom Hauptgerinne zu dem zweiten Abschnitt, den Überflutungsflächen bilden.

Dies begründet sich dadurch, dass von Anbeginn des Abflussereignisses die Ufer und Sandbänke, zumindest teilweise, von Wasser bedeckt werden. Konsequenterweise beginnt sich hier der Speicher von diesem Zeitpunkt an zu füllen.

Andererseits erfolgt die Überschwemmung der Überflutungsflächen erst dann, wenn der Fluss über die Ufer tritt. Daraus resultiert, dass dieser Speicher sich ausschließlich dann füllen kann, wenn ein bestimmter Wasserstand überschritten wird. Nur die Erfüllung dieser Bedingungen führt in diesem Bereich dazu, dass auch die Infiltrationskapazität abnimmt.

Eine wichtige Einflussgröße auf den Infiltrationsprozess stellt der Gehalt an Vorfeuchte im Alluvium dar. Um diesen berechnen zu können, wird ein Vorfeuchte Index in das ZIN-Modell integriert. Dieser Index ist eine einfache Empirische Exponentialfunktion, welche vom Zeitintervall zwischen jeweils zwei aufeinander folgenden Ereignissen abhängt.

Sowohl die Infiltrationsrate, als auch das maximal mögliche Infiltrationsvolumen ist von der Vorfeuchte abhängig. Die Green Ampt Gleichung beinhaltet die Vorfeuchte und wird daher direkt von ihr beeinflusst. Der Einfluss der Vorfeuchte auf die zusätzlich überschwemmten Gebiete, wird durch die Multiplikation der Infiltrationsrate mit dem Vorfeuchte Index simuliert.

Ein weiterer Prozess, der die maximal mögliche Infiltrationsmenge sowie den zeitlichen Verlauf der Transmission Losses stark beeinflusst, ist das Aufbrechen oder das Verschlämmen der Gerinneoberfläche. Letzteres ist eine Folge der Einlagerung von Feinmaterial. Die verschiedenen Kräfte, welche auf die Flussfracht oder auf das Alluvium einwirken, bestimmen ob das Fliessgewässer erodiert oder sedimentiert. In der vorliegenden Arbeit werden zwei unterschiedliche Ansätze, um die komplexen Erosions- und Sedimentationsprozesse zu simulieren, angewandt und miteinander verglichen. Als Kriterium, ob Erosion oder Sedimentation auftreten und damit auch, ob die Infiltration ungehindert oder blockiert stattfindet, wird in einem Ansatz die Scheerspannung und in dem anderen Ansatz die Fließgeschwindigkeit benutzt.

Bei einer neu entwickelten mathematischen Beschreibung des Flussquerprofils ist die Unterteilung der Überflutungsflächen in zwei Abschnitte miteinbezogen worden. Das ursprüngliche ZIN-Modell berechnete die Breite der Überschwemmungsfläche linear in Abhängigkeit des Wasserstandes, beginnend beim Hauptgerinne bis hin zur maximalen Gerinnebreite. Die neue Beschreibung unterscheidet zwischen dem Abschnitt der Ufer und Sandbänke sowie dem der Überschwemmungsflächen. Diese werden durch zwei miteinander verbundene Exponentialfunktionen angenähert, deren Steigungen justierbar sind. In der vorliegenden Arbeit wurde als Steigung der Ufer und Sandbänke eine konvexe Form gewählt, sowie eine schwach konkave für die Überschwemmungsflächen.

Die jeweiligen Modifikationen benötigen verschiedene geländespezifische Parameter. Aufgrund mangelnder Geländedaten wurden einige Werte aus Quellen der Literatur bezogen (Porosität, Saugspannung an der Feuchtefront und teilweise hydraulische Leitfähigkeit). Waren Geländedaten bekannt, wurden sie genutzt, um fehlende Parameter zu berechen (hydraulische Leitfähigkeit), oder direkt verwendet (Anfangsinfiltrationsrate und teilweise die geometrische Gerinnedaten). Ferner wurden verschiedene Gerinneeigenschaften erfasst, indem Luftbilder des Einzugsgebietes mit geographischen Informationssystemen analysiert wurden.

Die verschiedenen Versionen des veränderten Modells wurden in mehreren Simulationen getestet und mit gemessenen Abflussganglinien des Kuiseb River in Namibia und des Nahal Zin in Israel evaluiert. Zusätzlich wurde diese in zwei Skalen, der Meso- und Makroskala, im Einzugsgebiet des Nahal Zin in Israel getestet.

Die Abflusssimulationen zeigen, dass die modellierten Abflussganglinien, trotz gewisser Ungenauigkeiten der gewählten Parameter, von den vorgenommenen Änderungen des Modells beeinflusst werden. Durch die Simulation der Erosion und Sedimentation, sowie durch die zeitabhängige Berechnung der Infiltrationsraten, zeigen die Transmission Losses im modifizierten ZIN-Modell einen zeitlich variablen, von den Abflusseigenschaften abhängigen Verlauf. Zudem beeinflussen Vor- und Rahmenbedingungen wie der Vorfeuchtegehalt des Alluviums oder die Beschreibung des Flussquerschnittes merklich die Gesamtmenge und die räumliche Variabilität der Transmission Losses.

I Introduction

Water resources are limited and under serve pressure in arid and semiarid regions of the world. This is caused due to an expanding population, an increasing urban development and an increasing use of water for irrigation. In regions with shortage of water hydrology plays an important role in quantifying and qualifying usable water volumes for a sustainable catchment management. This has to meet the domestic, agricultural, industrial and environmental needs with regard to the availability of water resources and with regard to flood protection. Therefore, an accurate scientific understanding of the various hydrological processes is essential to ensure a constant water supply and to avoid damage to human and material objects due to floods.

Basic research and data collection are the foundations to achieving scientific knowledge and to understand the complex hydrological processes. Hydrological models are supplementary powerful tools to describe and to gain insight into the natural systems. Due to continuous improvements and developments in hydrological modelling and computing power, the applicability and the benefit of hydrological models have grown in importance. They have contributed enormously to the scientific understanding and support decision making in water management.

Despite of the precarious situation in arid regions, most hydrological models are designed for humid environments. These models hardly ever reflect the water related processes of the arid hydrology, hence the models that have been tailored to the arid characteristics are of great significance for these regions.

This thesis deals with the flow behaviour of ephemeral rivers in arid environments. It is carried out for and at the Institute for Hydrology in Freiburg i. Br., Germany under the supervision of Prof. Dr. Ch. Leibundgut and Dr. J. Lange. The aim of this work is to give a deeper insight into the various and complex processes of transmission losses and to improve an existing rainfall-runoff model with regard to those losses.

The original ZIN-model, to be modified in this thesis, was developed by Dr. J. Lange. It is a non-calibrated rainfall-runoff model for large arid catchments. The evaluation of the modified ZIN-model was executed using discharge data from two hyper arid watersheds, in particular the Kuiseb River in Namibia and the Nahal Zin in Israel.

II General aspects

2.1 Dryland hydrology

Drylands are characterized due to water shortage. More than one third of the world's total landmass can be characterized as semi-arid, arid or hyper-arid (Le Houérou, 1996).

There are different methods to classify a region by its humidity, for example based on the climatic conditions or due to the water balance. Following the classification of the UNESCO (1984), a region can be characterized by an aridity index (AR) which is the ratio of mean precipitation and potential evaporation. The UNESCO classifies regions into humid ($AR \geq 0.65$), dry sub-humid ($0.65 > AR \geq 0.5$), semiarid ($0.5 > AR \geq 0.2$), arid ($0.2 > AR \geq 0.05$) and hyper-arid ($AR < 0.05$).

Table 2.1.1 Percentage of dryland of total world land area (modified from Le Houérou, 1996)

Zone	Percentage of world land area	AR
Semiarid	17.7	0.20-0.45
Arid	12.1	0.05-0.20
Hyperarid	7.5	<0.05
Total	37.3	

The importance of understanding hydrological processes in regions with scarceness of water with regard to water management is emphasized in the introduction. Hydrology in arid and semiarid regions differs from the hydrology in humid regions. To give the reader a general idea, the following section describes briefly the important components of the water cycle in an arid environment.

The potential evaporation is high due to high radiation, low humidity and high temperatures whereas the actual evaporation is low due to the lack of water. According to Evenari et al. (1971), the potential evaporation reaches values up to 2700 mm per year in the desert Negev, Israel.

Rainfalls are limited to the rainy season of the year and sometimes they fail to occur at all. Rainstorms occur infrequently and they often show a high intensity with huge amounts of precipitation bringing a major portion of the annual rainfall to the surface in a short period of time (Vivoni, 2005). Low intensity showers often directly evaporate in the atmosphere or on the surface, without infiltrating into the soils or creating any runoff.

The intensive rainfalls can generate runoff when the precipitation intensity exceeds the infiltration rate (Hortonian overland flow). This process is supported by surface crusts, which are able to significantly curtail infiltration. This overland flow flows together into the river channel network. Therefore, streams that stay dry most of the year can react quickly to high intensity precipitation events (e.g. Lane 1990; Lange et al. 1997, 2005; Vivioni 2005). The characteristics of these floods are a relative short duration (hours to weeks in arid regions and weeks to months in semiarid regions), transmission losses, high erosion potential and high sediment load (e.g. Schwartz 2001; Ben-Zvi et. al. 2001; Alexandro 2003; Lange 2005). In arid regions, the ephemeral stream flows play an essential role for vegetation, wildlife and man. Ben-Zvi et. al. (2001) writes that 'runoff in arid areas is an essential source for water supply through appropriate storage installations and for groundwater recharge'.

These runoff events can recharge aquifers as a result of infiltration into the channel bed. However, this indirect linear recharge occurs only under favorable circumstances. These conditions include events of large magnitude (i.e. runoff volume, wetted perimeter and duration of flow) and highly permeable underlying strata (Shentsis et al., 2001). Direct recharge due to rainfall seldom replenishes the aquifer. The above-mentioned surface crusts hinder infiltration and due to the high evaporation rates, large amounts on the surfaces and in the unsaturated zone evaporate back into the atmosphere (e.g. Parissopoulos et al. 1991; Scanlon et al. 1997; Lange et al. 2003).

2.2 Hydrological modeling

A hydrological model is a simplified representation of a complex natural system (Uhlenbrook, 1999). This chapter deals with mathematical models, which simulate natural systems by using mathematical expressions. Besides mathematical models, physical and analogical models exist which will not be discussed further though.

Mathematical models can be divided into deterministic and stochastic models. A deterministic model simulates the physical processes operating in the system and the results are reproducible. A stochastical model considers the chance of occurrence of hydrological variables or the probability distribution of hydrological variables (Ward et al., 2000), so here different results for model runs under the same conditions are possible.

The deterministic models can be classified according to their spatial distribution into lumped, distributed and semi-distributed models (Uhlenbrook, 1999; Ward et al., 2000). In lumped models, one spatial unit represents the entire system (e.g. area of the catchment). In distributed models, the parameters and variables have the possibility to vary in space (e.g. 3-D grids). A semi-distributed model is somewhere between the above-mentioned models, in this case the parameters and variables vary for different parts of the model (e.g. areas with the same hydrological characteristics).

Another differentiation into physical, conceptual and empirical model is possible when looking at the physical background used in the model. According to Uhlenbrook (1999), a physically based model realizes the conservation of energy and mass. In contrast to a physically based model, an empirical model does not consider the physical background of the different processes. The conceptual models are based on a limited representation of the hydrological variables.

The conceptual and physically based models have to face two major problems i.e. the heterogeneity of the system and the issue of scaling (both spatial and temporal) (Feddes, 1995; Wheater et al., 1998). Table 2.2.1 shows different spatial scales in hydrology according to Dooge (1988).

Table 2.2.1 Spatial scales in Hydrology (according to Dooge, 1988)

Class	System	Typical length (m)
MACRO	Planetary	10 000 000
	Continental	1 000 000
	Large basin	100 000
MESO	Small basin	10 000
	Sub- catchment	1000
	Catchment module	100
MICRO	Elementary volume	0.1
	Continuum point	0.000 01
	Molecular cluster	0.000 000 01

The problem of scaling, in particular up scaling is strongly linked to the heterogeneity of the system. Many studies have dealt with this issue (Parissopoulos et. al. 1990; Stewart et al., 1996; Kyle et al., 1999; Stomph et al., 2002; Wheater 2002; Martinez-Landa et al., 2005), pointing out the difficulties in scaling up, as hydrological theories and catchment data are based on observation and experimentations at the micro- and meso scale.

2.3 Transmission losses and developments in research

Transmission losses are abstractions of water volume along the flow path in the riverbed. Especially in ephemeral rivers, the amount of transmission losses can be very significant and a major part of the runoff volume does not reach the watershed outlet but is lost along its way trough the channel.

The loss is caused by different processes such as evaporation, artificial withdrawal, bank storage, depression storage and infiltration (Külls, 1994), whereas in general the infiltration into the riverbed, the bars, the banks and the floodplains is the major abstraction. In a recent study, Lange (2005) pointed out that the rate of transmission losses rises abruptly when over bank flow occurs caused by the flooding of additional areas. Here, other processes like temporary storage in waterholes and evaporation play an important role next to the infiltration in view on transmission losses.

Since the alluvial fills of ephemeral channel beds are usually dry, they can absorb large volumes of water from runoff events (e.g. Sorman et al. 1993; Schwartz 2001). A fraction of the infiltrated water can percolate through the unsaturated zone and recharge aquifers when the channels are hydraulically connected to deeper aquifers (Shentsis et al., 1999, 2001). The remaining fraction (interception and soil moisture) evaporates back into the atmosphere, leaving space that can be refilled from subsequent runoff events (Ben-Zvi et. al., 2001).

Infiltration from floods in ephemeral stream channels is a complex phenomenon, which depends upon the gradient of the total soil water potential at the ground surface (Reeder et al., 1980). It is influenced by:

- alluvial characteristics
- alluvial moisture content
- channel configuration
- water depth
- water velocity
- flow duration
- water volume
- stream sediment load
- storage potential
- depth of groundwater table

Various studies investigated the different processes contributing to the transmission losses. The following review classified the processes into processes related to flood characteristics and processes related to channel characteristics, where some foster and others limit infiltration. However, they are not independent from each other, but rather interact and influence one another.

2.3.1 Flood characteristics

The process of scour and fill plays an important role in ephemeral rivers. On the one hand, crusts or soil compactions can be eroded through the power of the water and its sediment load. On the other hand, deposition can occur and build up crusts or seal the riverbed surface. Crerar et al. (1988) showed that silt carried by flood waters can effectively seal the alluvial surface even during flood events even at relatively high flow velocities. They also pointed out that other processes controlling infiltration may become relatively unimportant for much of the duration of any given flood event. These observations also showed no clear connection between the amount of silt carried by floodwaters and the coating of the alluvial surface. Furthermore, the infiltration rate changed under identical conditions of flow. On the other hand, Lado et al. (2004) point out that clay as the important grain size plays a significant role for sealing the riverbed surface. Many studies looked at the process of scour and fill (e.g. Shields 1936; Wiberg 1987; Lee 1999; Vollmeret al. 2000; Briaud et al. 2001; Lang et al. 2001; Wyrwa 2003; Lado et al. 2004; Indlekofer 2005) but still it is difficult to apply the findings to a spatially and temporally varying wadi systems.

The surface water depth influences the infiltration rate. Various studies (e.g. Reeder et al. 1980; Freyberg et al. 1980; Parissopoulos et al. 1991) deal with changing infiltration rates under ponded conditions and varying surface water depths. Reeder et al. (1980) found that infiltration rates may increase with time in response to rapid rates of increase in water depth (see also Figure 2.4.1). Parissopoulos et al. (1991) also investigates the change of infiltration rate under time-varying ponding water depth. This study was based on a two-dimensional unsaturated-saturated flow model, which was a numerical solution of the two-dimensional Richard's equation. Here the cumulative infiltration was found to be primarily a function of the infiltration opportunity time and the mean ponding depth of water but not of the temporal distribution of the depth of water.

Another process, which reduces infiltration rate under ponded conditions, is the entrapment of air. When the air cannot escape ahead of the infiltrating water, or even when it can, air movement offers an appreciable resistance to downward water flow at high soil water contents near saturation (Morel-Seytoux et al., 1985).

As mentioned before the flooded area, which is linked to the discharge magnitude and the cross sectional geometry, plays an important role for the total volume of water losses. Lange (2005) showed that transmission losses increased considerably, when the floodplains are flooded. Knighton et al. (1994) examined outflow to inflow ratios against event magnitudes with the result that this ratio increases with event magnitude only to an intermediate maximum at bank full discharge in the channel. With a further increasing event magnitude, the ratio declines due to the additional flooded floodplain.

Depending on the flood volume the transmission losses behave very differently from event to event. Sorman et al. (1993, 1997) note that transmission losses were highly correlated to thw inflow volume. Schwarz (2001) points out that the total losses grow with water volume, whereas the relative losses shrink with increasing water volume.

2.3.2 Channel characteristics

Apart from the flood characteristics, the stratigraphy and the properties of the alluvium of the flooded area are dominant aspects controlling the infiltration rate.

The governing parameters to describe water movement in the unsaturated (vadose) zone are the hydraulic conductivity and porosity. Both show a great variability due to the heterogeneity of natural systems. The specific characteristics and the influences on transmission losses will be discussed in detail in the chapters 2.4, 5.1 and 5.2.

The vertical extension of the alluvial body plays a role for the losses with regard to the total volume that an alluvium can absorb. It is strongly realated to the geomorphologic characteristics and history of the reach of interest.

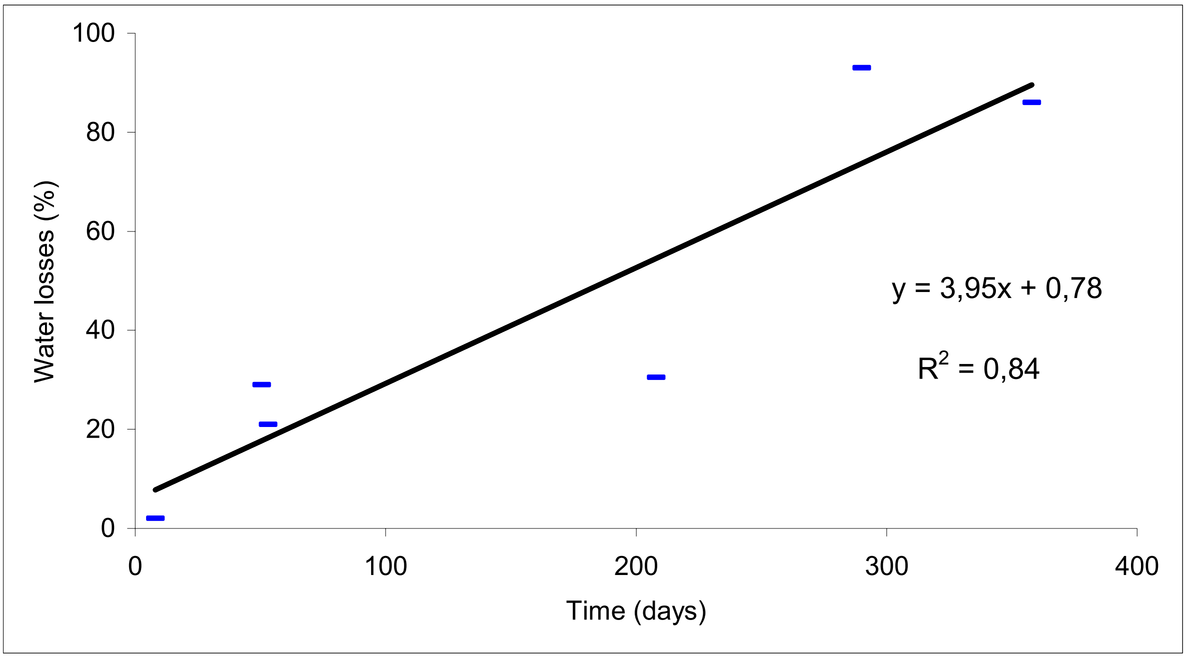

Figure 2.3.1 Percent of water losses vs. time from last flood (modified from Schwartz 2001)

The antecedent moisture content depends on the alluvial characteristics and the time between two runoff or rainstorm events. It influences the losses as it directly affects the infiltration rates (e.g. Freyberg 1981; Reeder et al. 1980; Serrano 2001) and determines (together with the porosity and the geometry of the alluvial body) the total possible volume that the alluvium can absorb (Rawls et al. 1992; Lado et al. 2004). Schwartz (2001) mentions that for at least five days after the last runoff event the infiltration rate is hugely decreased. He also derives a correlation between the losses in percent and the time passing between two runoff events, with the result that the percentage of water loss grows with the duration between two events (see Figure 2.3.1). With regard to aquifer recharge Sorman et al. (1993) point out that larger contributions to replenish an aquifer may occur as a result of high initial moisture content. This happens because percolation through the unsaturated zone only takes place after the alluvium has reached field capacity.

2.3.3 Determination of transmission losses

To evaluate transmission losses Schwartz (2001) segregates the possibilities into three basic methods.

1. Water balance method - comparing input and output data (e.g.; Sorman et al. 1993, 1995; Shentsis et al. 2001; Schwartz 2001)

2. Theoretical modeling founded on physical infiltration equations. This can further be separated into

- simple regression equations (e.g. Lane et al. 1971; Sorman et al. 1993)
- simplified differential equations (e.g. Jordan 1977; Peebles et al. 1981)
- combination of regression with differential equations (e.g. Lane 1990; Osterkamp et al. 1994)
- stream-flow routing (e.g. Knighton et al. 1994; Lange 2005)

3. Artificial tracer (e.g. Külls et al. 1995; Lange et al. 1997)

Problems often consist in the scarcity and the quality of data needed for the different methods. To obtain reliable data on discharge a well-structured system of measurements is required, which is likely only to be set up in experimental watersheds. Assessments of other watersheds must rely upon incomplete records, refer to analogy from experimental watersheds and creative assumptions (Ben-Zvi et. al., 2001).

When using the water balance method another problem is to determine discharge correctly. Due to degradation and aggradation, the channel geometry can change strongly from event to event and so it is difficult to gain an accurate water depth – discharge relation. Schwartz (2001) estimated the failure for discharge measurement at about 15%. In addition where data on contributing rainfalls and tributary flow are lacking no concrete estimation are possible for the lateral inflow and as a consequence the water balance remains with unknown variables Nevertheless, transmission losses are often assessed through the water balance equation

According to Shentsis et al. (2001), equation 2.3.1 is conveniently established for a reach extending between hydrometric stations:

$$TL = V_u + V_a - V_d$$ **equation 2.3.1**

TL Transmission Losses

V_u runoff volume at the upstream station

V_a lateral inflow

V_d runoff volume at the downstream station

Different kinds of estimation tools for transmission losses were developed.

A commonly used estimation tool for transmission losses is the development of linear relations between transmission losses and other parameters. E.g. correlating inflow volume to losses (e.g. Jordan 1977; Sorman et al. 1993, 1997; Schwartz 2001), or the rise of the groundwater table to losses (Sorman et al., 1993) or water losses in percent to days since the last event (Schwartz, 2001).

Lane (1985) developed a more general relationship between the amount of inflow and outflow considering channel and flood characteristics

$$Q_0 = \begin{cases} 0; & P_o \geq V_u \\ d + e * V_u; & P_o < V_u \end{cases}$$ **equation 2.3.2**

V_u volume of inflow (acre-feet)

P_0 threshold volume (acre-feet)

d; e functions of channel and flood characteristics

Dunkerly et al. (1992) in Lange et al. (2003) examined geomorphic downstream channel modifications along two stream reaches in an un-gauged watershed. Critical flow velocities, mean flow velocities and discharges were estimated and with the downstream decline of these parameter mean rates of discharge were approximated. Lange et al. (2003) points though out that the estimates of flood discharge cannot substitute measured flow data.

All these correlations between transmission losses and other parameters remain site-specific and the transfer to other watersheds brings large uncertainties or is simply impossible.

Several models for arid or semi-arid regions for different purposes have been constructed considering transmission losses, for example:

Sharma et al. (1994) modeled transmission losses as a function of inflow, distance, channel width, time parameters of flow and effective hydraulic conductivity in a differential equation.

Lange (1999) developed a non-calibrated rainfall-runoff model and modeled transmission losses with constant infiltration rates depending on the channel surface characteristics and the flooded area.

Shentsis et al. (2001) modeled transmission losses and groundwater recharge by using a hydrological-lithostratigraphical analogy. Here the lost volume is subdivided into channel moistening, which ultimately evaporates, and deep percolation, which replenishes aquifers.

2.4 Infiltration, soil water movement and developments in research

Infiltration is the process of water entry into the soil trough the soil surface. Soil water movement is the process of water flow from one point to another within the soil (Rawls et al., 1992) along soil-potential gradients. The two processes are tightly connected to each other as the rate of infiltration is determined by the rate of soil water movement.

These two processes depend on physical soil properties like the grain size, porosity, bulk density, macro pores or particle density and on soil water properties such as hydraulic conductivity, water retention characteristics, soil moisture content or hysteresis. It is important to keep in mind that the natural field conditions and the above-mentioned factors controlling infiltration and soil water movement are mostly heterogeneous and anisotropic in space and time (Ward et al. 2000; Rawls et al. 1992).

Soil water movement is separable into unsaturated flow and saturated flow. Unsaturated flow is a process of simultaneous flow of two immiscible fluids (Morel-Seytoux et al., 1985) such as air and water whereas saturated flow describes this process for only one fluid that is water. If the air cannot escape, it will constrain the flow of water, as an air pressure will build up below the wetting front, which will decrease infiltration.

A precise description of infiltration and soil water movement should consider the above-mentioned factors. However, most of the theoretical and experimental infiltration and soil water movement theories are based on the assumption of a homogeneous soil with uniform water content and assume that the air phase is interconnected so that it can easily escape as the water moves down thus offering a negligible resistance to water flow (Morel-Seytoux et al. 1985; Rawls et al. 2000).

2.4.1 Darcy’s law and the Richard’s equation

It is assumed that both, saturated and unsaturated flow, obey Darcy’s law (equation 2.4.1) and that the yield is a function of the hydraulic conductivity and the hydraulic gradient. Both depend on physical properties of the soil and properties of the soil water.

$$Q = k(\theta) * A * \frac{\Delta H}{\Delta L}$$ **equation 2.4.1**

where Q volumetric discharge of flow rate (m^3/s)

A cross sectional area (m^2)

ΔH difference in hydraulic heads of water between two ends of the soil column (m)

ΔL length of soil column (m)

$k(\theta)$ hydraulic conductivity (m/s)

θ soil water content

or in differential form

$$q = -k(\theta) * \frac{\delta H}{\delta z} \qquad \textbf{equation 2.4.2}$$

where q specific discharge (m/s)

z distance in flow direction (m)

The combination of Darcy's law and the mass conservation equation leads to the Richard's equation (equation 2.4.3), which is governs the time-dependent infiltration rate.

$$C(\Psi) * \frac{\delta \Psi}{\delta t} = \frac{\delta}{\delta z}\left(k(\Psi) * \left(\frac{\delta \Psi}{\delta z} + 1\right)\right) \qquad \textbf{equation 2.4.3}$$

where $C(\Psi)$ specific moisture capacity

Ψ soil water pressure potential

z vertical space coordinate

t time

Figure 2.4.2 shows the Richards model that describes the vertical movement of soil water. The soil is divided into a shallow saturated zone at the ground surface (saturated zone), a zone trough which water from the upper zone is transmitted (transmission zone, almost saturated) and into the last zone which has a steep moisture gradient and where the water content changes with time.

2.4.2 Modeling infiltration and soil water movement

The characteristic curve of the infiltration rate over the time shows a decline as illustrated in Figure 2.4.1 in curve one. The variations in infiltration capacity result from the decrease of the gradient for the water potential in the soil. Nevertheless, other processes such as varying water surface depths, clay swelling, raindrop impact or in-washing of fine material can also change the infiltration capacity (Reeder et al. 1980; Crerar et al. 1988; Rawls e al. 2000). Curve two in Figure 2.4.1 schematically shows a temporary increase of the infiltration rate due to a temporary rise of the surface water depth.

The difference between curve one and curve two can be explained by examining Darcy's law. A temporary rise of the surface water depth results in a temporary increase of the hydraulic gradient, therefore the decline of the infiltration rate can be weakened, stopped or as in Figure 2.4.1 the declining rate changes to an increasing rate. So for varying surface water depth it is possible for the slope of the infiltration curve to be either negative, zero or positive.

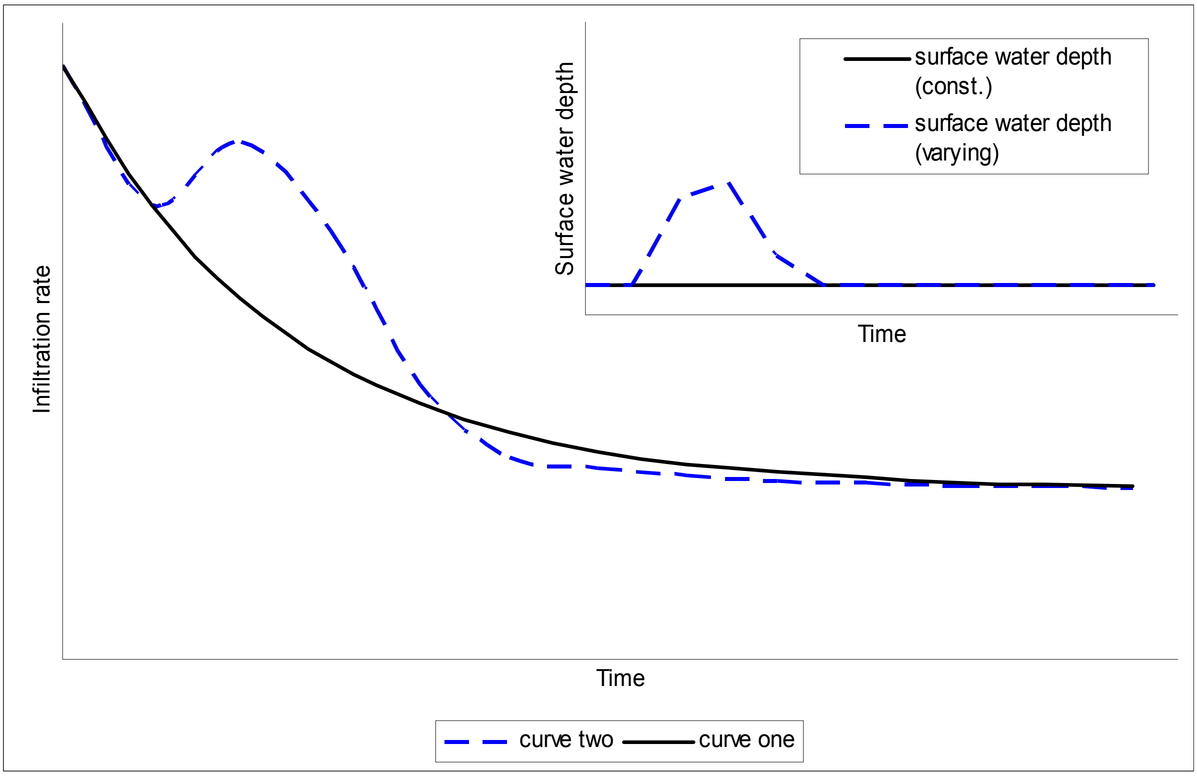

Figure 2.4.1 Schematic decline of infiltration rate over time; curve 1(black): constant surface water depth or incipient condition, curve 2 (dashed blue): with temporary rise of the surface water depth

Different models have been developed to describe the process of infiltration and according to Rawls et al. (1992) they can be divided into

- rainfall excess models
- empirical infiltration models
- approximate theory-based infiltration models

One example for each type of model with a short description of it will follow whereas the Green-Ampt model as an approximate theory-based model will be described in more detail.

Rainfall excess models - SCS runoff curve number model:

The SCS Model is an empirically developed approach to modeling the water infiltration process provided with a physical explanation of the process. The losses depend on the soil curve number and the precipitation. The soil curve number is derived from the type of soil, the land use and the antecedent soil moisture (precipitation of the previous five days).

Empirical infiltration models - Kostiakov model:

The Kostiakov model relates the infiltration rate f(t) to the time t using an algebraic power law usually stated as

$$f(t) = k_k^{t-\alpha} * f_\infty \qquad \textbf{equation 2.4.4}$$

where k_k, α constants

t time

f_∞ final constant rate when the soil is saturated

The function f(t) is a simple decay-curve where k_k and α are empirical constants depending on soil properties and initial conditions.

Approximate theory based models –Green-Ampt model

In contrast to the above mentioned infiltration models the model originally proposed by Green and Ampt (1911) explicitly considers surface water depth and thus warrants consideration for application in ephemeral stream channel modeling (Freyberg et al., 1980). In the Green-Ampt approach water is assumed to infiltrate into the soil as piston flow resulting in a sharply defined wetting front which advances but does not change shape (see Figure 2.4.2 Green-Ampt infiltration model). This progressing wetting front divides the wetted from un-wetted zones and the soil moisture profile is assumed to be a step function.

Applying Darcy's law to the saturated portion of the profile, while assuming a time dependent pressure head H(t) at the ground surface due to the surface water depth and an effective suction head h_e at the wetting front discontinuity (Freyberg et al., 1980) the infiltration rate of a homogeneous soil can be calculated as

$$f(t) = k\left(1 + \frac{(h_e + H(t)) * (\theta_s - \theta_i)}{F(t)}\right) \qquad \textbf{equation 2.4.5}$$

or

$$f(t) = k\left(1 + \frac{h_e + H(t)}{Z(t)}\right) \qquad \textbf{equation 2.4.6}$$

where k hydraulic conductivity (mm/h) in the portion of the profile above the discontinuity

θ_s volumetric soil moisture content at residual air saturation

θ_i uniform initial volumetric soil moisture content

F(t) cumulative infiltration or net change in total soil moisture above the moving wetting front (mm)

$Z(t) = \dfrac{F(t)}{\theta_s - \theta_i}$ depth of the moving wetting front (mm)

Its integrated form (Rawls et al., 2000) reads as

$$k * t = F - (h_e + H) * (\theta_s - \theta_i) * \ln\left(1 + \frac{F}{(h_e + H) * (\theta_s - \theta_i)}\right) \qquad \textbf{equation 2.4.7}$$

The first term ' $k * 1$ ' in equation 2.4.5 describes the steady rate of flow due to the gradient of soil water potential between the surface and the soil below, whereas the second term ' $k * (h_e + H(t)) * \frac{(\theta_s - \theta_i)}{F(t)}$ ' describes the diffuse flow into the soil ahead of the moving wetting front (Freyberg et al. 1980; Rawls et al. 2000).

The problem of solving equation 2.4.5 is that the infiltration rate f at the time t_i depends on the cumulative infiltration F at the time t_i. Two solutions for solving the Green-Ampt equation are proposed in chapter 3.3.

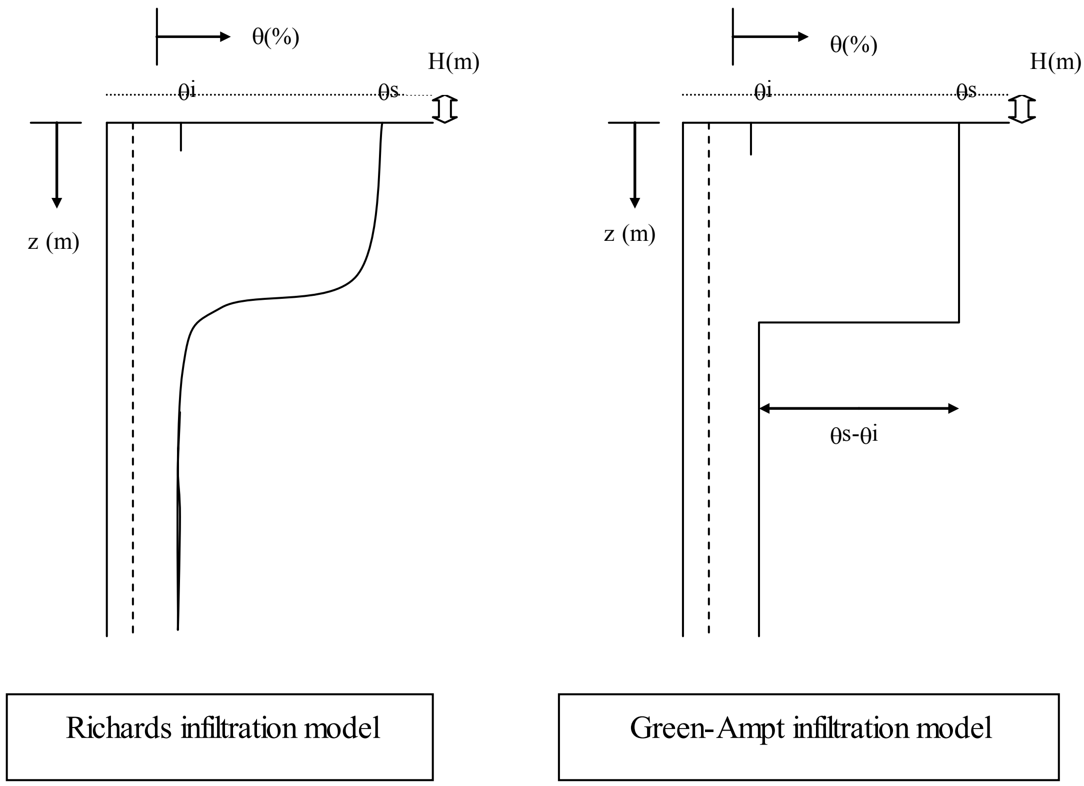

Figure 2.4.2 Comparison of the Richard's model and the Green-Ampt model (z-depth; H-surface water depth; θ_s-saturated soil water content; θ_i-initial soil water content)

The Green-Ampt equations for homogeneous soils can be extended to describe infiltration into layered soils where the hydraulic conductivity of the successive layers decreases with depth (Childs 1969; Hachum et al. 1980; Moore 1981; Ahuja et. al. 1983).

As long as the wetting front is in the first layer, the equation remains equal to equation 2.4.5. After the wetting front enters the second layer, the effective hydraulic conductivity k is set as the harmonic mean

$$k_h = (k_1 * k_2)^{0.5} \qquad \textbf{equation 2.4.8}$$

for wetted depths of the first and second layer. The capillary head is set equal to the one of the second layer. This principle is then applied to all succeeding layers.

For a crusted soil, in which the saturated hydraulic conductivity of the subsoil is greater, the above Green-Ampt equations as phrased above cannot be used after the wetting front enters the higher-k layer. For such cases, one can assume that infiltration through the higher-k layer continues to be governed by harmonic mean of the upper layers (Moore 1981).

2.5.3 Macro pore flow

Another process strongly influencing the infiltration is macro pore flow. Macro pore flow takes place in wormholes, decayed root channels or structural cracks and is not considered in the above-mentioned models. An approach to integrate this fast component of infiltration is to adjust the effective hydraulic conductivity or to consider the soil porosity as two domains, the macro pores and the soil matrix with an interaction between the two (Rawls et al., 1992). Dong (2003) for example calculated the hydraulic conductivity for the macro pores k_{mp} as a function of radius and fractional macro-porosity (n_{mp}) and then computed the weighted effective conductivity of k_{mp} and k for different matrix potentials (ψ) as

$$k_{eff} = n_{mp} * k_{mp}(\Psi) + (1 - n_{mp}) * k(\Psi) \qquad \textbf{equation 2.4.9}$$

where the pressure equilibrium between the soil matrix and the macro pores is reached immediately.

2.5 Conclusion

In arid regions, the ephemeral rivers stay dry most of the year. In these regions, which are hydrologically characterized by high potential evaporation rates and low annual precipitations, the rare high intensity rainfalls can create runoff. A feature of those runoff events is the decrease of water volume along the course of flow in the riverbed (transmission losses). This is caused through miscellaneous processes like evaporation, artificial withdrawal, bank storage, depression storage and infiltration. The amount of transmission losses varies in space and time and depends on various processes that are related to the channel and flood characteristics (e.g. scour and fill, antecedent moisture, flooded area or infiltration characteristics). Different techniques are developed and applied to determine transmission losses. The three main methods are the appliance of the water balance equation, theoretical modeling and the use of artificial tracer.

In general, infiltration is the most relevant process with respect to transmission losses. This process and the associated process of soil water movement depend on soil and water properties and therefore they are aptly described by Darcy's law and the Richard's equation. Several methods have been developed to simulate infiltration, which can be classified into rainfall excess models, empirical models and approximate theory based models. The Green-Ampt model belongs to the physically based models assuming a sharply defined advancing wetting front that considers the surface water depth.

The introduced ways to simulate transmission losses or the related processes indicate the problem to describe these complex processes in a heterogeneous system with only a few and rigid parameters. So when simulating the infiltration of an ephemeral stream the Green-Ampt approach should be preferred to empirical or rain excess models as it considers the surface water depth and it grants a certain physical background. The problems of modeling in general and in specific modeling transmission losses are the spatial and temporal heterogeneity of natural systems and the choice of suitable simulation tools.

The following chapter describes how the ZIN-model was modified to simulate transmission losses considering the above-mentioned processes that influence the losses.

III Methodology

3.1 The ZIN-model

Dr. Lange developed the ZIN-model during his dissertation. It is a distributed rainfall-runoff model for large-scale catchments in arid regions that requires no calibration with runoff data. Originally, it was developed for the Nahal Zin catchment in the Israeli desert Negev but has also successfully been applied to other regions and purposes (e.g. application in the hyperarid Kuiseb catchment in Namibia (Lange, 2005), in a small hyperarid catchment in Israel (Thormählen, 2003), for urban hydrology in Freiburg, Germany (Guwang, 2004)…).

It is possible to subdivide the distributed ZIN-model into three different units, in particular runoff generation (described with model elements), runoff concentration and channel routing (described with channel segments).

A short description of the model follows with an emphasis on the routing module and the transmission losses, as the main aim of this work is to modify and to improve this part of the model. For further detailed information, the reader should refer to the dissertation 'A non-calibrated rainfall-runoff model for large arid catchments, Nahal Zin, Israel', Lange 1999.

3.1.1 Runoff generation

The input-size is a spatial distributed rainfall rate, which generates Hortonian overland which varies with the surface type. Hortonian overland flow is assumed to be the main process for runoff generation in arid regions (Lange, 1999).

To apply the ZIN-model, the catchment has to be disaggregated into different surface types according to their hydrologic characteristics. The original model used 21 terrain types for the Nahal Zin catchment in Israel. The important hydrologic characteristics to classify the surfaces concerning Hortonian overland flow are the initial loss volume and the final infiltration rate. The time dependent infiltration rate is interpolated between these two values using a decay-function.

The ZIN-model computes runoff concentration as rainfall excess in dependence of the rainfall and the infiltration rate for the different terrain types.

3.1.2 Runoff concentration

To describe runoff concentration the catchment has to be divided into tributary catchments (model elements) according to the topography and into channel segments according to the tributary catchments.

The spatial pattern of overland flow, resulting from the runoff generation and the tributary catchments, is transformed to the channel segments as lateral inflow through a mean response function. The mean response function was determined in a similar experimental catchment.

3.1.3 Routing

As mentioned above the channel network is divided into segments. These channel segments, which begin and end with a node, are grouped into four channel types according to their morphological features as shown in Table 3.1.1.

The ZIN-model uses a distributed routing scheme where the channel segment properties like cross sectional geometry, slope, flow length and channel roughness are considered. Here a non-linear Muskingum-Cunge method, to be accurate the MVPMC3-method (Ponce & Chaganti, 1994), is used to route the discharge from node to node with respect to lateral inflow and transmission losses.

Table 3.1.1 Channel types (abridged according to Lange 1999)

Channel type	Description
1	Flat loessial valley fills with a dense vegetation cover and limited channel incision
2	Single clearly definable main channel with pronounced entrenchment and a rather coarse riverbed alluvium. Vegetation is limited to banks and high bars. This unit is subdivided according to their underlying strata
3	Braided channel systems with large cross sectional widths
4	Steep headwaters with waterfalls and rocky reaches

3.1.3.1 Channel geometry

The ZIN-model assumes that the channel consists out of the inner channel and the bars, each with a certain proportion of the total width. The flood always covers the inner channel, whereas the covering of the bars by the flood depends on the water depth. This dependence of flooded area and water depth is realized by a linear interpolation between the total width (bankful stage) and inner channel width (see Figure 3.1.1).

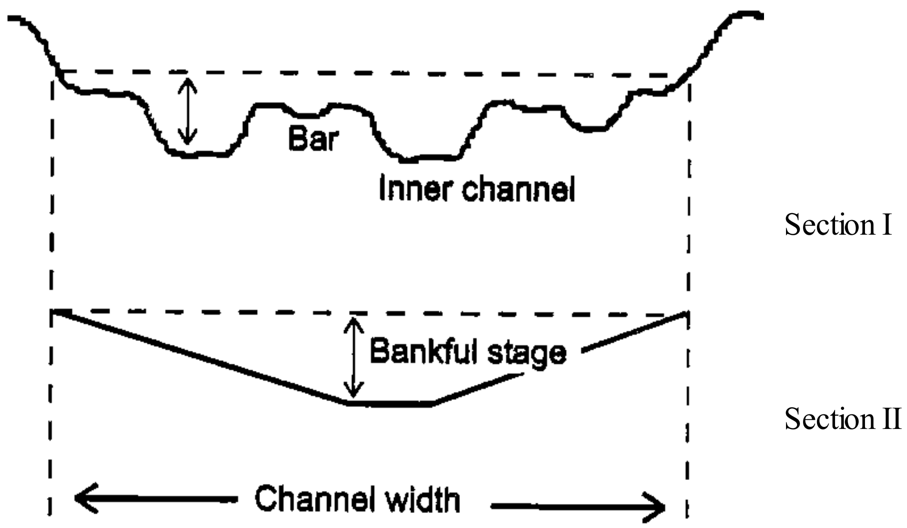

Figure 3.1.1 Simplified representation of cross-sectional geometry (modified from Lange 1999); Section I-real cross section, Section II-model approximation

3.1.3.2 Transmission losses

In the ZIN-model, the process of infiltration represents the transmission losses. For each channel type two different but constant infiltration rates are assumed, one for the inner channel and one for the bars. The values vary between zero and 420 mm/h for the inner channel and between zero and 110 mm/h for the bars. The inner channel infiltration occurs on the entire inner channel area of each segment, whereas the infiltration into the bars depends on the flooded area. The calculation of the additionally flooded area depends on the cross-sectional geometry (see chapter: 3.1.3.1 Channel geometry) and increases linearly with the water depth. The process of infiltration stops when the active alluvium is completely saturated. The channel type characterizes the depth of the alluvium and according to Lange (1999), it varies between zero and two meters for the Nahal Zin catchment in Israel.

The infiltrated water volume is then subtracted from the actual discharge in each time step and segment.

3.2 Modifications

It is often adequate to use simple, non-physical models such as an initial abstraction and constant loss rate model when calibrating an event-simulation model with gauged data (Goldman, 1989). However, it is desirable to relate loss rates to physical characteristics of the watershed (Reed et al., 1998) or to physical characteristics of the channel. In addition, a model with a physical basis may be suitable for application in unmeasured areas.

Therefore, in this study the transmission losses in the ZIN-model are modified in different ways to achieve a more physically based background.

The previous constant infiltration rate into the inner channel is now described by using the approximate theory-based solutions to the Richard's equation, in particular the Green-Ampt model. To solve the Green-Ampt equation, in a first step the cumulative infiltration is computed in order to calculate the infiltration rate in a next step. Different methods are used to compute the cumulative infiltration, in particular an approximation procedure according to Sir Isaac Newton (1669) and a decomposition series according to Serrano (2001, 2003). The different methods are applied to the ZIN-model and the two versions are tested (chapter 6.1.1) and discussed (chapter 7.1).

Transmission losses on flooded bars, banks and floodplains are described by using a simple empirical approach based on a linear storage model. The additional flooded area is approximated with a grow-function.

To simulate the process of scour and fill, an empirical factor has the function of reducing the infiltration rate. Whether this factor is active or not depends on the critical shear stress or on the critical flow velocity. Both methods are tested and the results compared (chapter 6.1.2).

The antecedent soil moisture content is modeled with a 'days-since-last-event' dependent power function according to Dames & Moore (1988) in Sorman et al. (1993). This antecedent soil moisture has an impact on the infiltration rate and on the total volume of infiltration.

The above-mentioned modifications of the ZIN-model are described in detail in the following chapters and the different computer codes are presented in the Appendix (chapter 9.2).

3.3 Computing infiltration into the inner channel with the Green-Ampt equation

The Green-Ampt model has been introduced in chapter 2.4. It has been chosen because it is a model with a physical basis that relates the rate of infiltration to measurable soil properties such as the porosity, hydraulic conductivity and the moisture content. Further, it considers the effects of a varying surface water depth on the infiltration rate as Freyberg et al. (1980) states, 'for infiltration problems where the depth of water above the ground surface is varying, conventional algebraic power law models of infiltration rate are unsatisfactory'.

To solve equation 2.4.5 (Green-Ampt equation) two different methods are presented and described in detail, whereas the calculation of the infiltration rate f(t) always follows the same pattern. Depending on the method, the cumulative infiltration F(t) is approximated for the each time step. Afterwards the infiltration rate f(t) is computed according to equation 2.4.5, considering other aspects such as the sealing of the alluvial surface. To approximate the cumulative infiltration, an iteration method and a decomposition series has been used.

In determining the cumulative infiltration, both approximation methods do not consider the circumstances of the previous time steps. That means that $F(t_i)$ for time step t_i is calculated with the water depth of time step t_i without considering changing water depths and possibly hindered infiltration in preceding time steps. The influence of varying infiltration rates due to clogging is demonstrated schematically in Figure 3.3.1. Here, a constant water depth is assumed. Infiltration rates and cumulative infiltrations are compared for case one (f1, F1) where infiltration is unhindered and for case two where infiltration is blocked twice (f2, F2). It becomes evident that cumulative infiltration F1 in case one differs in comparison to F2 in case two from that moment on where infiltration rate f2 becomes zero (totally blocked - period T1). Corresponding to this, the infiltration rate in case two (f2) exceeds the infiltration rate in case one (f1) between the blocking periods T1 and T2 and after period T2 as the amount of infiltrated water is lower.

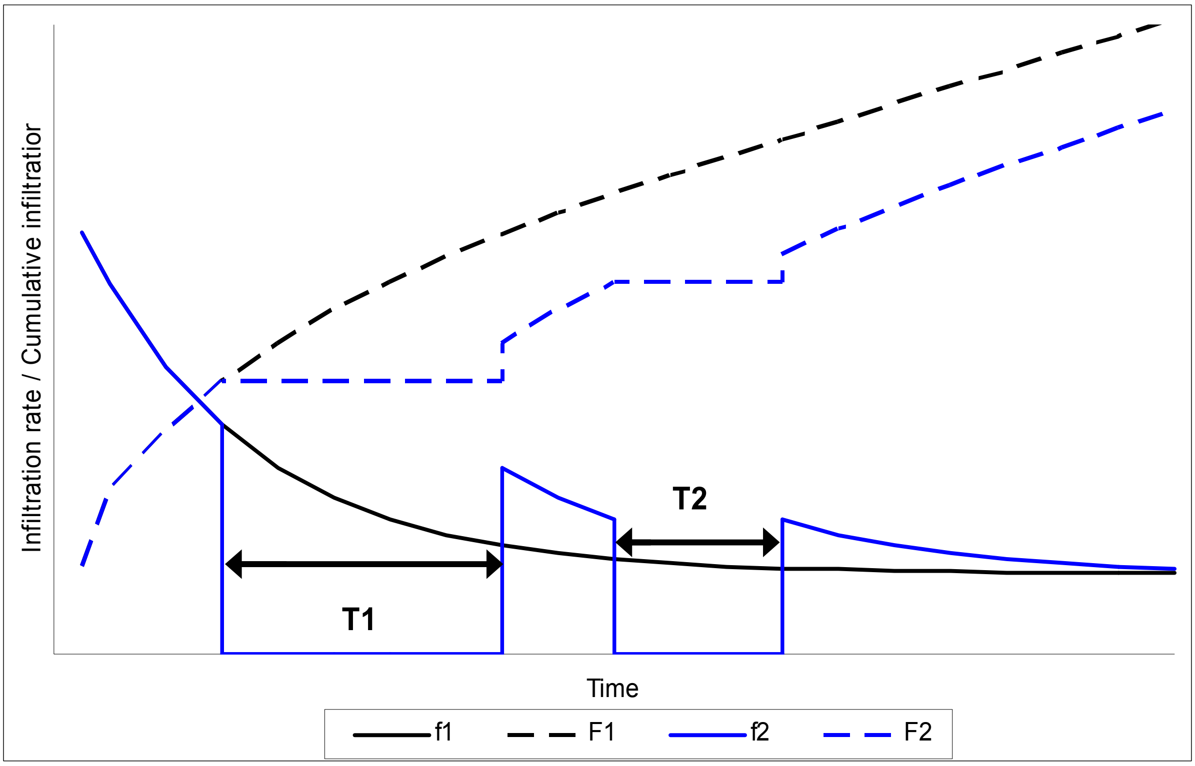

Figure 3.3.1 Schematic comparison of infiltration rate (f-dashed 'declining' curves) and cumulative infiltration (F) without (1-black curves) and with (2-blue curves) blocking. Before period 1 (T1) the blue curveoverlays the black curve

In order to avoid this error, F(t) is approached in a different way after an initial cumulative infiltration of five centimeters. This threshold is mostly reached in the first time step of the ZIN-model (five minutes) as the initial infiltration capacity is very high because of the shallow depth of the wetting front. Afterwards the infiltrated water from each time step, that is calculated as infiltration rate multiplied with time and reduction factor, is added up and this value is used to compute the new infiltration rate.

Unfortunately, this method is not accurate either as $f(t_i)$ is computed with the cumulative infiltration of the last time step $F(t_{i-1})$ and not with the current amount of infiltrated water $F(t_i)$. Still this systematic error is smaller than it would be when using any of the above-mentioned approximation method because F(t) is computed with regard to real infiltration rates for each time step with changing water depths and processes affecting infiltration.

3.3.1 Cumulative infiltration calculated with an iteration

The Newton approximation procedure is used to solve numerical non-linear equations. For a continuous differentiable function g with a single variable x this procedure can approximate the variable x so that the function reaches zero (g(x) = 0). The idea is to determine the tangent in one point of the function by the differentiating with respect to x $\left(\frac{\partial g(x)}{\partial x}\right)$. The value where the tangent is null is then used for the following approximation to advance the approximation accuracy according to equation 3.3.1

$$x_{n+1} \equiv x_n - \frac{g(x_n)}{g'(x_n)} \qquad \textbf{equation 3.3.1}$$

The accuracy of the result grows with the index n. In this study n is chosen as five (tests showed that the final value is reached for n =3), and the starting-value (x_1 or here F_1) as half of the possible storage volume of the alluvium. So rewriting equation 2.4.7 as shown below in equation 3.3.2and differentiating with respect to the cumulative infiltration (F), equation 3.3.1 yields the form of equation 3.3.3

$$0 = F - (h_e + H) * \ln\left(1 + \frac{F}{(h_e + H) * (\theta_s - \theta_i)}\right) - k * t \qquad \textbf{equation 3.3.2}$$

$$F_{i+1} = F_i - \frac{F_i - (h_e + H) * \ln\left(1 + \frac{F_i}{(h_e + H) * (\theta_s - \theta_i)}\right) - k * t}{1 - \left(\frac{(h_e + H) * (\theta_s - \theta_i)}{(h_e + H) * (\theta_s - \theta_i) + F_i}\right)} \qquad \textbf{equation 3.3.3}$$

3.3.2 Cumulative infiltration with a decomposition series

Serrano (2001) approximated the non-linear Green-Ampt equation with a decomposition series. Decomposition generates a series, much like the Fourier series, that converges fast towards the exact solution (Serrano, 2001). In 2003, Serrano published an improved decomposition solution to the Green-Ampt equation. He derived a new form for the cumulative infiltration that includes more terms in the decomposition series and a criterion for its convergence. The derivation of the cumulative infiltration F follows, in doing so this study assumed incipient ponding, so the time to ponding as well as the amount of infiltrated water before the ponded conditions are realized is zero.

According to Serrano (2001) equation 2.4.5 can be rewritten as

$$F = k * t + \ln\left(\frac{F + ai}{ai}\right) \qquad \textbf{equation 3.3.4}$$

with $ai = (H + he) * (\theta s - \theta i)$ **equation 3.3.5**

or $F = k * t + NF$ **equation 3.3.6**

with $NF = a * \ln\left(\frac{F + ai}{ai}\right)$ **equation 3.3.7**

The non-linear term NF can be expressed as a sum of polynomials

$$NF = \sum_i A_i \qquad \textbf{equation 3.3.8}$$

Where the polynomials are defined as

$$A_0 = NF_0; \qquad A_1 = F_1 * \frac{dNF_0}{dF_0};$$

$$A_2 = F_2 * \frac{dNF_0}{dF_0} + \frac{F_1}{2!} * \ldots \qquad \textbf{equations 3.3.9}$$

A_0 only depends on F_0; A_1 on F_0 and F_1; A_2 on F_0, F_1 and F_2 and so on. All of the F_n components are analytic and calculable (Serrano, 2001).

From equation 3.4.2 and equation 3.3.9 one may get the different F_n's

$$F_0 = k * t; \qquad F_1 = A_0 = a * \ln\left(\frac{F + ai}{ai}\right)$$

$$F_2 = A_1 = ai * \ln\left(\frac{k * t}{ai}\right) * \frac{ai}{k * t + ai} \ldots \qquad \textbf{equations 3.3.10}$$

These terms can be factorized and the cumulative infiltration can be expressed as

$$F(t) = k * t + ai * \ln(m_1) * \left(1 + \frac{m_2}{(1 - m_2) * (1 + m_2 * \ln(m_1))}\right) \qquad \textbf{equation 3.3.11}$$

for $t \geq t_{pon}$ (t_{pon} time till ponding)

$$m_1 = \frac{k * t + ai}{ai}$$ **equation 3.3.12**

$$m_2 = \frac{ai}{k * t + ai}$$ **equation 3.3.13**

The convergennce criterion of the series is

$$1 > 2 * \frac{ai}{F_0 + ai}$$ **equation 3.3.14**

The accuracy of the decomposition series depends on the number of terms. According to Serrano (2001), the maximum error in comparison with the exact implicit solution was about 0.15 % when using three terms in the series and it is reduced to 0.02 % when including one more term.

In case that the convergence criterion (equation 3.3.14) is not satisfied, cumulative infiltration and infiltration rates are overestimated when equation 3.3.11 is applied. Serrano (2003) emphasized that equation 3.3.14 is not satisfied when the rainfall rate exceeds the hydraulic conductivity many times, or the effective suction head is large. But if the condition for convergence is not satisfied the errors decrease with increasing time. The plausibility of applying equation 3.3.11 for incipient ponding will be discussed in chapter VII Discussion.

3.4 Infiltration into the remaining area

As mentioned above, the Green-Ampt infiltration model does not simulate the transmission losses on the residual area like bars, banks and floodplains. Still, they are modeled as losses due to infiltration but with an empirical approach with regard to a single linear storage model. For these areas, such an approach is chosen preferentially over the Green-Ampt model as the processes causing the transmission losses differ from the processes in the inner channel. According to personnel communication with J. Lange and C. Külls, the over-bank areas can remain flooded or swamped many days after the event. So here, different processes amongst the process of infiltration, such as depression storage (e.g. surface water storage in dead end channels) and evaporation are responsible for the losses. Considering this, the Green-Ampt approach loses the physically based legitimation to simulate the losses in this area. However, a linear storage approach reflects these processes in a suitable way, as the outflow of or in this case, the inflow into the linear storage is strongly connected to the present water volume in the storage. It is important to mention that the storage is not constant in volume as it depends on the flooded area.

Therefore, this approach has to meet two criteria. First, the transmission losses increase with increasing flooded area as the storage grows with additional flooded area. Second, the losses on the flooded area decrease with time as the storage fills up. Both criteria are strongly connected with the simulation of the cross sectional geometry that is described in chapter 3.7. To consider the two criteria the residual area is separated into two sections, the bars plus the banks and the over-bank area. Details of the simulation of the infiltration into these two sections are given below.

3.4.1 Modified linear storage model

In general, the linear storage approach is used to describe the outflow of the storage dependent on the storage content whereas the yield grows with rising storage content. This realationship is reversed in this study. Here the inflow decreases with rising storage content whereas an equivalent mathematical description is used.

The following simplified derivation of the linear storage equation follows Maniak (1997) and Nestmann et al. (2002).

The variation of the storage contents S over time t depends on the difference of inflow $Q_i(t)$ and outflow $Q_o(t)$. This is expressed in equation 3.4.1

$$\frac{dS}{dt} = Q_i(t) - Q_o(t)$$ **equation 3.4.1**

It is assumed that $Q_o(t)$ is proportional to S, so

$$S = c * Q_o(t)$$ **equation 3.4.2**

with c proportionality constant

Combining of equation 3.4.1 and equation 3.4.2 one gets

$$\frac{dS}{dt} + \frac{1}{c} * S = Q_i(t)$$ **equation 3.4.3**

Assuming $S_0 = 0$ and $Q_i(t) = x * \delta(t)$ **equation 3.4.4**

where $x * \delta(t)$ is a Dirac impulse of an inflow of x m^3 water at the time t = 0 one gets the equation for the single linear storage model:

$$Q_o(t) = x * \frac{1}{c} * \exp(\frac{-t}{c})$$ **equation 3.4.5**

Reversing the conditions so that the inflow into the storage decrease with a rising storage content and assuming that the outflow is zero, the equivalent to equation 3.4.2 is

$$S = c * Q_i(t)$$ **equation 3.4.6**

Combining equation 3.4.1 and equation 3.4.6 with $Q_o(t) = 0$, one gets a linear differential equation of first order

$$\frac{dS}{dt} = \frac{S}{c}$$ **equation 3.4.7**

By rearranging equation 3.4.7 and forming the integral one gets

$$\int_{S(t_0)}^{S(t)} \frac{1}{S} dS = \int_{t_0}^{t} \frac{1}{c} dt$$ **equation 3.4.8**

$$= \left[\ln S(t)\right]_{S(t_0)}^{S(t)} = \frac{1}{c} * (t - t_0) + b$$ **equation 3.4.9**

b integration constant

with $t_0 = 0$ and $S(t_0) = S_0$ can be written as

$$S(t) = S_0 * \exp(\frac{-t}{c}) + b$$ **equation 3.4.10**

Combining equation 3.4.10 with equation 3.4.6 the general solution for $Q_i(t)$ is

$$Q_i(t) = \frac{S_0}{c} * \exp\left(\frac{-t}{c}\right) + b$$ **equation 3.4.11**

The next step is to find plausible values for the proportionality constants c and $\frac{S_0}{c}$. The proportionality constants should consider the storage characteristics of the flooded area, described with a constant value k_b (equivalent to the initial infiltration rate) and the variable width bv.

So with the boundary conditions that at the beginning of the event $Q_i(0) = k_b$ and $Q(\infty) = k_f$, one gets

$$\frac{S_0}{c} = k_b - b$$ **equation 3.4.12**

and $b = k_f$ **equation 3.4.13**

Consequently equation 3.4.11 takes on the form of Horton’s infiltration equation.

$$Q_i(t) = kf + (kb - kf) * \exp\left(\frac{-t}{c}\right)$$ **equation 3.4.14**

The losses on the banks, bars and over-bank areas are now described by equation 3.4.14.

To establish a relation between the variable width bv and the proportionality constant c, with the intention that additional flooded area slows down the decline or even enlarges the infiltration rate, the proportionality constant c changes to a proportionality variable that depends on the variable width. This is reasonable, as with growing flooded width the additional flooded area has not been flooded yet. Therefore, the capability on these areas to assimilate water is higher than on the previous flooded areas. Consequently, the infiltration rate for the whole area is a mix out of the infiltration rates for the several, temporal different, flooded areas.

Hence, the variable c is chosen as k_b [mm/h] + bv [m].

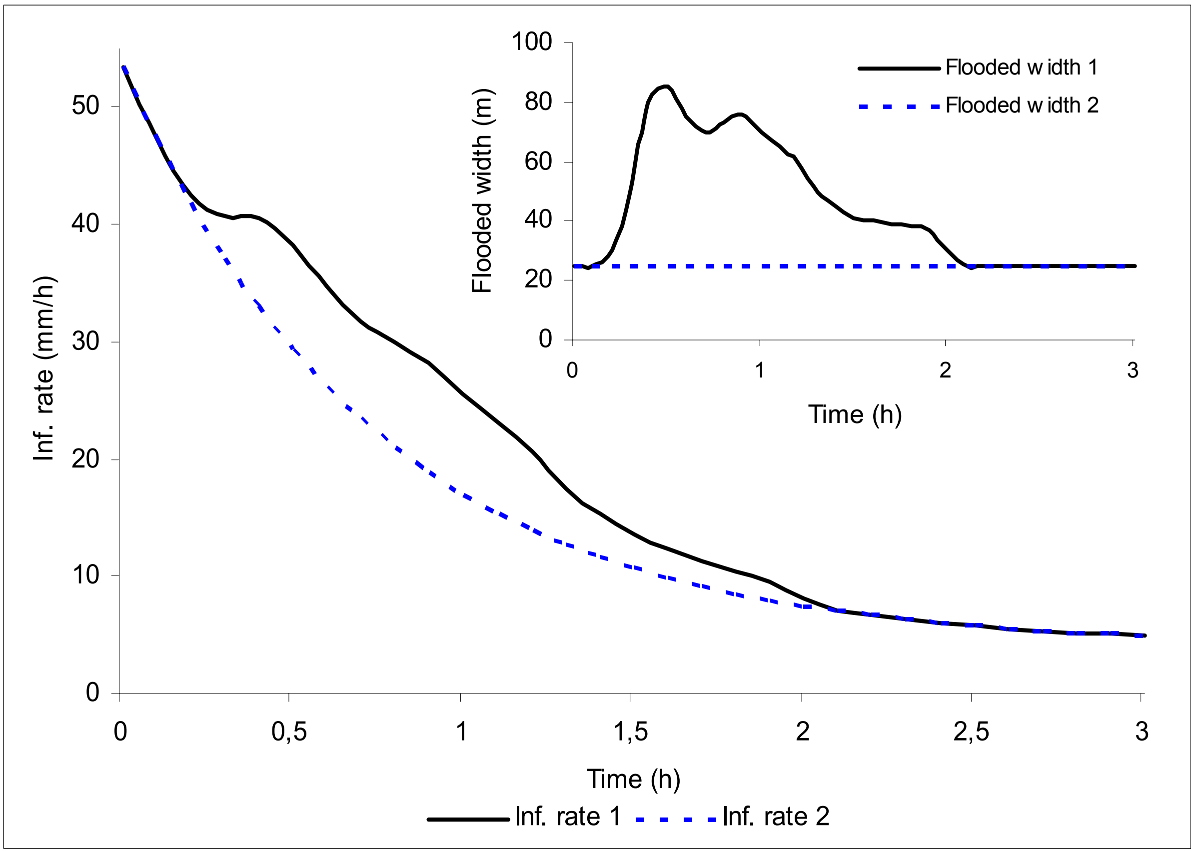

Figure 3.4.1 Infiltration rate according to the single linear storage approach, dependent on the flooded width; comparison of a constant width (dashed blue curve) and a varying width (black curve)

Figure 2.3.1 shows a comparison between the loss rates when the width is constant (blue curve) and when the width changes with time (black curve). For both curves, kb and kf are the same, namely 50 mm/h and 4 mm/h. The infiltration rate (for the completely flooded area) decreases slower from the moment on when additional area is flooded (black curves). This is reasonable as the additional flooded area has a higher infiltration capacity as the already previously flooded part and therefore the infiltration rate for the entire area lies between the minimum and maximum rates. After the flooded width reaches the initial width (black curve), the infiltration capacity amounts the same values as the infiltration rate with a constant flooded with (blue curve) as these area was flooded for the same time in both cases.

3.4.2 Infiltration into bars and banks

The ZIN-model assumes that the inner channel is immediately and completely covered by the flood at any time of the event. Consequently, bars and banks are, depending on the water depth, at least partly covered by the flood as well. Therefore, this part of the whole cross sectional area is chosen as one section representing one linear storage.

For this section, the infiltration depends on the variable flooded area of each segment and on the time since the beginning of the event because this is the point of time when the storage (banks and bars) starts to fill. The flooded area for each time step is calculated as the product of constant segment length and variable segment width. Chapter 5.4 describes the determination of each segment length and chapter 3.7 describes the computation of the variable width.

For each time step (Δt), the transmission losses (TL) are computed by multiplying the area (A) times the infiltration rate

$$TL = \Delta t * A * (k_b - k_f) * \exp\left(\frac{-t}{k_b + bv}\right) \qquad \textbf{equation 3.4.15}$$

3.4.3 Infiltration into floodplains

The computing of the transmission losses into over-bank areas basically follows the same method as the one into bars and banks. In contrast to bars and banks, over-bank areas are not partly flooded right from the start of the event. Only when the water depth surpasses a certain height this area is activated with regard to transmission losses and the storage can be filled. Consequently, this area is deactivated when the water depth falls below this height. Considering this, the computation of the transmission losses remains like equation 3.4.15 with the difference that time is just starts running (and so the decline of the infiltration rate) when the water depth exceeds a certain height. As a result, infiltration occurs only when the over-bank areas are flooded.

3.5 Scour and fill

According to different authors (Shields 1936; Wiberg 1987; Briaud et al. 2001 or Wyrwa 2003), the processes of deposition and erosion are strongly connected to the shear stress affecting the riverbed surface. Another factor controlling these processes is the initial concentration of particles in the water whereas Lee (1999) points out that with an increasing shear stress the impact of the initial concentration decreases exponentially. In principle, deposition occurs when the shear stress imposed by the water on the soil falls below a critical value τ_d whereas erosion occurs by exceeding a critical value τ_e. This critical shear stress for non-cohesive sediment is derived from the balance of forces on individual particles at the surface of riverbeds (Wiberg, 1987).

Already in 1936, Shields investigated the behavior of sediment in relation to the shear stress. He found non-dimensional parameter (the Shields parameter) for non-cohesive sediments, describing incipient sediment motion. So, initial motion occurs when the Shields parameter is larger than a critical threshold. Surpassing this threshold means that the drag forces exceed the gravitational force and the electromagnetic and electrostatic forces that are effective against the downstream movement of the particle.

Clean sands and gravel erode particle by particle (Briaud et al., 2001). The electromagnetic and electrostatic forces between these particles are insignificant compared to the gravitational force. However, for fine gained soils, in addition to the gravitational force, the electromagnetic and electrostatic inter-particle forces increase distinctly the scour resistance (Briaud et al., 2001). In this case, according to Briaud et al. (2001) two ways of erosion are possible; particle-by-particle and block-by-block. So when observing cohesive sediments the critical value τ_e depends apart from the grain size distribution on the history of the underground, especially on the depth and the idle period.

The relation between incipient motion, entrainment in suspension and the shear stress is illustrated in the Shields diagram (Figure 3.5.1) where density and diameter are adequate for the description of the sediment.

In addition to the power of water, the bed load itself has the ability to erode the surface due to its own mass and velocity. When the bed load is rolled, shoved or saltated on the surface the energy or the momentum might be used for erosion.

A closely related attempt for the description of erosion and sedimentation is to use the flow velocity. Similar to the shear stress a particle with a certain grain size on the riverbed surface will be eroded when exceeding a threshold velocity v_e and on the other hand deposition takes place when the velocity falls below a threshold velocity v_d. The Hjulström-diagram (Figure 3.5.2) shows the relationship between the grain size, the flow velocity and the resulting process (deposition, transport or erosion).

The critical shear stress and the critical flow velocity rely on different factors as shown below in the following two chapters. It is evident that the ability of water to erode or to deposit depends on the properties of the sediment and on hydraulic characteristics as shown in Table 2.2.1.

In this thesis, the modeling focuses on the suspended load and not on the bed load or dissolved load, as according to Crerar et al. (1988) the suspended load in particular silt clearly inhibits infiltration by sealing the alluvial surface.

To simulate the silt related clogging two approaches are chosen in this work. First, a shear stress dependent factor and second a flow velocity dependent factor that both reduce the infiltration rate.

Table 3.5.1 Sediment and hydraulic characteristics in view on erosion and deposition

Sediment characteristics	hydraulic characteristics
grain size (d)	flow velocity (v)
grain structure	shear stress (τ)
density of the particle (ρ_s)	shear stress velocity (u)
particle sink velocity (w)	density of water (ρ)
	viscosity of water (ν)

3.5.1 Critical shear stress

This shear stress depends on the kinetic energy of the moving water and therefore on the depth of water, the slope and the flow velocity. The shear stress can be expressed as

$$\tau = \rho * g * R_h * I_e \qquad \textbf{equation 3.5.1}$$

where τ shear stress (N/m²)

ρ density of the fluid (kg/m³)

g acceleration due to gravity (9.81m/s²)

R_h hydraulic radius (m)

I_e energy slope

and

$$R_h = \frac{A}{U} \qquad \textbf{equation 3.5.2}$$

$$I_e = I_w + \frac{v_1^2 - v_2^2}{2 * g * L} \qquad \textbf{equation 3.5.3}$$

where A cross sectional flow area (m²)

U wetted perimeter (m)

I_w declination of water level

v_1-v_2 difference of flow velocities in a distance L (m/s)

L distance (m)

As mentioned above, scour takes place when τ exceeds τ_e, which individually differs for different surfaces and grain sizes. Below the value τ_e the processes of transport or sedimentation occur. In 1936 Shields introduced a non-dimensional parameter describing initial motion for non-cohesive sediment, the Froude number or Shields parameter (Fr). The non-dimensional parameter for entrainment in suspension is the Reynolds number (Re).

where

$$Fr = \frac{u^2}{\left(\frac{\rho_s}{\rho - 1}\right) * g * d}$$ **equation 3.5.4**

$$Re = \frac{u * d}{\nu}$$ **equation 3.5.5**

For the Shields diagram (Figure 3.5.1) nother two more parameters are required, the shear stress velocity (u) and the particle diameter of the (d)

with

$$u = \sqrt{\frac{\tau}{\rho}}$$ **equation 3.5.6**

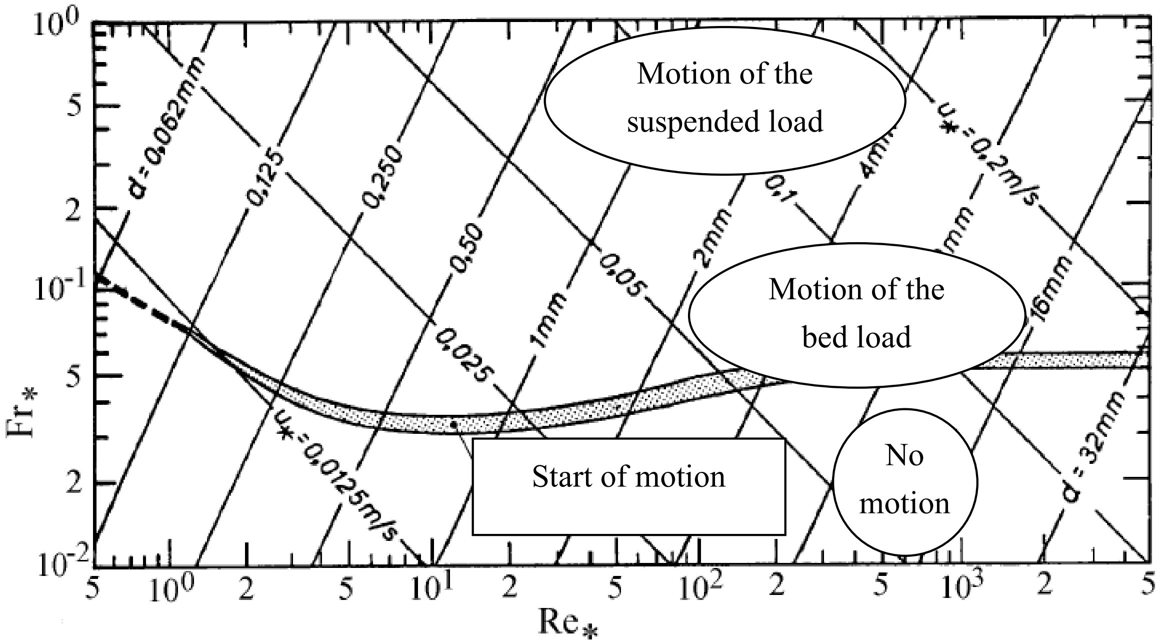

Figure 3.5.1 Shields diagram for ρ_s/ρ = 2.65 and ν = 1.3*10^{-6} m²/s (water-temperature: 10°C) (modified from Indlekofer, 2005)

Lane (1955) in Chang (1988) developed a differnt method to estimate the critical shear stress. He showed that coarse material behaves independently of the Reynolds number and that the critical shear stress can be expressed simply as a function of the grain size as

$$\tau_e = 0.0164 * d_{75}$$ **equation 3.5.7**

with τ_e in pounds per square foot and d_{75}, grain size such that 75 % is finer than d, in millimeters.

Briaud et al. (1999) in Briaud et al. (2001) established a simple relationship (equation 3.5.8**)** between the shear stress and the diameter based on experimental research with sand and gravel.

$$\tau_e = d_{50}$$ **equation 3.5.8**

with τ_e in Newton per square meter and d_{50}, grain size such that 50% is finer than d, in millimeter. Equation 3.5.8 and equation 3.5.7 correspond well with the critical shear stress obtained from the Shields-diagram for grain sizes larger than circa 0.1 mm but they cannot be applied to fine grained soils (like soils with high amounts of silt or clay).

When assunig a grain size of 0.05 mm (silt: 0.05 mm - 0.002 mm according to USDA soil textural classification system), a viscosity of $1*10^{-6}$ m^2/s (water temperature at 17°C), the tabulated density of silt as 2650 kg/m^3, the density of water as 1000 kg/m^3 and the Shields number as 0.13 than the critical shear stress for erosion becomes about 0.1 N/m^2 and the critical shear stress for entrainment in suspension about 0.04 N/m^2.

(According to equation 3.5.8, τ_e is about 0.05 N/m^2 and according to equation 3.5.7 τ_e is about $8.2*10^{-4}$ lb/ft^2 or 0.04 N/m^2).

As in nature, one does not find homogeneous alluvial silt surfaces but mixtures of different grain sizes, the above computed values are undervalued. The additional momentum of larger particle and the presence of places with more or less turbulence are not taken in account in this computation.

According to Briaud et al. (2001), the measured values of τ_e for fine grained soils reported in the literature vary between zero and five N/m^2. In his own experiments, τ_e was about 0.25 N/m^2 for a soil containing very fine sand and silt and 3 N/m^2 for coarse sand. In the work of Simon et al. (2003), τ_e varies between 10 N/m^2 and 0.31 N/m^2 depending on the grain size.

3.5.2 Critical flow velocity

As mentioned above the flow velocity can also be used as a criterion for incipient motion of particles. In this case, the permissible or critical velocity corresponds to the maximum velocity at which no erosion takes place.

Several studies have been carried out to determine the critical flow velocity for different grain sizes (e.g. Hjulström (1935); Briaud et al. 2001; Indlekofer 2005). A very popular and often used way to estimate the critical velocity is by employing of the Hjulström-diagram (Figure 3.5.2). In Figure 3.5.2 one can see that the erosion-curve declines with declining grain size until a value of about 0.3 mm is reached. Afterthat the critical velocity increases due to additional cohesive forces.

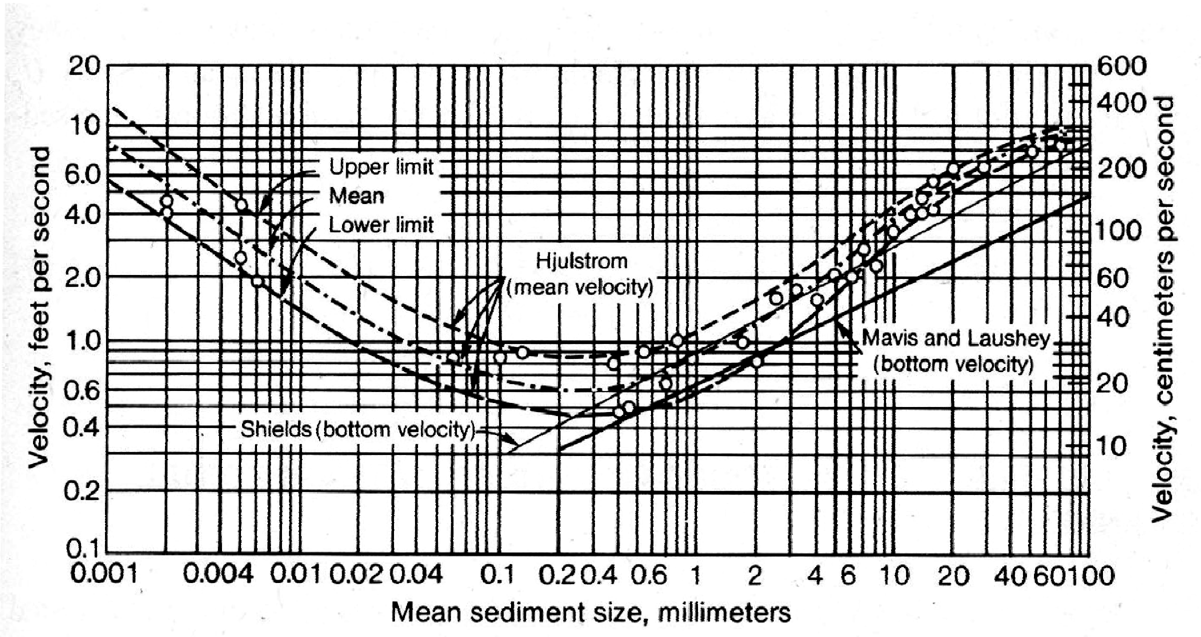

Figure 3.5.2 Hjulström diagram; processes erosion (section above the curves) and sedimentation (section below the curves) dependent on the flow velocity (source: Chang, 1988)

Referring to silt as important grain size for sealing the surface, one can interpret in Figure 3.5.2 in such a way that silt (grain size < 0.05 mm) erodes at velocities faster than circa 0.3 m/s and deposits at velocities lower than circa 0.002 m/s.

According to experimental results by Briaud et al. (2001), the critical flow velocity for a soil containing very fine sand and silt is circa 0.26 m/s.

3.6 Antecedent moisture

Many studies (e.g. Sorman et al. 1993; Dick 1997; Schwartz 2001; Schmitz 2004) described a relation between transmission losses and the time since the foregoing runoff or precipitation event.

Dick (1997) reported that the storm runoff response is highly sensitive to antecedent moisture that greatly reduces the infiltration capacity. In his study, the largest flow events occurred in situations with high antecedent moisture content coupled with low intensity and long duration rainstorms (Dick, 1997).

Schwartz (2001) observed large differences in transmission losses in the Nahal Zin, Israel. He examined the relationship of the observed transmission losses (in %) and the time from the preceding flood (see Figure 2.3.1). The study illustrates that the absorption of water by the alluvium is significantly inhibited for at least five days after the occurrence of a flood (Schwartz, 2001).

Schmitz (2004) observed two flow events in the Kuiseb River, Namibia with only four days between them. The first flood was large with a peak of about 90 m^3/s (estimated by Schmitz) compared with the second one with a peak of about eight m^3/s (estimated by Schmitz). Still the travel distances of both were approximately the same. This phenomenon is explained by the slacking of the first flood which lead to sealing of the alluvial surface so that the infiltration of the second flood was hindered.

This relation between transmission losses and the time from the preceding flood can be seperable into three main effects:

- Processes from the previous or current event that affect the riverbed surface, like slacking, eroding or building up of crusts, which influence the entry of water into the ground. These processes vastly depend on the deposited material and they are considered in chapter 3.5 Scour and fill.
- The soil moisture content directly influences the infiltration rate as the process of infiltration depends, amongst others, on the initial soil moisture content. So according to the Green-Ampt equation (equation 2.4.5) a higher initial soil moisture content (θ_i) in a soil lowers the infiltration rate as (θ_s - θ_i) in the numerator of equation 2.4.5 gets smaller.
- The potential total volume that the alluvium is able to infiltrate depends on the initial soil moisture content.

The ZIN-model did not consider the initial moisture content. In this thesis an antecedent moisture index (Antec) developed by Dames & Moore (1988) (in Sorman & Abdulrazzak, 1993) is integrated into the model. This index is an empirical power function with the number of days (T) since the last event as independent variable (see Figure 3.6.1) and simulates the decay of the soil moisture content due to evapotranspiration (see Figure 3.6.2).

Table 3.6.1 Antecedent moisture index for the four different channel types

Channel type	Antec	Channel properties
1	$= 1 - 0.9^T$	Surfaces with a high silt content – high matrix potential
2	$= 1 - 0.85^T$	Deep alluvial sediments – evaporation energy is lessened with depth
3	$= 1 - 0.\ 8^T$	Surfaces with high transmission losses
4	$= 1 - 0.75^T$	Rocky surfaces – little possibility of infiltration

Such an index is normally based on regional and seasonal characteristics such as the climatic situation or the soil properties. To consider at least the soil properties this index is modified with respect to the four different channel types (see chapter 3.1) as detailed in Table 3.6.1.

Figure 3.6.1 shows the different functions according to Table 3.6.1. It is visible that the index for channel type one rises not as steeply over time as the others do. So here, the loss of the soil moisture takes more time than is the case with the other channel types (e.g. fine grained soils). In contrast, the index for channel type four rises rapidly with the consequence that the soil moisture content vanishes relatively fast compared to the others (e.g. coarser material with less resistance against evaporation).

The antecedent moisture index is used to compute the initial moisture content θ_i as shown in equation 3.6.1 dependent on the different channel types.

$$\theta_i = \theta_s * (1\text{-Antec})$$ **equation 3.6.1**

equation 3.6.1 is a simple approach describing the time-dependent changes in soil moisture content without considering any processes involved (e.g. evapotranspiration or percolation). It can be seen as a functional method as the soil is nearly saturated directly after the event and the moisture content approaches zero after roughly 55 days. Three days after the event the water content varies between 0.73 % of the saturated value for channel type one and 0.34 % of the saturated value for channel type four. These values should represent the canonical field capacity. According to Ward (2000), the amount of water held in a soil after gravitational water has drained away varies between circa 0.51 to 0.79 % of the saturated value for clay and circa 0.23 to 0.31 % of the saturated value for sand. Therefore, equation 3.6.1 seems to adequatly to simulate the antecedent moisture content

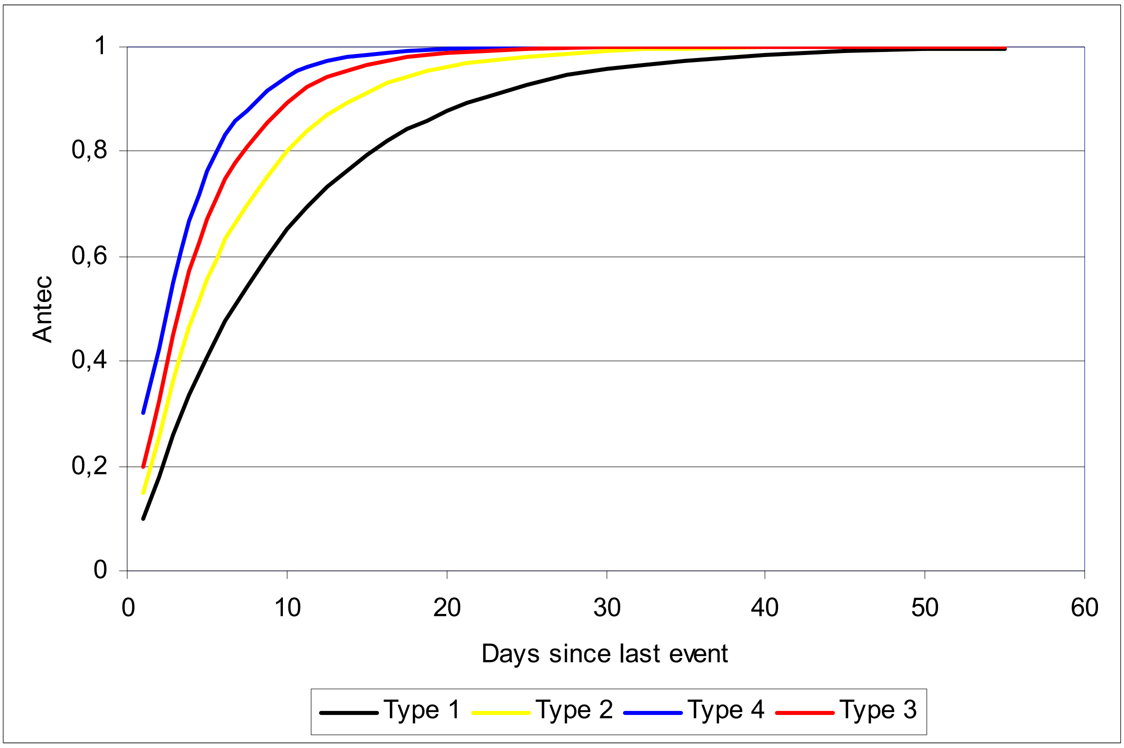

Figure 3.6.1 Antecedent moisture index for the four different channel types

Figure 3.6.2 shows soil moisture measurements in two arid stream channels in particular the Kuiseb River (Schmitz, 2004) and the Nahal Zin (Schwartz, 2001) (note: the initil moisture values after 60 days represent measured minimum values with a span of time of at least 60 days). Additionally, it shows the soil moisture contents computed with the antecedent moisture index (channel type one and three). In both channels, the measured values did not reach zero after a period of 60 days. The corrected values in Figure 3.6.2 are standardized to a relative scale from zero to one for a better comparison of the simulated moisture content and the measured moisture content. This fact will be discussed in the chapter VII ‘Discussion and outlook’.

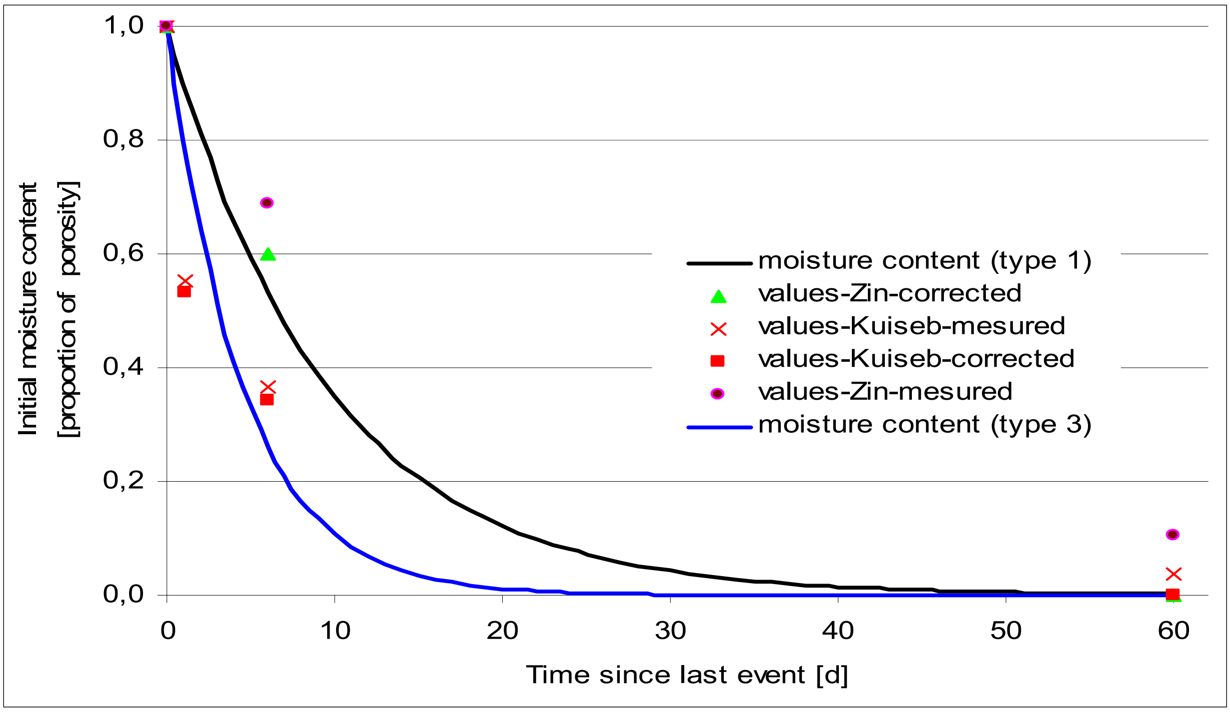

Figure 3.6.2 Measured soil moisture as fraction of porosity (points; corrected values: standardized to vary between one and zero in 60 days) compared with simulated soil moisture (curves)

As mentioned before, the initial soil moisture directly influences the Green-Amt equation and the total volume that can be absorbed by the inner channel alluvium.

The calculation of the initial moisture content with the antecedent moisture index affects the infiltration rate in the ZIN-model in various ways.

The infiltration into the floodplains is affected by the antecedent moisture index only when the preceding runoff event was large enough to flood these areas. As the process of infiltration in this section is described empirically (see chapter 3.4), the Antec index is also used empirically for this area. The infiltration is reduced by multiplying the infiltration rate with the Antec index, which reaches values between one (>55 days→ no influence) and zero (zero days→no infiltration).

3.7 Cross sectional geometry

The amount of infiltration among other factors depends on the size of the flooded area, which again is correlated to the water depth and the description of the cross sectional geometry. In this study, two composite power functions replace the linear approximation of the flooded area in the ZIN-model.

It is important that the developed functions consider two major aspects:

- the stability of the model
- an approach to describe the cross sectional geometry in a realistic way.

Too fast of an expansion of the flooded area goes hand in hand with large losses, which reduce the amount of discharge and the water depth in the next time step. This reduces the flooded area and therefore the losses, followed by an immense increase of the discharge and water depth in the next time step. This process repeats and the hydrograph becomes instable and shows a zigzag shape.

Considering this, the expansion of the flooded area has to be approximated with a slow growing function. On the other side, a slowly growing function hardly ever reflects the real cross sectional geometry. On the contrary, the floodplains are often huge and smooth, so that a small rise of the water level can result in flooding of large areas. So in addition to a slowly growing function, the floodplains have to be simulated with a fast growing function.

Therefore, the entire channel width was divided into three sections (schematically shown in Figure 3.7.1).

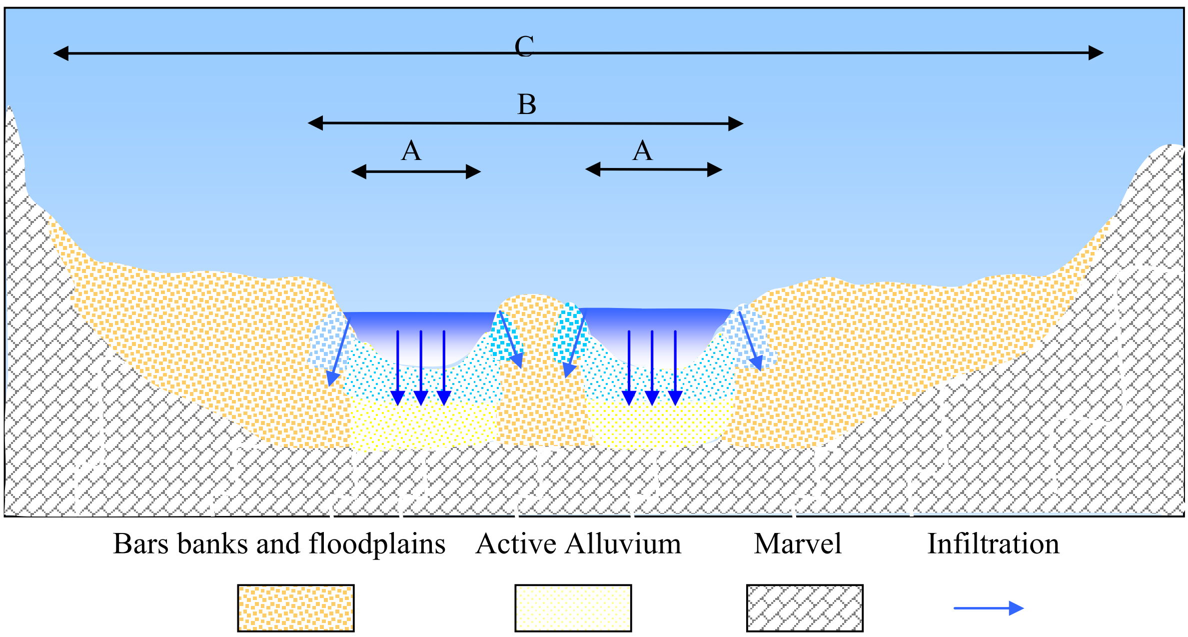

Figure 3.7.1 Schematic profile of a cross sectional channel geometry; A – approximation of inner channel area, B – Approximation of banks and bars; described by equation 3.7.1, C – Approximation of floodplains area, described by equation 3.7.2

The first section $(A; bc*v)$ represents the inner channel is assumed to be flooded immediately and completely.

The second section (B) represents the bars and the banks with a steep incline. In section B the growth of the flooded area is simulated by equation 3.7.1 (see also Figure 3.7.2)

$$bv_1 = bc * v * \left(1 + H^x\right)$$ **equation 3.7.1**

with bv_1 variable channel for section B

H water depth

bc maximum channel width

x constant, determines the inclination of bars- and banks-function (bv_1)

v percentage of inner channel of maximum width

The third section (C) represents the floodplain. For this section equation 3.7.2 describes the additional width (see also Figure 3.7.2).

$$bv_2 = \sqrt[d]{\left(\frac{H - f_a}{f_b}\right)}$$ **equation 3.7.2**

with bv_2 variable water width for section C

d constant, determines the inclination of the floodplain-function (bv_2)

f_a; f_b functions to fulfill the criterion of continuity as shown in equation 3.7.1 and equation 3.7.2

Hf water depth where maximum segment width is over-flooded

y relative fraction of bars and banks of total inner channel width

$$f_a = Hf - f_b * bc^d$$ **equation 3.7.3**

$$f_b = \frac{Hf - \sqrt[x]{y}}{bc^d * \left(1 - \left((1 + y) * v\right)^d\right)}$$ **equation 3.7.4**

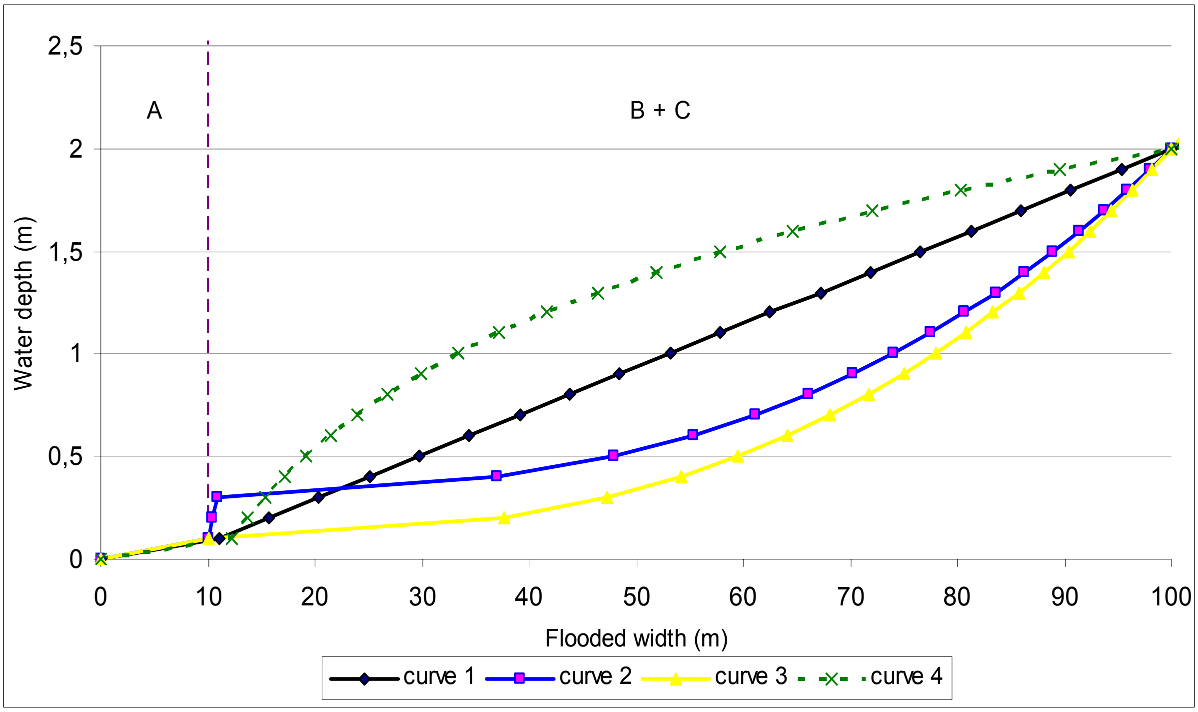

Figure 3.7.2 Approximated cross sectional geometry for v=0.1 bc=100 m and Hf=2m; A – Approximation of inner channel area, immediately flooded; B+C – Approximation of banks and bars, described by equation 3.7.1 plus approximation of over-bank area; described by equation 3.7.2. Curve one: x =1, d =1, y =0.1; curve two: x =2, d =3, y =0.1; curve three: x =2, d =3, y =0.01; curve four: x =0.01, d=0.01, y = 0.1

Figure 3.7.2 shows different cross sectional approximations for a channel segment. In this example the water depth, when reaching the maximum channel width of 100 m, is two meter. Curve one shows a linear approximation (d = 1, x = 1) and therefore it is equivalent to the formerly linear approximation of the ZIN-model. Curve two (d = 2, x = 3) shows a more realistic cross section as the slope for the channel bank is steeper and the floodplain smoother. By varying d and x it is possible to change the slopes of these two sections. Curve four shows an example where the chosen values for d and x are smaller than one (x =0.01, d = 0.01). In this case, the slopes are reversed and the bars and banks have a concave whereas the floodplain has a convex shape. Curve three shows an example similar to curve two but the percentage of bars and banks of inner channel (y) is reduced from 10 % to 1 %. Obviously, for y =1 % (10cm) bv_1 has almost no influence on the cross sectional geometry.

3.8 Improvements of the routing scheme

The output of the ZIN-model sometimes shows a sharp decline to a discharge value of zero. Furthermore, the simulation of the 1979 event in the Nahal Zin catchment showed a preceding flood wave, which build up ever more from node to node. These two unintended features are caused by the way the Muskingum Cunge routing procedure calculates the discharge. For this, it uses the discharge of the last node at the last time step, the discharge of the last node at the current time step and the last discharge of the actual node at the current time step. These three values are weighted with different factors (positive and negative) and then added up to yield the current discharge (for a detailed description see Lange 1999: 'A non-calibrated rainfall-runoff model fore large arid catchments, Nahal Zin, Israel'). One problem consist in that when one of the several products of weighting parameter and corresponding discharge is small compared to the others, the balancing effect vanishes. Therefore, the computed discharge can be negative (i.e. it is set to zero) when the positive values are too small or the computed discharge builds up unnaturally when the negative values are too small. These anomalies in the model do not always occur. This seems to happen mostly with either steep channel gradients or abrupt hydrograph declines (as input values) indicating that the one-dimensional description of the flow processes is insufficient for those cases.

To avoid these situations the ZIN-model is modified in such a way that when such a situation occurs, meaning when one of these products falls below a certain threshold value (in this study: one m³/s), the discharge is calculated with the average of the three above mentioned discharge values divided without considering the weighting factors. Figure 3.8.1 shows an example where after the first peak the original simulation (dashed red curve) drops to zero. The modified model catches this fall at a value of about 10 m³/s.

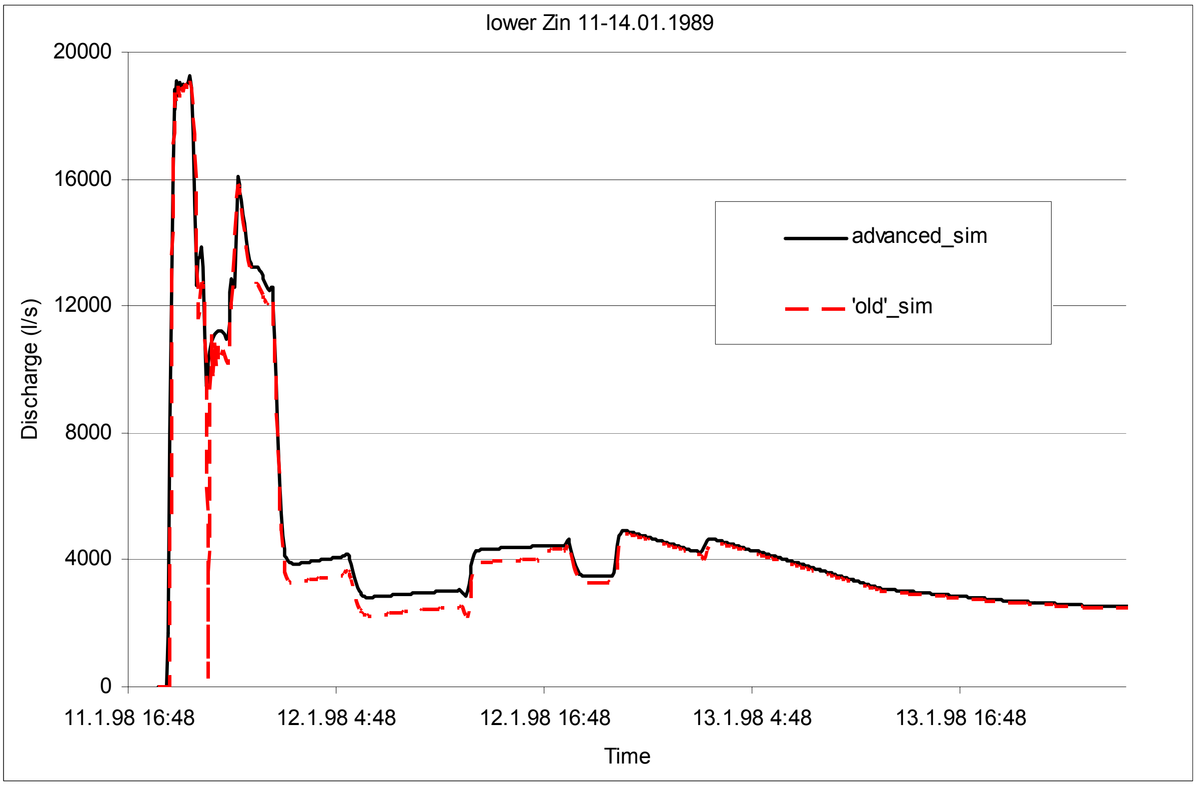

Figure 3.8.1 Comparison of a simulation with the improved (black curve) and the original (dashed red) routing scheme

Chapter 3.7 addressed the problem of an oscillating hydrograph. Despite a new cross sectional geometry, this problem still can occur. A simple way to avoid or to reduce these oscillations is to compute the discharge as the average between the last and the current discharge. The value that is calculated in this way belongs to a time point that is half of the time step earlier.

3.9 Conclusion

The ZIN-model (Lange, 1999) is a distributed non-calibrated rainfall-runoff model for large arid catchments. The routing procedure is realised by applying the non linear Muskingum Cunge method, whereas a constant infiltration rate is assumed and the flooded width is approximated with a linear interpolation depending on the water depth.

Different modifications to the ZIN-model (Lange, 1999) are accomplished to improve the simulation of the transmission losses and associated processes. Thought has been given to the effects of varying surface water depth, antecedent moisture content, the processes of scour and fill on the infiltration. Moreover, a function has been developed to describe the cross sectional geometry and it has been attempted to improve the routing scheme. The simulation of the process of scour and fill is realized by using either a critical flow velocity criterion or a critical shear stress criterion. Infiltration is separated, depending on to the location where it takes place, into a physically based approach and an empirical approach. The physically based approach, which models infiltration into the inner channel, is implemented by using the Green-Ampt equation. The empirical approach, which simulates infiltration into bars, banks and floodplains, is implemented by a reversed single linear storage model. Both approaches to simulating infiltration are influenced by an antecedent moisture index, which is calculated with respect to the number of days since the last event. The developed function that describes the cross sectional geometry is variable with regard to the slopes of the riverbanks and the floodplains. So depending on the ‘real’ shape of the cross section it is possible to adjust the ‘virtual’ shape. In addition, the routing scheme is improved by an add-on, which prevents the calculated discharges from plunging unintendly and abruptly down to zero or from artifactual build-up.

The aim of these modifications was to integrate the temporal and spatial variability of transmission losses into the ZIN-Model. For that, the various complex processes are described in more or less complex ways. But since the ZIN-model was developed for large catchments the difficulties in obtaining the several parameters to accomplish the modifications are evident. The next chapter describes the catchments where the modified model versions were tested to give the reader a rough idea about the catchment characteristics. The chapter following the next one deals explicitly with the different parameters.

IV Sites of application

4.1 Nahal Zin, Israel

4.1.1 Geography and climate

According to Evenari et al. (1971), the Israeli desert Negev occupies about 12,500 km² and forms an isosceles triangle with its base facing north, running from a point near Gaza on the Mediterranean coasts to the shores of the Dead Sea. Its southern reach ends at the northern end of the Gulf of Aqaba. The Negev can be divided into four major regions, the northern, the central and the southern Negev plus the Arava.

The 1.400 km² watershed of Nahal Zin with a main channel length of about 120 km is located in the central Negev. According to Köppen's classification, two climatic regions can be assigned to the Nahal Zin catchment. One is a desert climate with the dry season in the summer and a mean annual temperature under 18 °C (BWks) in the upper, southwestern part of the catchment (region around Advat) and the other is a desert climate with the dry season in the summer and a mean annual temperature over 18 °C (BWhs) (see Figure 4.1.1). Figure 4.1.1 shows the average annual rainfall that varies between 100 mm (headwaters, near Mitzpe Ramon) and 50 mm (Dead Sea) from the southwest to the northeast.

4.1.2 River description

In this study, two different kinds of routing dimensions in the Nahal Zin catchment are investigated. On the one hand, a runoff event is simulated, where runoff data are available from Lange (1999). The flow distance for the simulation averages approximately 76 km. On the other hand, several runoff events in the lower part of the catchment are simulated (lower Zin). Here discharge data from a reach with approximately 5.5 km are available from Schwartz (2001). Therefore, the first section of the following river description focuses on the entire catchment and the second section will give details on the small reach (lower Zin).

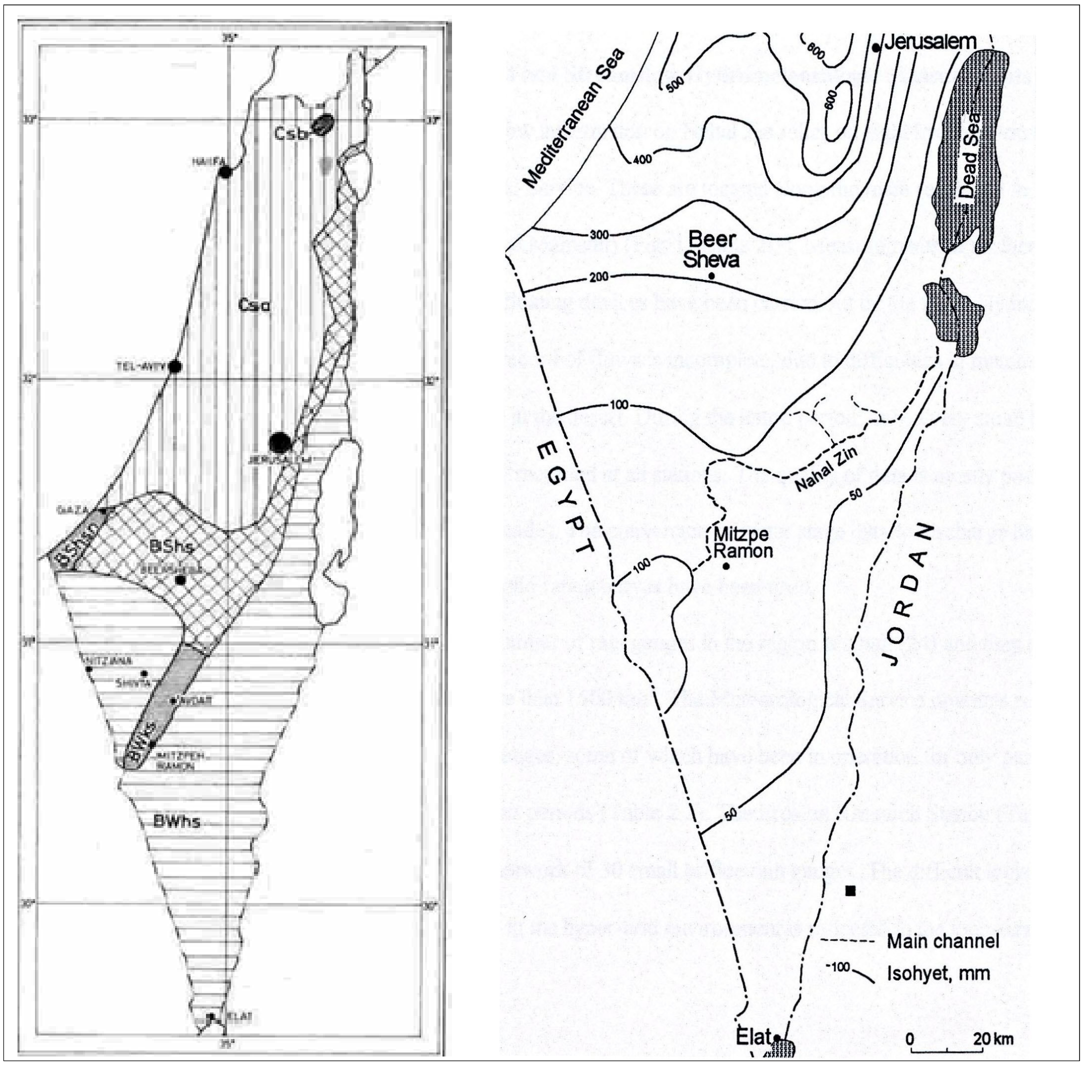

Figure 4.1.1 Left: Climatic regions of Israel according to Köppen's classification: B-dry climate; C-warm temperature climate; BS-steppe climate; BW-desert climate; a-mean temperature of warmest month over 22°C; b-mean temperature of warmest month under 22°C with means of at least four months over 10°C; h-dry ad hot, mean annual temperature over 18°C; k-dry and cold, mean annual temperature under 18°C, mean annual temperature of the warmest month over 18°C; n-high humidity, mean summer temperature between 24 and 28°C; s-dry season in summer (modified from Evenari, 1971); Right: Mean annual rainfall in the Negev (source: Schwartz, 2001)

4.1.2.1 Entire catchment

According to Lange (1999) the Nahal Zin catchment can be divided into discrete morphological units in particular the Advat Plateau, the Zin valley, the northern Negev Fold Belt, the Rotem plain, Rift valley, Makhtesh Katan and Makhtesh Gadol. The following description mainly owes to the explanations given in Lange (1999) and Schwartz (2001).

The upper part of the catchment, the Avdat Plateau in the south-west reaches altitudes up to 950 m.s.l.. This area is situated in eocenic resistant marine limestone. The rocky slopes consists of hard carbonatic rocks alternating with small pockets of Hamada soils and the valleys are filled with loessial silty sediments with thickness up to 40 cm (Lange, 1999). According to Schwartz (2001) the channel forms a canyon type sequence of steps and waterfalls.

The Zin valley with is a wide entrenched canyon that is situated geologically in the upper cretaceous with chalky-marly sediments and with partial flint cover. The soils, which were able to developed, are shallow calcareous desert litho-sols on marl and clay and reg soils when a flint cover is presence.

The northern Negev Fold Belt in the Nahal Zin catchment consists of three northeast-southwest trending anticlines (Hatira, Hazera and Ramon). The geological sequence of the anticlines is the upper cretaceous with resistant marine limestone. According to Lange (1999) gravely reg soils were able to develop along the main channels on the alluvial terraces whereas on the steep slopes no soils are present. The geological sequence of the Synclines is also the upper cretaceous but with chalky-marly sediments and partly with a flint cover like in the Zin Valley. Consequently, the soils correspond to the soils of the Zin valley that are shallow calcareous desert litho-sols on marl and clay and reg soils when a flint cover is present. According to Schwartz (2001) some 25 m of Pleistocene and Holocene alluvial sediments were deposited in the 25 km channel reach of the Zin syncline.

The channel reach between the gauging stations (see Figure 4.1.2) Mapal and Massos, measure a length of approximately 42 km. Here the channel slope averages almost 0.01 m/m and the mean channel width is some 27 m. The almost 34 km long reach between Massos and Aqrabim is partly characterized by a thick alluvium and a broadened channel width due to a major tributary inflow (Nahal Hava). In this section, the mean channel width reaches circa 245 m and the channel slope averages circa 0.0084 m/m.

4.1.2.2 Lower Zin

The Arava Rift Valley forms the last morphological unit before the Nahal Zin reaches its alluvial fan at the southern end of the Dead Sea. Here the channel is incised into Pleistocene marly sediments and the development of shallow calcareous desert lithosols was possible. Over the last 15 km the channel width reaches up to 100 m with a shallow alluvium (0 – 2 m) and it is incised into the impermeable lacustrine sediments. The channel reach between the two gauging stations Mpl and Brg (see Figure 4.1.2) in the lower part of the catchment measures approximately 5.5 km. The gauging station Mpl is located at the lower waterfall. From here, the channel is incised into Lisan marl. The average channel width is about 90 m with an average depth of the alluvium of about four meters (Schwartz, 2001).

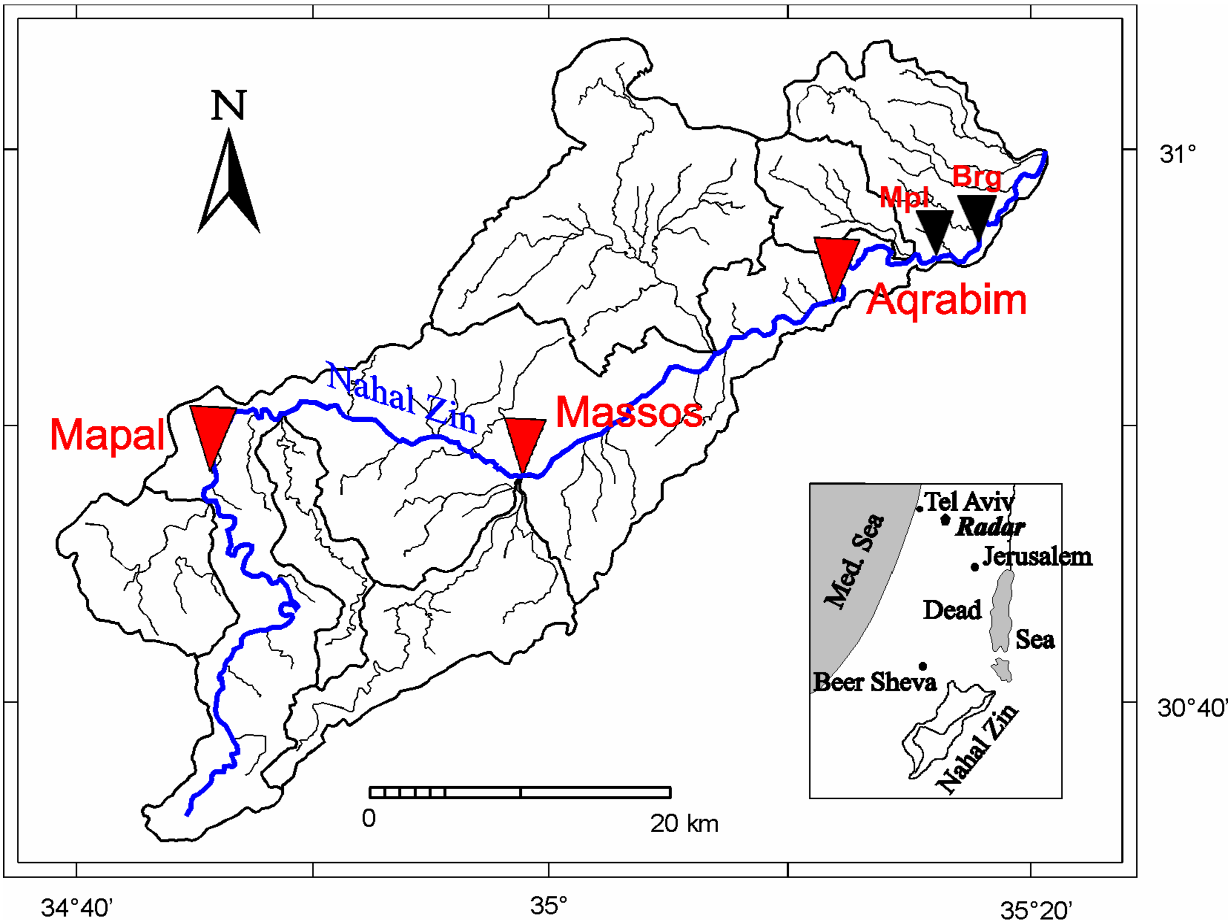

Figure 4.1.2 Catchment Nahal zin, Israel (modified from: http://www.hydrology.uni-freiburg.de/forsch/zinmod/zinmod.htm)

4.2 Wadi Kuiseb, Namibia

4.2.1 Geography and climate

Namibia is located on the southwestern Atlantic coast of Africa. The mean annual rainfall of 284 mm ranges from less than 50 mm/year in the western region along the coastline to 700 mm/year in the north-eastern Caprivi (see Figure 4.2.1). The coastal strip is occupied by the Namib Desert. The Namib Desert reaches circa 150 km inland to the base of the Great Western Escarpment (see Figure 4.2.2). The climatic region according to Köppen's classification is BWk; dry and cold desert climate with a mean annual temperature under 18 °C and a mean annual temperature of the warmest month over 18 °C.

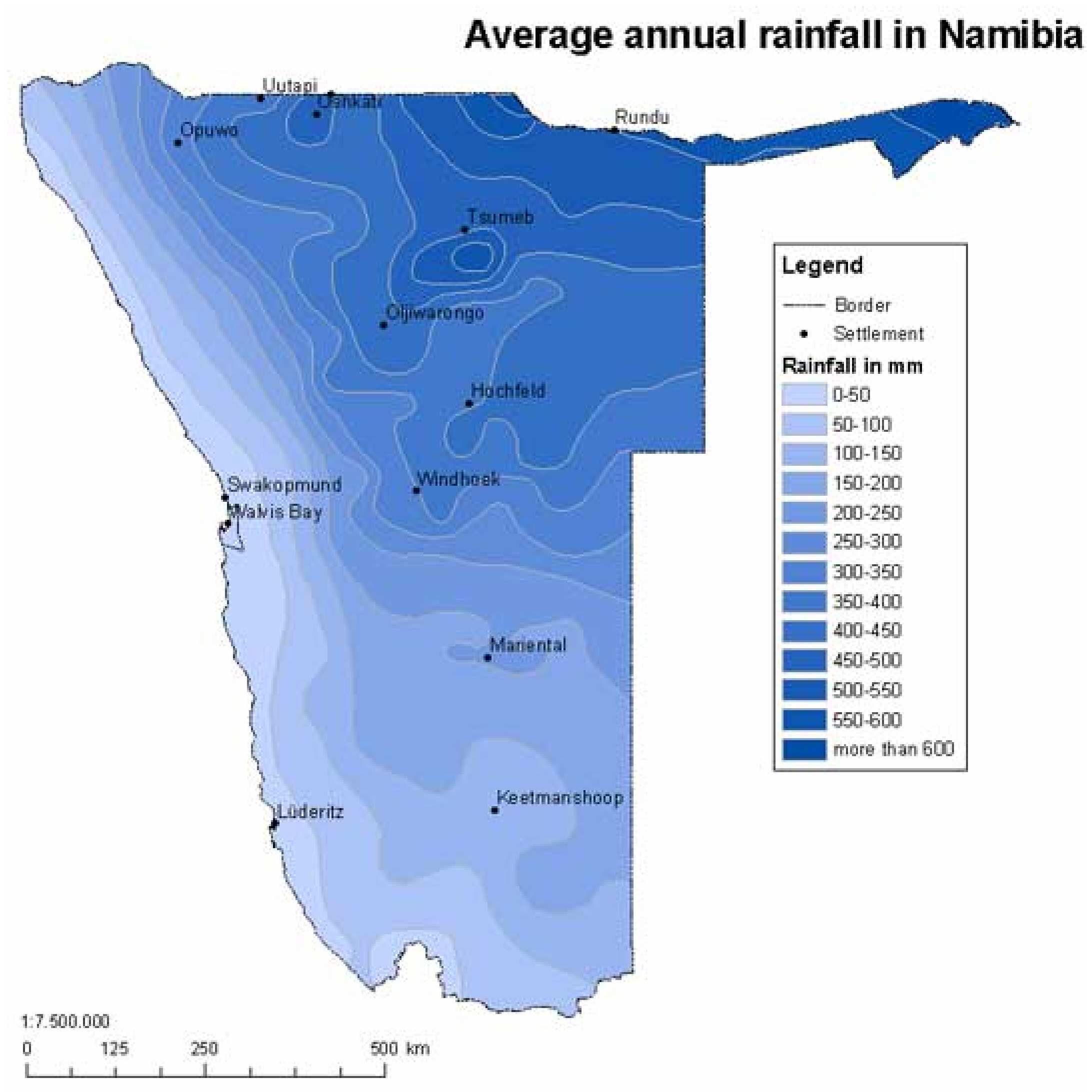

Figure 4.2.1 Map of Namibia with average annual rainfall (modified from: www.uni-koeln.de/inter-fak/sfb389/e/e1/download/atlas_namibia/e1_download_climate_e.htm#annual_rainfall)

According to Jacobson (1997) the Wadi Kuiseb, with a length of about 560 km and a catchment size of abut 15.000 km², originates on the interior Kohmashochland plateau of central Namibia at an elevation of roughly 2000 m. The Kuiseb runs east to west crossing the Namib Desert along the northern border of the Namib Sand Sea and flows into the Atlantic near the city Walvis Bay. The mean annual rainfall ranges from the headwaters to the coast from about 350 mm to almost zero mm.

4.2.2 River description

Jacobson (1997) divided the Kuiseb catchment into two main parts, the upper and the lower Kuiseb.

According to Jacobson (1997) the Kuiseb has formed a shallow, sinuous valley westwards of the headwaters. Here the dominant rock types are schists and quartzites. After crossing the escarpment that divides the inland plateau from the coastal plains the river has burrowed a deep canyon. The canyon has a mean width of about 20 m with maximums of circa 100 m and depths of over 200 m (Jacobson, 1997). Due to a steep slope that averages 0.0034 m/m (Jacobson, 1997) in the upper Kuiseb the river often flows over bedrock with no alluvial deposits.

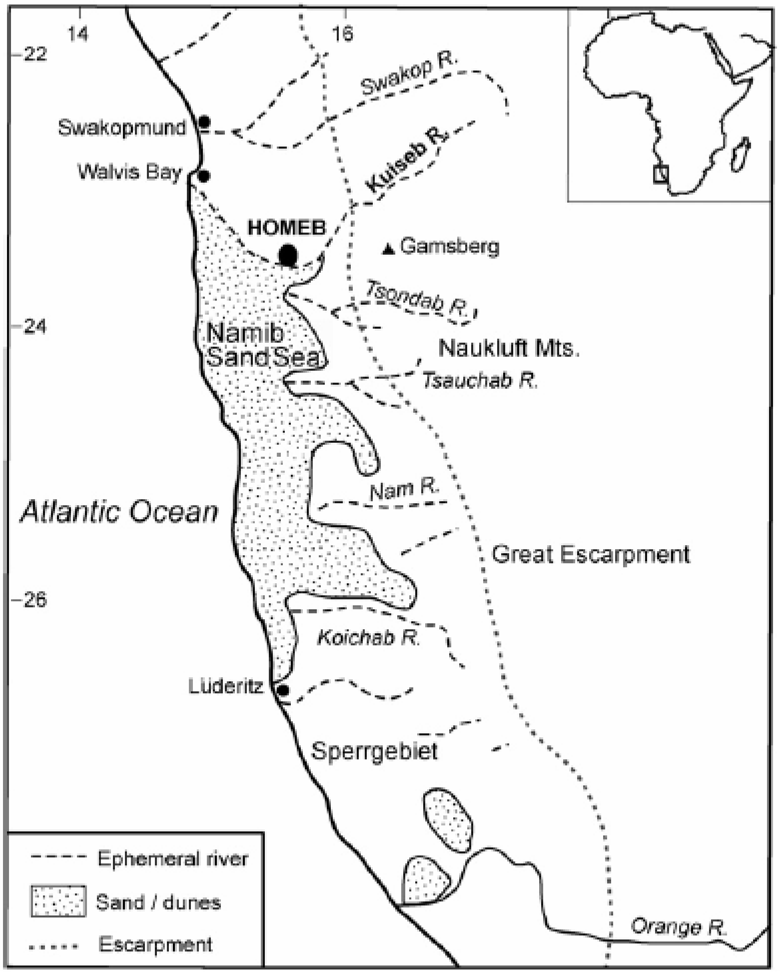

Figure 4.2.2 South-west part of Namibia with ephemeral rivers (source: Bourke, 2003)

Approximately 80 km upstream of the desert research station Gobabeb, the canyon widens and the river flows into the second part of the Kuiseb catchment. The widening of the channel width goes along with a decrease in the mean slope from 0.0034 m/m to 0.0019 m/m (Jacobson, 1997) and as a result of the decreasing valley limitation, the channel width expands onto wide floodplains. This continues downstream over the 92 km reach to the Gobabeb gauging station, where according to Ward (1987) the Homeb Silt Formation is located. According to Bourke et al. (2003) the Homeb silts are variously described as lacustrine sediments emplaced behind an aeolian dune dam, valley fill and slack water deposits. The lower Kuiseb forms a frontier between the Damara sequence in the north and the Namib Sand Sea in the south.

Below the Gobabeb weir the Kuiseb occupies a wide, shallow valley and the width of the floodplain can exceed one km. 20 km from the coast the valley becomes indistinct. Here, low cresentic dunes cross the river. Over the last 80 km the slope increases again to a mean value of about 0.00466 m/m (Jacobson, 1997).

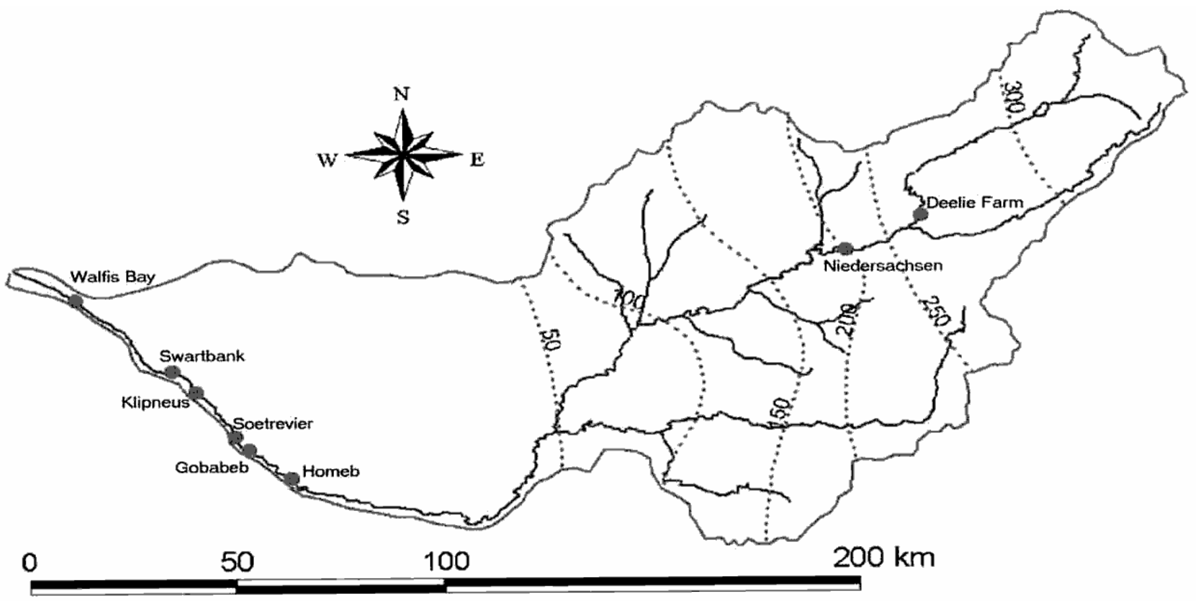

Figure 4.2.3 The Kuiseb catchment (modified from Schmitz, 2004)

4.3 Conclusion

Discharge data are available for two large catchments in arid regions. One is the 1,400 km² watershed of Nahal Zin in the Israeli desert Negev. The river has an approximate length of 120 km and it draws through resistant limestone and chalky-marly sediments. The other one is the watershed of the Kuiseb River in Namibia, mainly located within the Namib Desert. The catchment of the Kuiseb River exceeds the catchment of the Nahal Zin in size. It measures approximately 15.000 km² and has a channel length of about 560 km drawing through schist, quartzite and lacustrine sediments. Both catchments are located in hyper-dry environments with mean annual rainfalls varying from about 100 mm to 50 mm (Zin catchment) and 350 mm to almost zero (Kuiseb catchment) respectively.

The important river segments with regard to transmission losses are those, where the river broadens or where the alluvium is deep. The Zin watershed shows these characteristics downstream of the gauging station Massos (channel width ~250 m) and in the lower part of the catchment (lower Zin) with an average width of 90 m. The Kuiseb River starts to broaden in the above-mentioned second part (lower Kuiseb) where channel widths can measure up to one kilometre.

V Parameter

5.1 Hydraulic conductivity

The hydraulic conductivity k quantifies the capacity of the soil to transmit fluids. It depends on the properties of the soil and the fluid as listed in Table 5.1.1. Furthermore, k is not constant but a non-linear function of soil water content. k decreases with increasing water content resulting in the saturated hydraulic conductivity k_f when the soil is fully saturated. The connection between k and the moisture content is a result that k is a function of the matrix potential which varies with the moisture content (e.g. Freyberg 1981; Rawls et al. 1983, Ward et al. 2000).

Table 5.1.1 Properties of the soil and the fluid influencing k (according to Rawls, 1992)

Soil	Fluid
Total porosity	Viscosity
Pore size distribution	Density
Moisture content	Salinity
Pore continuity	Temperature
Macro pores/cracks	

Therefore, a homogeneous soil k is separable into a constant saturated hydraulic conductivity k_f and a variable unsaturated hydraulic conductivity k.

The Green-Ampt model assumes a sharply defined wetting front that separates the wetted and un-wetted zone in the soil, with constant soil water content in the wetted zone and therefore a constant hydraulic conductivity between the surface and the discontinuity. The hydraulic conductivity k above the wetting front controls the rate of infiltration (Reed et al. 1998; Rawls et al. 1992).

According to Freyberg (1981) k is expected to be somewhat less than the saturated hydraulic conductivity k_f and in fact k may not be constant for a homogenous soil, because of the changing volume of entrapped air in the soil. Therefore, he proposed to utilize the hydraulic conductivity at residual air saturation k_a instead of k_f for the Green-Ampt model. Bouwer (1966) in Freyberg et al. (1980) and Rawls et al. (1983) suggests values for k as half of k_f. Morel-Seytoux et al. (1985) introduced a correction factor for the Green-Ampt equation to take in account that the wetted zone builds up a viscous resistance to airflow, which reduces the infiltration rate. Depending on the soil type, this correction factor varies between 1.1 and 1.7.

The above-mentioned hypotheses are idealized assumptions for a homogeneous medium and do not consider aspects such as the spatial heterogeneity of the soil or macro-pores.

As the ZIN-model is constructed for macro scale catchments and infiltration is computed for each channel segment depending on the channel types, the hydraulic conductivity is described using a uniform value for each different channel type. Obviously, the spatial variability is not accounted for in detail and the chosen values for k represent average values for the vertical and horizontal extensions of the different channel types.

5.1.1 Values from the literature

Rawls et al. (1983)gives values for the saturated hydraulic conductivity k_f between 0.6 mm/h for clay to 235.6 mm/h for sand. Accordingly, the hydraulic conductivities for the Green-Ampt equation (half of the value of the saturated values) are 0.3 mm/h for clay and 117.8 mm/h for sand. Lane (1985) related bed material characteristics to k and divided them into five groups as shown in to Table 5.1.2.

Table 5.1.2 Relationship between bed material characteristics and hydraulic conductivity k (modified from Lane 1985)

Bed material group	Bed material characteristics	Hydraulic conductivity k (mm/h)
1 Very high loss rate	Very clean gravel and large sand	127
2 High loss rate	Clean sand and gravel, field conditions	50.8-127
3 Moderately high loss rate	Sand and gravel mixture with low silt-clay content	25.4-76.2
4 Moderately loss rate	Sand and gravel mixture with high silt-clay content	6.35-2.54
5 Insignificant to low loss rate	Consolidated bed material; high silt-clay content	0.0254-0.254

Considering macro pores, Dong (2003) calculated a value of 400 mm/h with equation 2.4.9 (k is circa 18 mm/h without macro pores) for a silty loam. Here the problem of scaling up point measurements becomes distinct.

Külls et al. (1985) examined the infiltration characteristics in the lower Nahal Zin with two infiltration experiments. One is executed on a silty bar resulting in a k value of 110 mm/h, the other one was carried out in the inner channel resulting in a k value of about 420 mm/h. For the same reach, Schwartz (2001) calculated values for k for several recorded runoff events by equating the total volume of losses with the product of the effective hydraulic conductivity multiplied by the duration of flow. When calculating k this way, the values ranged between 0.014 and 300 mm/h.

5.1.2 Calculated values

Data of the vertical advance of the wetting front are available from both catchments. Schwartz (2001) measured the arrival times of the wetting front with TDR sensors. He measured them at different depths in the alluvium near the gauging station 'Brg', lower Nahal Zin. Schmitz (2004) calculated two vertical advance velocities for two runoff events near the gauging station Gobabeb, Wadi Kuiseb.

It is possible to calculate the hydraulic conductivity from to the Green-Amt equation. Substituting f(t) with dF/dt and F = Z(t)*Δθ and rewriting equation 2.4.5 as

$$k = \frac{dZ(t)}{dt} * \Delta\theta * \left(1 + \frac{H + h_e}{Z(t)}\right)^{-1} \qquad \textbf{equation 5.1.1}$$

one can determine k.

Nahal Zin: k can be calculated in two possible ways. One is to calculate k for the vertical distances between the sensors (sensor to sensor). The other way is to calculate k for the whole depth (surface to sensor) in which the sensors were placed. It should be noted that the sensors are not placed directly below each other so the second way to calculate k should be preferred. Further, these calculations do not consider channel surface changes due to erosion or deposition. When a change occurs, the vertical advance velocity is calculated with wrong sensor depths and therefore the values for k are over- (erosion) or under- (deposition) estimated. Schwartz (2001) measured channel accumulations up to almost one meter and channel degradation of almost half a meter in the period between Dec. 4, 1996 and Feb. 21, 1997. During this period, two runoff events took place. A relatively small one (peak discharge 1.5 m^3/s) and the January event from which the moisture data are derived (peak discharge 84 m^3/s).

Table 5.1.3 shows the measured data from the January runoff event 1997 (Schwartz, 2001), the resulting values for vertical advance velocities (dZ/dt) and k. The calculated values for the distances between the sensors are listed in column 'a' (italics), the calculated values for the distance from surface to sensor depth 'b'. When k is calculated with equation 5.1.1 different values for Δθ, and h_e have to be assumed. Here Δθ is chosen as 0.3, h_e as 0.2 m. A surface water depth (H) of 0.7 m is used as the computed water depth of the model for these time steps lies between 0.66 m and 0.79 m.

Table 5.1.3 Calculation of k according to equation 5.1.1 with H=0.7

Z (mm) (from Schwartz, 2001)	t (h) (from Schwartz, 2001)	dZ /dt (mm/h)		k according to equation 5.1.1 (mm/h)	
		a	b	a	b
400	0.083	*4800*	4800	*444.856*	444.856
750	0.167	*4200*	4500	*350.000*	612.412
1050	0.583	*720*	1800	*54.087*	290.935
1220	0.833	*680*	1464	*123.208*	252.848

b – Mean average of k: 400.26 mm/h (*a – weighted 264.08 mm/h*)

Table 5.1.3 shows four different values for k (calculation according to method b). k should be constant according to the theoretical Green-Ampt infiltration model. The mean average value is approximately 400 mm/h; still the value at a lowest depth (k ~ 250 mm/h) is used for the simulations in this part of the Nahal Zin catchment. This point will be discussed in chapter VII ‘Discussion and outlook’.

Wadi Kuiseb: According to Schmitz (2004) the vertical advance velocities are 0.3 m/h (300 mm/h) for event one and 0.15 m/h (150 mm/h) for event two. When using equation 5.1.1 again with $\Delta\theta$ as 0.3, h_e as 0.2 m and H as 0.1 m and 0.6 m, one gets:

H: 0.1 → event one: k = 69.23 mm/h, event two: k = 34.62 mm/h, average k = 51.92 mm/h

H: 0.6 → event one k: 50 mm/h, event two: k = 25 mm/h, average k = 37.5 mm/h

5.2 Porosity

The values chosen for porosity ‘n’ together with the depth of the alluvium determine the maximum volume that can be absorbed by the alluvium. With regard to influence the infiltration rates n does not have as much weight as the other parameters. The final infiltration rate is not influenced by the porosity but by the initial infiltration rates. Low values for n will reduce the initial infiltration rates whereas large values will increase the initial infiltration rates. Together with the antecedent moisture index Antec, n is used to calculate the initial moisture content.

5.2.1 Values

According to Ward et al. (2000), the porosity for soils varies between 0.30 and 0.65. The effective porosity, the porosity that plays an active role in the storage and movement of water, varies between 38 % for clay and 48 % for silt loam (e.g. Rawls et al., 1993). When using the Green-Ampt equation Rawls et al. (1983) suggested values between 39.8 % (33.2 % - 46.4 %) for sandy clay loam, 43.7 % (37.4 % - 50 %) for sand and 50.1 % (42 % - 58.2 %) for silt loam.

One can see that the porosity varies within a range of about 15 % for different grain sizes. This range can be extended on closer examination of the heterogeneous multi layered soils in ephemeral streams. Soil profiles of the two catchments, where the modified model is applied, are scarce. The existing ones just represent single points and they are not representative for larger section or even the whole catchment.

Nevertheless, Schwartz (2001) analyzed the alluvium properties in the lower Nahal Zin and divided them into five units, which are described briefly below:

- Granules, coarse sand and small pebbles; 93 % matrix. The coarse sand alternates with the granules.
- Cobbles; 70 % cobble and 30 % matrix. The matrix is composed of coarse sand and granules.
- Small pebbles, clast supported.
- Cobbles and pebbles, clast supported.
- Very coarse sand layers and lenses.

Schmitz (2004) investigated several soil profiles in the active channel and on over-bank areas near the research station Gobabeb. The inner channel is described as heterogeneous with three main units:

- purely sand (depth of profile: 1.75 m)
- layers of fine material alternating with layers of sand
- layers of coarse material alternating with layers of sand and fine material

Schmitz (2004) also described a silty surface cover that varies in depth from one millimeter to several centimeters.

5.3 Effective hydraulic suction head

Here in this thesis the effective hydraulic suction head h_e is assumed to be constant over time. In reality, this is not completely correct because h_e is a function of time, surface water depth, moisture content and soil type. Freyberg et al. (1980) examined h_e for different soils and showed that h_e decreases monotonously over time for a constant water depth. He pointed out that the practicality of the Green-Ampt models lies in its ability to reproduce observed data reasonably well when a constant value of h_e is used. He pointed out, though, the dilemma of choosing a single representative value for h_e.

The fractional error strongly depends on the water depth H(t) because a large H(t) dominates the numerator in the Green-Ampt equation and h_e becomes less important. Nonetheless, the practicability of the Green-Ampt model depends upon the appropriate selection of a constant value of h_e.

5.3.1 Values from the literature

The values for the effective suction head vary over a wide range according to different authors. In his study, Freyberg et al. (1980) estimated values between 150 mm and 300 mm for Yolo light clay and values between 280 mm and 460 mm for Monterey sand. Rawls et al. (1983), on the other side suggested 49.5 mm (9.7 mm - 253.6 mm) for sand and 316.3 mm (63.9 mm – 1565 mm) for clay.

Phillips (1954) related the permeability to capillary potential as shown in equation 5.3.1

$$h_e[\mathrm{mm}] = 250 * \log(k[\mathrm{mm/s}]) + 100 \qquad \textbf{equation 5.3.1}$$

Applying equation 5.3.1 with k = 1 mm/h ($2.78*10^{-4}$ mm/s) and k = 150 mm/h (0.042 mm/s) h_e yields circa 989 mm and 444 mm (the sign is not considered).

For the sake of completeness, another method to estimate h_e according to Rawls et al. (1983) is presented below, but it is not used in this study to calculate values for the effective suction head.

$$h_e = \frac{(2+3\lambda) * h_b}{(1+3\lambda) * 2} \qquad \textbf{equation 5.3.2}$$

λ – Brooks Corey pore size distribution index

h_b - Brooks-Corey bubbling pressure head

5.4 Geometric channel properties

The ZIN-model requires the parameter slope, segment length, segment width, percentage of inner channel and the Manning-value for routing and the depth of the alluvium to calculate the transmission losses. These values are determined for each segment. The program reads in the channel length, width and slope for each segment. The other parameter (percentage of inner channel, the Manning value and the depth of the alluvium) are averaged and assigned to the different channel types.

For the simulations in this work it was only necessary to determine the channel properties for the lower part of the Nahal Zin catchment, where runoff data from the work of Schwartz (2001) were available. The properties for the simulations of the entire Nahal Zin catchment and the Kuiseb River are adopted from Lange (1999 and 2005).

For the lower part of the Nahal Zin catchment (see Figure 5.4.1) the differentiation into the different channel types according to Lange (1999) was not feasible. Here the surface characteristics are too similar. Therefore, a differentiation into three channel types according to percentage of inner channel width was chosen. The description of the determinations of the different parameters follows in the next sections and the different values are listed in the Appendix in Tab. IX.1.

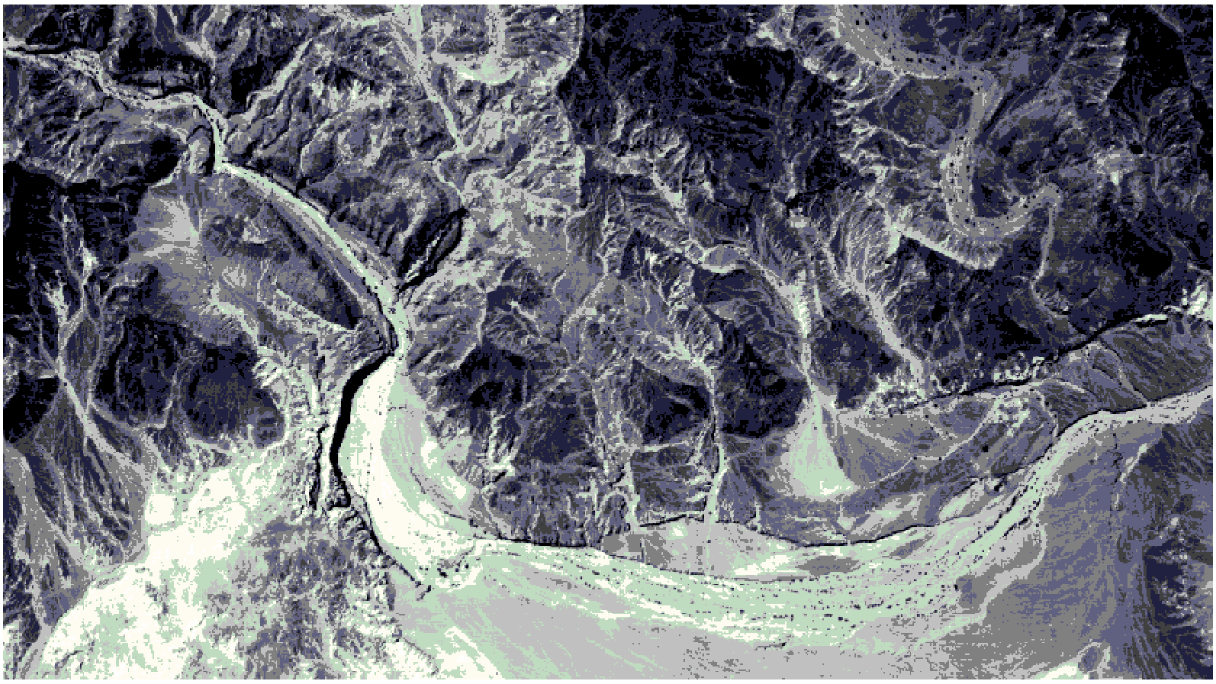

Figure 5.4.1 Aerial photo of the lower Nahal Zin (from Schwartz 2001)

5.4.1 Channel length, width and slope

The channel lengths and widths are determined by analyzing aerial photos with GIS (see Figure 5.4.1) in particular Arc Info. The width is calculated as a mean width of the total area that can be flooded (inner channel plus over-bank area). The slopes are determined by dividing the difference in height of the nodes (they were read out from a topographic map (1:50.000)) with the segment length.

5.4.2 Percentage inner channel, depth of alluvium

To obtain the percentage of inner channel of each segment, for each segment the area of the inner channel is divided by the total area that can be flooded. Then these values were assigned to the channel types and a mean percentage of inner channel according to the different types is calculated.

The depth of the alluvium is chosen according to the values provided by Schwartz (2001). In this reach, the values vary between a minimum of zero meters and a maximum of four meters.

5.5 Conclusion

To calculate the transmission losses various parameter like the hydraulic conductivity, the effective suction head, the porosity or the geometric channel properties need to be assigned. Different methods of obtaining the various parameters are used. The geometric channel properties are determined by analysing aerial photos and by using existing data from Lange (1999) and Schwartz (2001). For the effective suction head and the porosity, the values are taken from different literature sources (e.g. Freyberg et al. 1980; Rawls et al. 1993; Ward et al. 2000) whereas these values vary in certain ranges. Also, for the hydraulic conductivity numerous literature values are available for different soil types (e.g. Rawls et al. 1993; Lane 1985; Dong 2003). In addition, data from infiltration tests in the lower Zin (Külls et al., 1985) and soil moisture measurements from both catchments are available (Schwartz 2001, Schmitz 2004), which allow calculations for k. These calculated values include uncertainties but still they indicate a rough dimension for k. The calculated values in the lower Zin exceed the calculated values in the Kuiseb by a multiple. At the outset, it is visible that the values for the hydraulic conductivity, the effective suction head and the porosity are not clearly defined because of the heterogeneity of the channel properties and the lack of data. So for the simulations in the next chapter the available existing data and literature values are used. As far as possible, the literature values were chosen according to the channel characteristics but these values are flawed because of the too many uncertainties.

VI Simulations

6.1 Nahal Zin – Jan 23, 1997

In the following two sections, the previously introduced methods to calculate the infiltration and to simulate the process of scour and fill will be examined and compared. To this end the lower Zin reach is chosen as it provides, due the relative short channel length (circa 5.5 km), a certain overview on the processes. According to chapter 5.4, three channel types are assigned to this reach. The different parameters for the three channel types used for the simulations are listed in Tab. IX.3 in the Appendix**.** To compare the different methods all parameters are kept constant except for the ones, which are subjects of investigation. In addition to the hydrograph, which allows visual comparison of the different methods, the model efficiency is calculated according to equation 6.1.1

$$R_{eff} = 1 - \frac{\sum_i (y_i - x_i)^2}{\sum_i (x_i - x_{me})^2} \qquad \textbf{equation 6.1.1}$$

R_{eff} model efficiency
y_i simulated values
x_i measured values
x_{me} mean measured value

6.1.1 Comparison of iteration and decomposition

Figure 6.1.1 shows a runoff event in the lower Nahal Zin catchment, Israel (Jan 23, 1997). The dashed black curve represents the measured values (discharge data from Schwartz, 2001). The green curve shows the simulation without any transmission losses. The red and the dashed blue curves show simulations including transmission losses. The red hydrograph used the Newton iteration method whereas the dashed blue hydrograph used the decomposition series to calculate initial cumulative infiltration for the Green-Ampt equation.

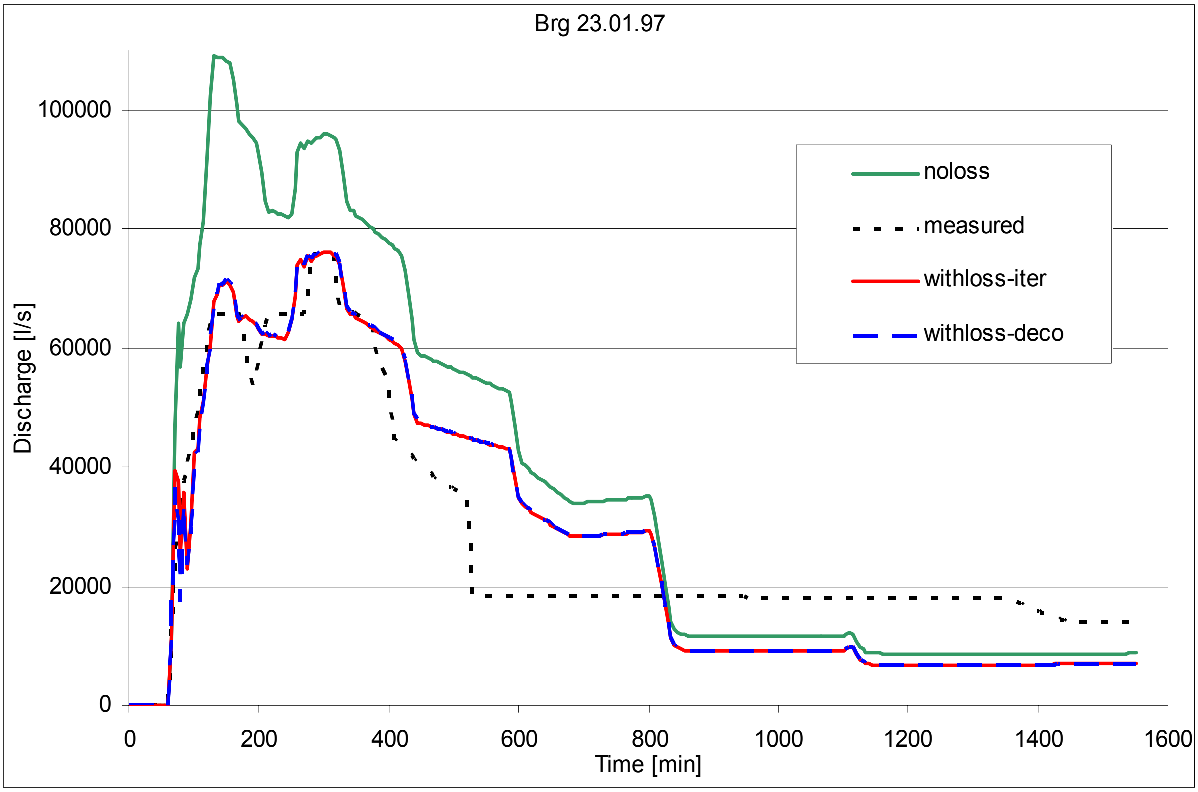

Figure 6.1.1 Comparisons of simulations without losses (green curve), with Newton iteration (red curve), decomposition series (dashed blue curve) and measured (dashed black curve) values in the lower Nahal Zin (23.01.1997)

The differences between the simulations considering transmission losses are hardly noticeable and according to equation 6.1.1, both simulations reach the same model efficiency R_{eff}, (at $R_{eff} = 0.733$). The model efficiency for the simulation without transmission losses is $R_{eff} = 0.169$.

Figure 6.1.2 shows only the simulated hydrographs with transmission losses and the difference between them (black curve). Clearly, the most obvious differences occur in the steep rise at the beginning of the runoff event where the simulation is unstable (zigzag shape). Over the rest of the course, the differences are imperceptible. The volume difference between the two simulations is approximately one percent of the total volume of each simulated flood.

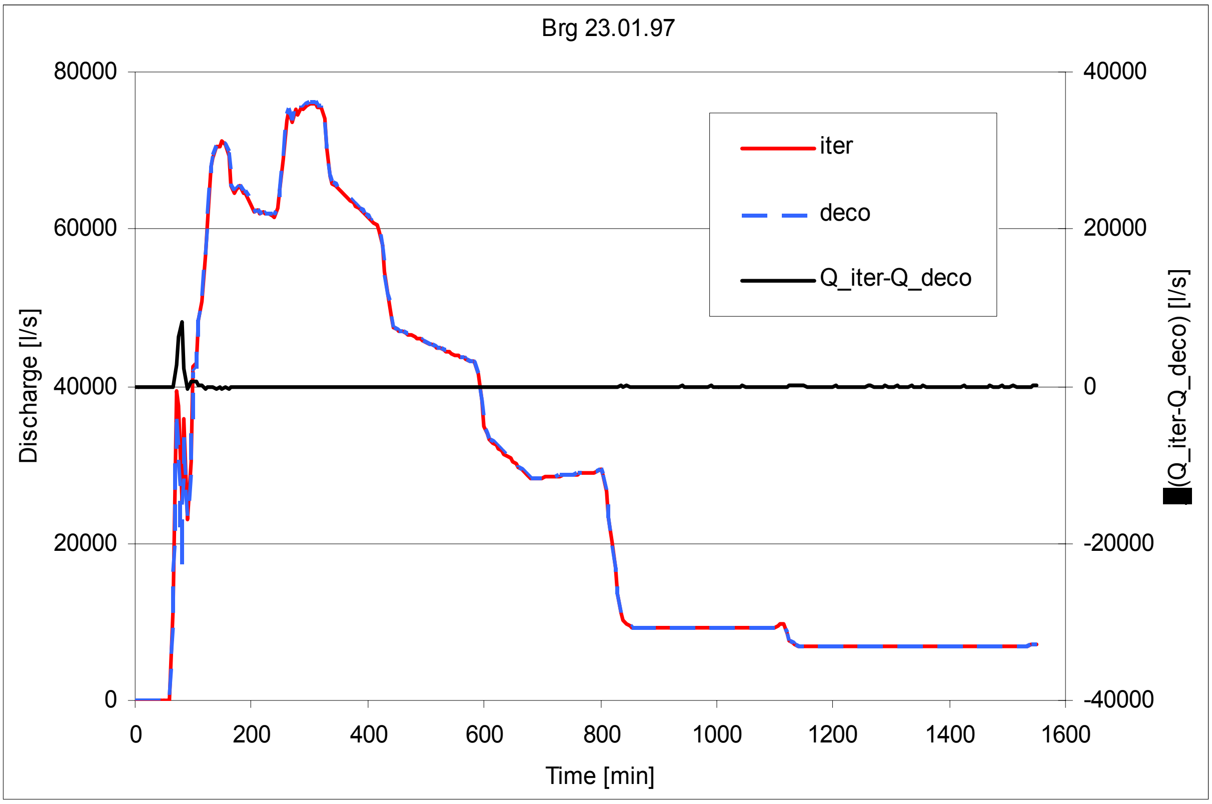

Figure 6.1.2 Comparison of Newton iteration (continious red curve) vs. decomposition series (dashed blue curve) in the lower Nahal Zin (23.01.1997). The black curve represents the difference between both methods

6.1.2 Comparison of critical shear stress and critical flow velocity

To compare the two parameters simulating the process of scour and fill, the same event as in section the above is chosen, whereas the initial infiltration is simulated with the Newton iteration method. Different values for the critical shear stress and the critical flow velocity are presented in chapter 3.5 and one quickly notices that both have a relatively wide range of possible values. For a better comparison, the factor (l) that reduces infiltration into the inner channel is set to zero.

In this section, a comparison of the two criteria with

- literature minimal values for erosion
- literature maximum values for erosion
- best fit values

follows.

1. The minimum values are chosen according to chapter 3.5.1 Critical shear stress and chapter 3.5.2 Critical flow velocity. For the three channel types the same critical values are chosen, in particular 0.05 N/m² as critical shear stress and 0.26 m/s as critical flow velocity.

Figure 6.1.3 shows the measured hydrograph (black curve), the simulated hydrograph using a critical shear stress of 0.05 N/m² (blue curve) and the simulated hydrograph using a critical flow velocity of 0.26 m/s (red curve).

The differences between the two simulated curves are obvious. In the beginning, the red hydrograph shows smaller values than the blue curve, implicating higher transmission losses or, more precisely, an earlier breaking open of the alluvial crusts. The red curve simulates the first peak more exactly but an additional third peak causes a deviation from the measured graph (shape). After approximately 255 min, the two hydrographs converge each other. The corresponding model efficiencies are: for the red hydrograph that is modeled with the shear stress criterion an R_{eff} of 0.7106 and for the blue hydrograph that is modeled with the flow velocity criterion an R_{eff} of 0.7389.

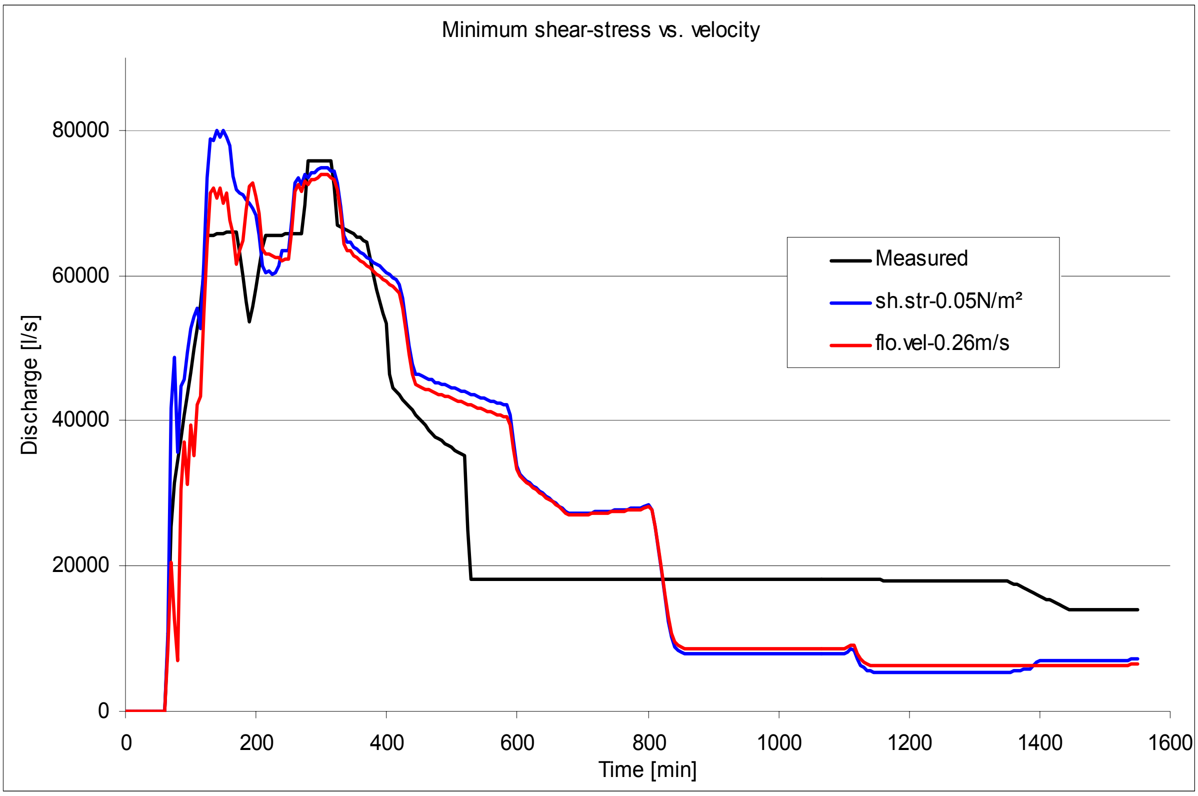

Figure 6.1.3 Comparison of minimal values (erosion occurs relatively fast) for the critical shear stress (blue curve) and the critical flow velocity (red curve)

2. The maximum values for the critical shear stress and the critical flow velocity are chosen as 3 N/m² according to Briaud (2001) for coarse sand and 3 m/s according to the Hjulström diagram for a grain size of about 0.002 m. The comparison of these values (with regard to the different grain sizes) is debarable, but the aim of these model runs is to compare the criterions and to test the sensitivity. Therefore, the upper boundary of the critical values according to literature is chosen.

Figure 6.1.4 shows the measured hydrograph (black curve) and the modeled hydrographs. The blue curve represents the modeled hydrograph for a critical shear stress of 3 N/m² and the red curve represents the simulated hydrograph for a critical flow velocity of 3 m/s.

Both curve show a zigzag shape in the steep rise at the beginning of the event whereas the discharge values of the red hydrograph are smaller compared to the blue one. This becomes more obvious at the first peak. After approximately 255 minutes, the modeled hydrographs converge each other. The corresponding model efficiencies are: for the blue hydrograph that is simulated with the shear stress criterion an R_{eff} of 0.6921 and for the red curve that is simulated with the flow velocity criterion an R_{eff} of 0.7095.

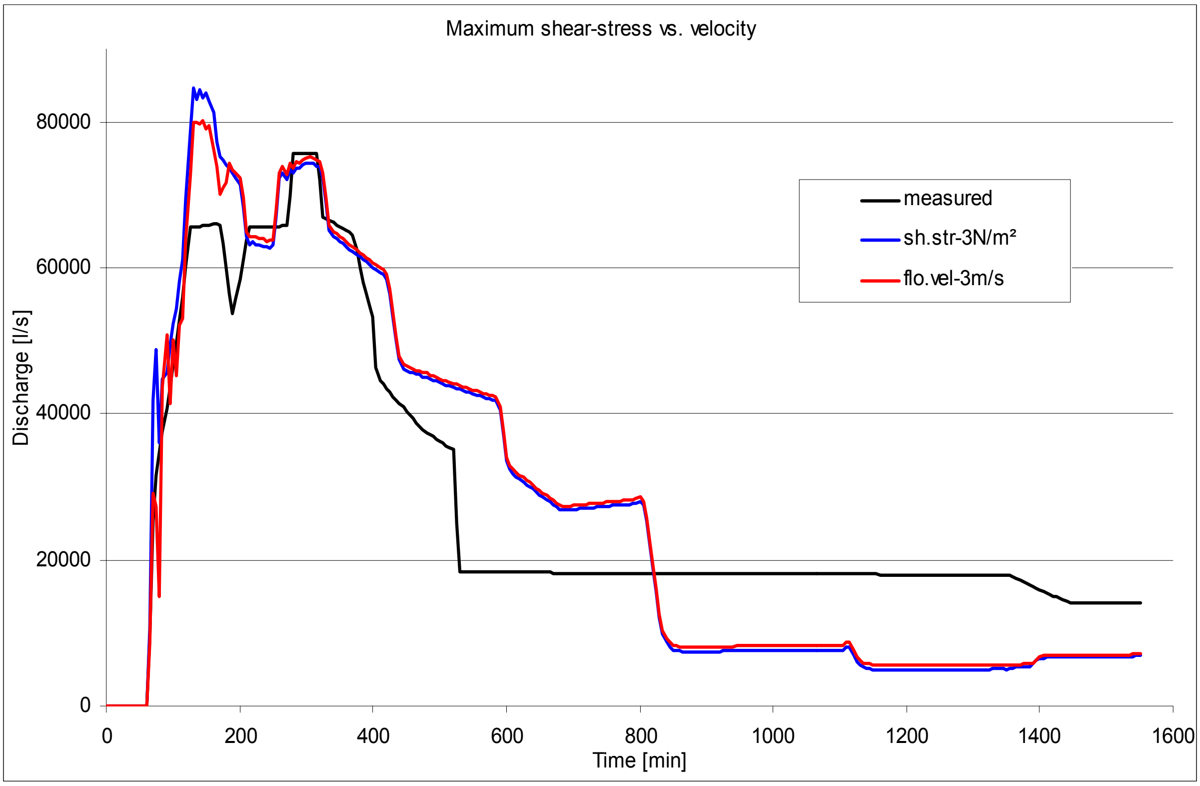

Figure 6.1.4 Comparison of maximum values (erosion occurs relatively late) for the critical shear stress (blue curve) and the critical flow velocity (red curve)

3. In the next model run, the two critical thresholds are fitted to the measured values. In this case, the critical values are fitted for each channel type unlike to the two previous comparisons (minimum values; maximum values) where the critical values are chosen unique for all three channel types. Table 6.1.1 gives the different fitted values for the critical shear stress and the critical flow velocity.

Table 6.1.1 Critical shear stress and flow velocity for different channel types – best fit

	Critical shear stress (N/m²)	Critical flow velocity (m/s)
Channel type 1	0.053	3.3
Channel type 2	0.025	5.8
Channel type 3	0.015	2.52

Figure 6.1.5 shows the model runs with the fitted and the measured values (dark curve). The hydrograph that is modelled with the criterion shear stress (blue curve) shows smaller values in the steep rise at the beginning, whereas the decline from the first peak (circa 70000 l/s) doesn'go as far as the red hydrograph that is simulated with the criterion critical flow velocity. Here again the graphs converge each other after approximately 255 minutes. The corresponding model efficiencies are: for the simulation with the shear stress criterion an R_{eff} of 0.7325 and for the simulation with the flow velocity criterion an R_{eff} of 0.7319.

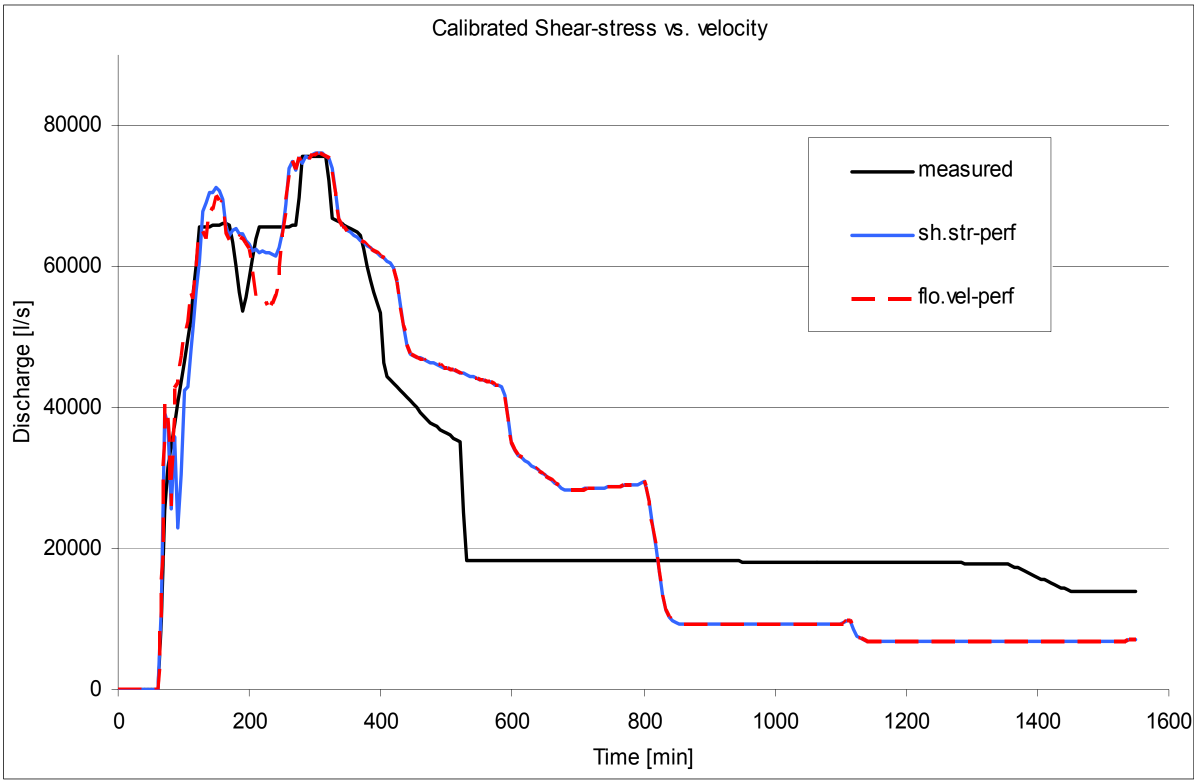

Figure 6.1.5 Measured hydrograph (black curve) and simulated hydrographs (blue and dashed red curve) with fitted critical values

The following simulations in the Nahal Zin and the Kuiseb catchment (chapters 6.2, 6.3, 6.4) use the Newton iteration method to calculate the initial cumulative infiltration to solve the Green-Ampt equation and critical flow velocities to simulate the process of scour and fill.

6.2 Nahal Zin event October 1979 ('large scale')

A single cell thunderstorm in the south-west part of the upper Nahal Zin catchment created the October 1979 event. Three gauging stations, in particular Mapal, Massos and Aqrabim (see Figure 4.1.2) recorded the single peak runoff event. The flow volume decreased from station to station (see Figure 6.2.1) and according to Lange (1999), additional tributary inflow can be excluded. So this event xan be viewed as a paradigmatic event for transmission losses. Figure 6.2.1 depicts the measured values (black curves) at the three stations (from Lange, 1999). The hydrograph recorded at the gauging station Mapal is used as the input function for the model and the channel properties are taken from Lange (1999). The additional parameters needed to simulate the transmission losses are listed in Appendix in Tab. IX.5.

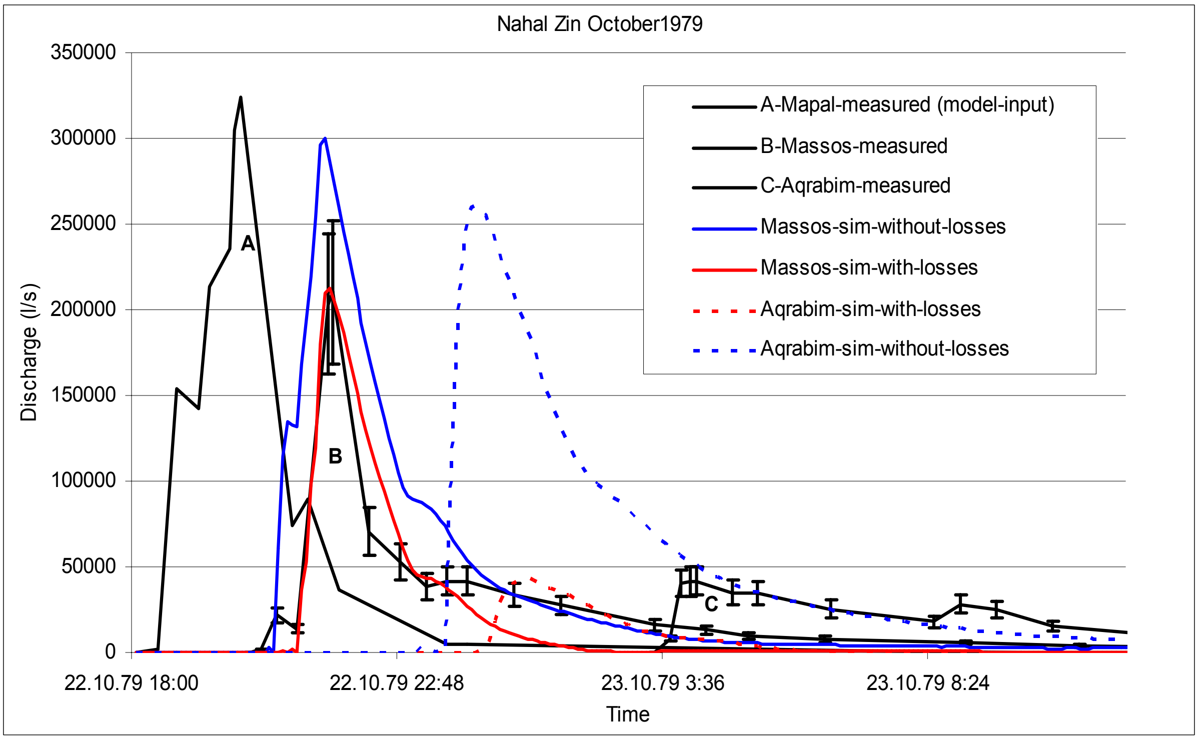

Figure 6.2.1 Nahal Zin October 1979 Single peak event recorded by three gauging stations (black curves, Mapal (A), Massos (B-with error bars (20%)) and Aqrabim (C with error bars (20%)), simulated hydrographs at the stations Massos (continuous curves) an Aqrabim (dashed curves) with (red) and without (blue) transmission losses

Station Massos (B): here, the simulated hydrograph evidently almost perfectly matches the peak of the recorded values. The steep fall-of in the hydrograph is a bit overestimated until circa 23:00 (Oct 22nd). From there on, the simulated hydrograph underestimates the measured hydrograph that declines very smoothly indicating that an additional slow component accompanies the fast (peak) component.

Station Aqrabim (C): the simulated hydrograph reaches the station Aqrabim too early (approx. 3 hours). This phenomenon will be discussed in chapter 'Discussion and outlook'. Otherwise, the simulated peak discharge of about 43 m³/s fits well the measured peak discharge of roughly 42 m³/s. Here again in the declining part of the hydrograph the measured values also show the already addressed second component that even creates a second peak.

6.3 Lower Nahal Zin ('small scale')

For the following three simulations, the same parameter set was used as for the simulation in chapter 6.1. The measured discharge data are taken from Schwartz (2001).

6.3.1 Runoff event Feb 2, 1996

The runoff event on the Feb 2 1996, is a small event with a maximum discharge of about ten m³/s. The measured hydrograph (black curve) shows a sharp increase to the maximum discharge. After reaching its peak value, it falls of sharply to a value of about 1.4 m³/s. Afterwards it rapidly rises again to circa 4 m³/s and then it increases smoothly to a discharge of about 5.5 m³/s. The peak discharge of the simulated curve (red curve) overeshoots the measured one by approximately 1.5 m³/s whereas the incline and the decline fit well to the measured hydrograph. In the interval after the minimum discharge (9.2.98 4:00) the modeled and measured hydrographs deviate from one another.

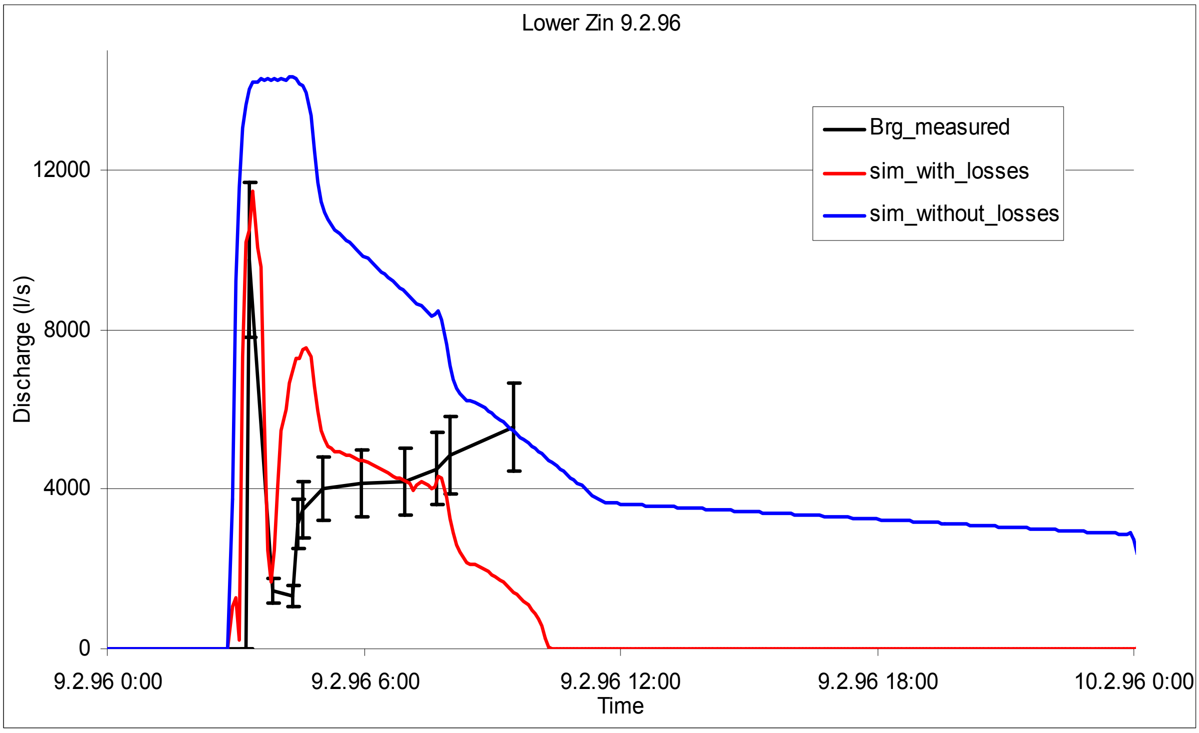

Figure 6.3.1 Lower Nahal Zin 9.2.96 Measured hydrograph (black curve with error bars (20%)) and simulations with (red curve) and without (blue curve) transmission losses

6.3.2 Runoff event 21.11.1996

The November 96 event is the smallest modeled event of the Nahal Zin catchment. The maximum measured discharge reaches almost five m³/s. In Figure 6.3.2, one can see that at the gauging station Brg the Zin River flows for about half an hour. After approximately another eight hours, the discharge rises again with values up to 0.9 m³/s. The model run with transmission losses (red curve) simulates the peak prematurely (circa 20 minutes) and too high (2.5 m³/s). Further, the simulation shows no more discharge values in the further discharge course.

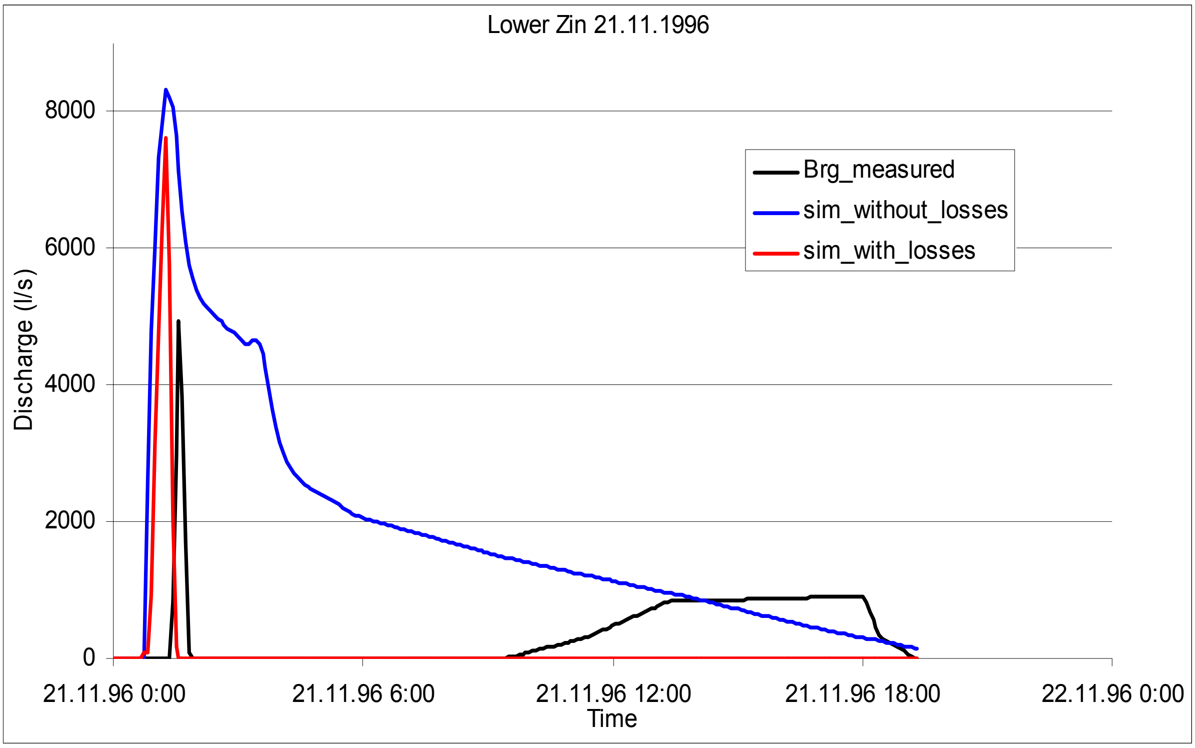

Figure 6.3.2 Lower Nahal Zin 21.11.96 Comparison of measured (black curve) and simulated hydrograph with (red curve) and without (blue curve) transmission losses

6.3.3 Runoff event Jan 11-14 1998

The January 98 event is modeled with (red curve) and without (blue curve) transmission losses as can be seen in Figure 6.3.3. However, by viewing the hydrograph it becomes clearly that the runoff event arrives at the downstream gauging station Brg earlier than at the upstream gauging station Mlp. The simulation shows a potential hydrograph (red graph) for the downstream gauging station when the inflow into the reach is equivalent to the data measured upstream (dashed black graph). Since no additional information was available to amend the contradictorily meausered data, this event is not discussed further.

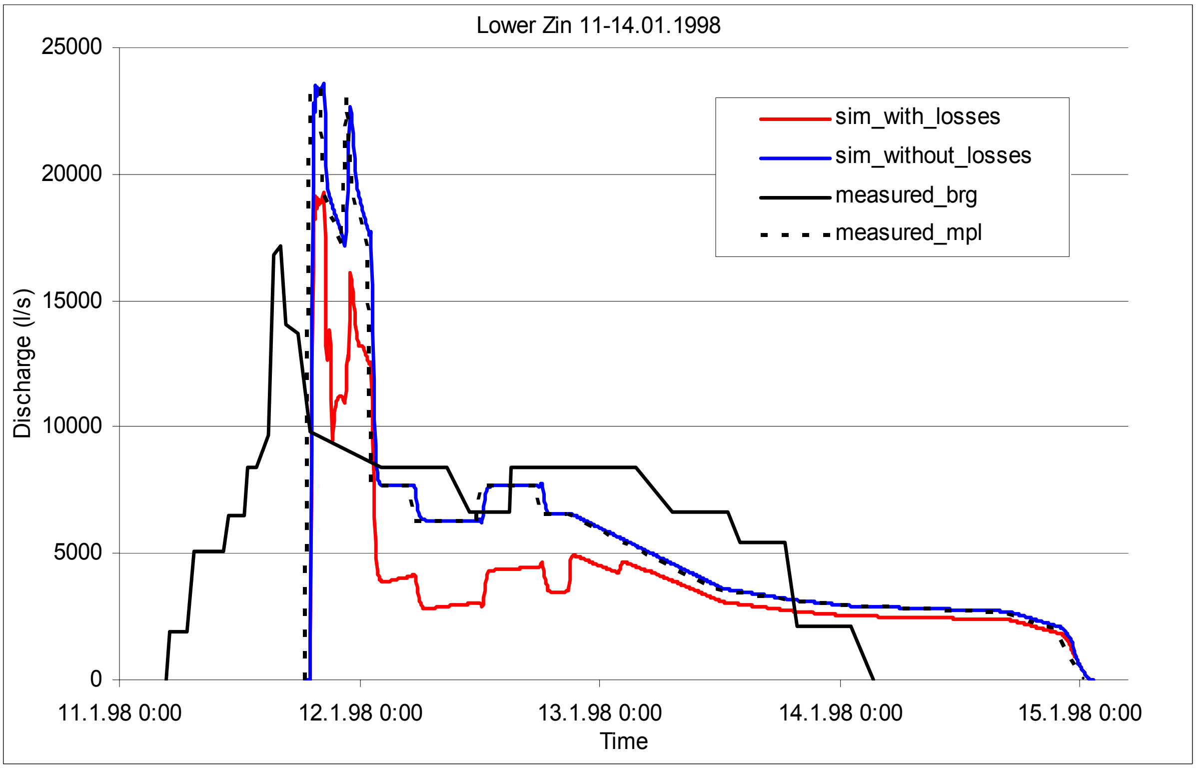

Figure 6.3.3 Lower Nahal Zin 11-14.1.1998 measured values at the (upstream) gauging station Mpl (dashed black curve) and (downstteam) gauging station Brg (continuous black curve) and simulation with (red curve) and without (blue curve) transmission losses

6.4 Kuiseb

In the Kuiseb catchment, different events were recorded. In this study three runoff events have been selected according to the criteria discharge dimension and antecedent moisture: so one relatively small event with a maximum discharge of about 4.5 m³/s, one relatively large event with a maximum discharge of about 88 m³/s and one event where time passed since the preceding flood was about one week.

6.4.1 Runoff event 18.02.1995 – small event

The runoff event on the 18.02.1995 was relatively small. The recorded maximum discharge at the gauging station Gobabeb reached approximately 4.5 m³/s. Figure 6.4.1 shows the measured hydrograph (black curve) and the simulated hydrographs. The blue curve is a model run without transmission losses, whereas the red curve is a simulation considering transmission losses. The different parameters used for this event, are listed in Tab. IX.6 in the Appendix.

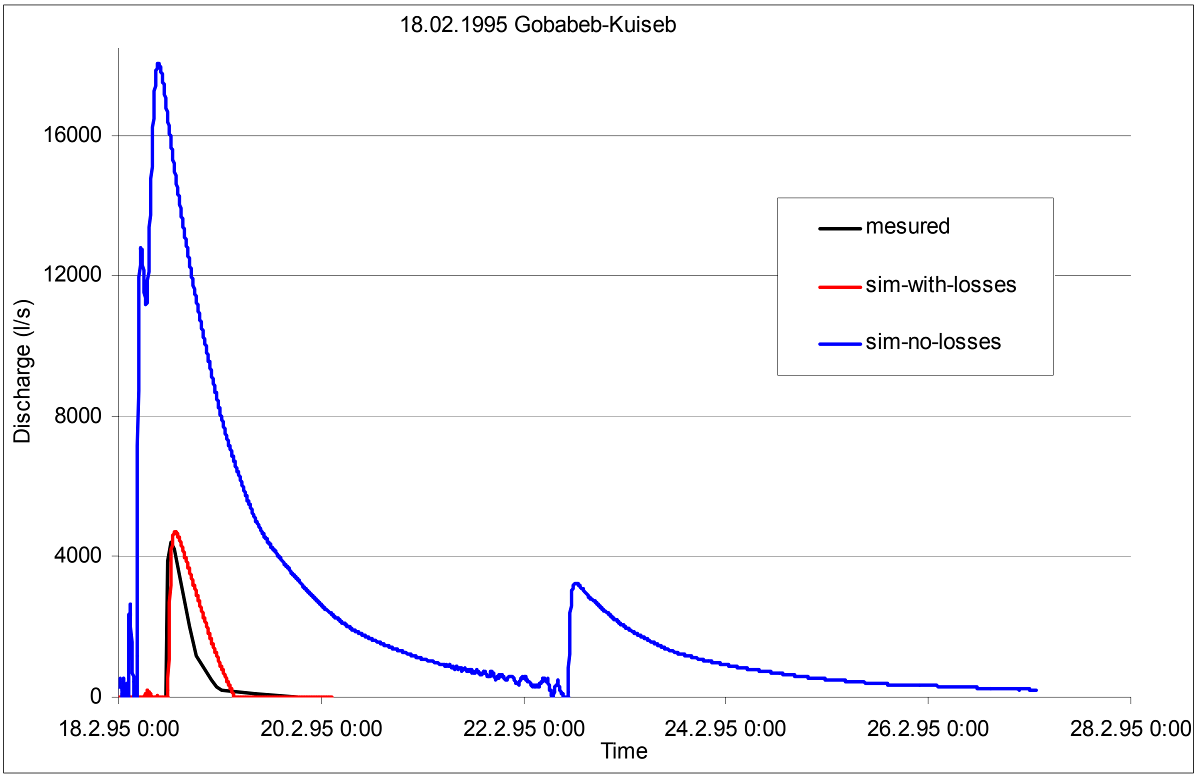

Figure 6.4.1 Runoff event on the 18.02.1995. Comparison of measured (black curve) hydrograph and simulations with (red curve) and without (blue curve) transmission losses.

Figure 6.4.2 shows the measured hydrograph and the model run with transmission losses in more detail. In addition, the measured hydrograph carries error bars (assumption: 20 % measurement uncertainty). The simulated curve is about one hour late in comparison with the measured one and shows a small oscillation already several hours before the actual arrival of the flood. Besides this, the peak discharge is overestimated by approximately 300 l/s, which lies within the margin of error. The almost linear decline of the simulated hydrograph does not reflect the shape of the measured one that is shaped like an outflow curve of a single linear storage model.

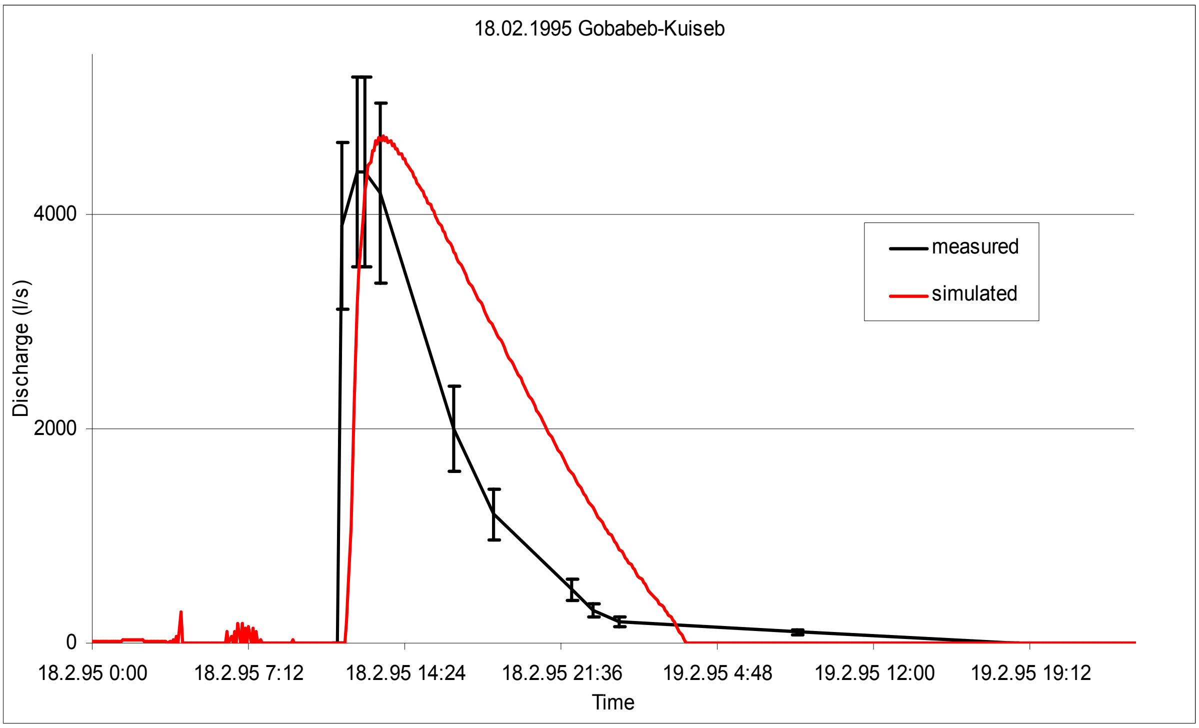

Figure 6.4.2 Close up of the measured (black curve with error bars (20%)) and simulated (red curve) hydrographs with transmission losses - Jan 18, 1995.

6.4.2 Runoff event Jan 17-30 1997 – large event

The following runoff event is large compared to the previous one. It is a multiple peak event with a maximum discharge of about 88 m³/s and an approximate duration of two weeks. Again, the measurements had been taken at the gauging station Gobabeb. The parameters used for the simulation can be found in Tab. IX.8 in the Appendix.

Figure 6.4.3 shows the measured (black curve) hydrograph with error bars (20%) and the simulations with (red curve) and without (blue curve) transmission losses. Contrary to the event of Feb 18 1995, the modeled hydrograph that includes transmission losses shows more or less the same shape as the simulation that does not consider transmission losses. The single striking difference in shape is the missing first peak in the red hydrograph. Otherwise, the losses are identifiable as the values are lower especially when the discharge is large but the hydrograph shape is more or less the same. The red curve underestimates the measured discharge with the exception of an overestimation of the maximum peak. Both simulations are about nine hours early and after the different peaks they converges (more or less) slowly towards zero, whereas the measured hydrograph remains approximately constant at values between 17 m³/s and 18 m³/s.

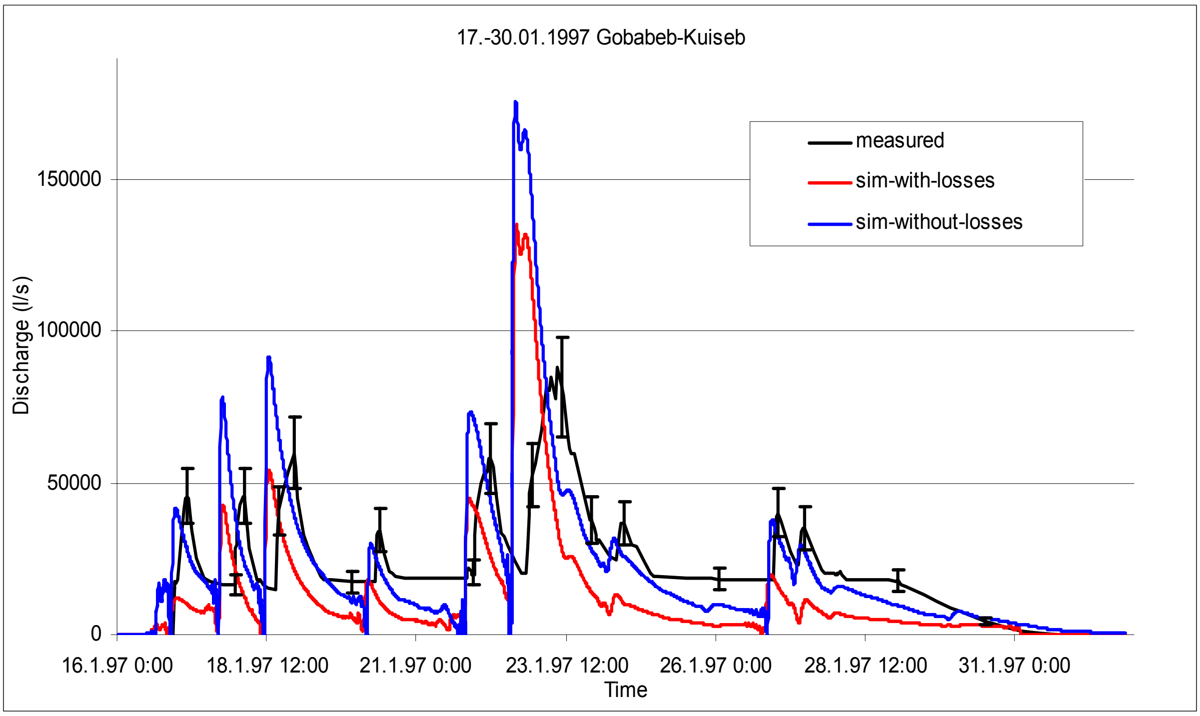

Figure 6.4.3 Runoff event between the 17. and the 30.01.1997. Comparison of measured (black curve) hydrograph with error bars (20%) and simulations with (red curve) and without (blue curve) transmission losses.

6.4.3 Runoff event 19.02-2.03.1985 – event with a preceding flood

The reason for the choice of the following event is that a preceding runoff event took place one week before. So here, it the influence of the initial soil moisture content and consequently the antecedent moisture index should influence the routine of the infiltration process. The parameters used for the simulations are listed in Tab. IX.7 in the Appendix. The runoff event was multiple peak event (two major peaks) with a relatively high maximum discharge peak (circa 55 m^3/s) and it lasted for almost two weeks at the gauging station Gobabeb. The preceding runoff event is considered as large enough to flood at least partly the floodplains so the antecedent moisture index also influenced the infiltration process into banks, bars and floodplains.

In Figure 6.4.4 it is visible that the measured hydrograph (black curve) and the simulations with (red curve) and without (blue curve) transmission losses start almost equally and the simulations show the first peak with a delay of approximately three hours. The red hydrograph underestimated the first peak, whereas the simulation without transmission losses fits well to the measured hydrograph. But the blue hydrograph overestimates the second peak (maximum discharge). Here the modeled hydrograph that includes transmission losses fits well to the measured values, but both simulated hydrographs have a retardation of almost three hours. In the decline after the maximum peak, both simulations run higher than the measured hydrograph.

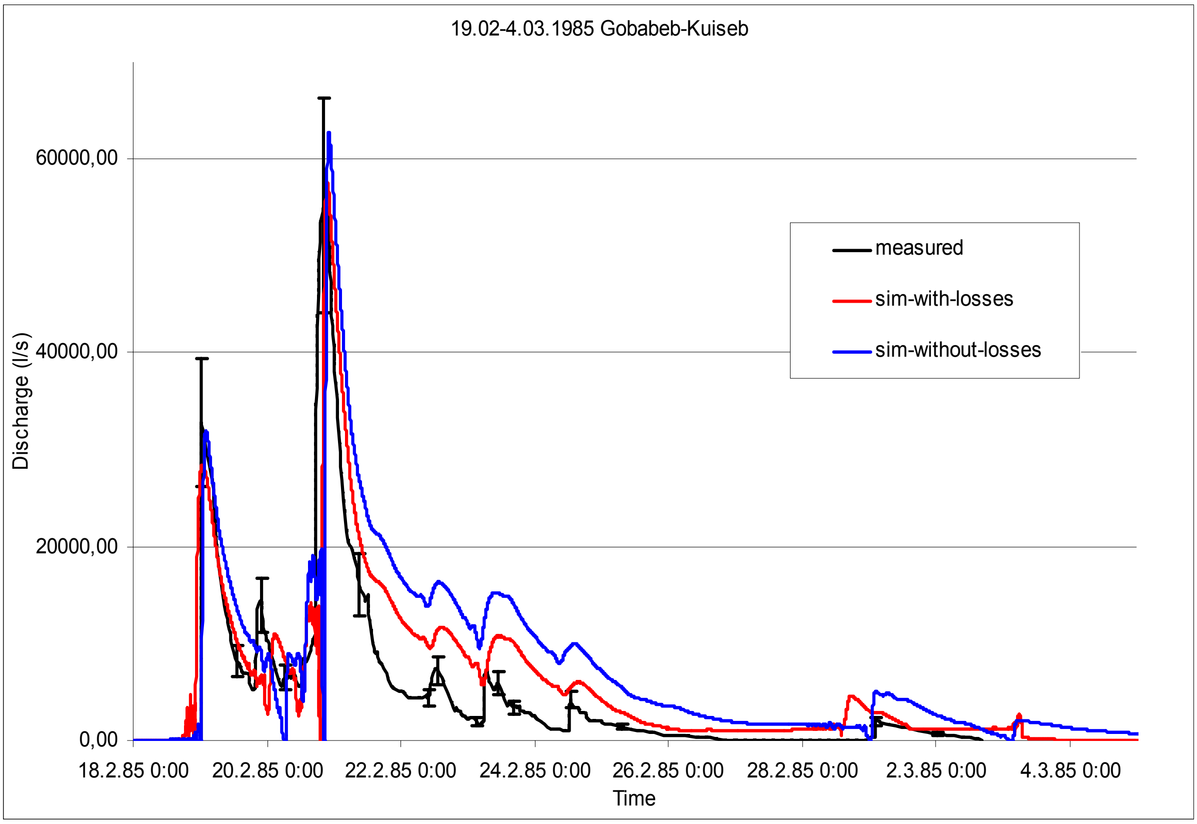

Figure 6.4.4 Runoff event between the 19.02 and the 2.03.1985. Comparison of the measured (black curve) hydrograph with error bars (20%) and simulations with (blue curve) and without (red curve) transmission losses.

6.5 Conclusion

Different methods that are described in the foregoing chapters are applied to the ZIN-model and tested respectively. Two ways to compute the initial cumulative infiltration, which are presented in chapter 3.3 for the inner channel area, are compared by simulating a flood event in the lower Nahal Zin. The analysis showed that the differences in the calculation methods are negligible. The hydrographs show the same shape with a small exception in the rising part of the graph. Further the two difference criterions to simulate the process scour and fill (see chapter 3.5) are tested. According to a certain range of literature values for the critical values, three runs are performed (maximum values, minimum values and 'best fit' values) to test the parameter sensitivity. The model runs with the maximum and minimum values showed that the model efficiency is slightly better when the flow velocity criterion is used. But when it is possible to adjust the critical values both methods yield similar results. It is conspicuous that the fitted values (see Table 6.1.1) for the critical shear stress and the critical flow velocity do not proceed similar from channel type to channel type. To achieve a good result, the critical shear stress has been lowered from channel type one to three with a maximum value for channel type one and a minimum value for channel type three. Contrary for the critical flow velocity, here the maximal critical value has been chosen for channel type two. This could be an indication that the two methods are not directly compareable.

A set of further runoff events in the Kuiseb River and the Nahal Zin are modelled. Three more runoff events are simulated in the lower Nahal Zin with a flow distance of about 5.5 km and one event in almost the entire catchment. The short distance simulations reflect the measured hydrograph in an acceptable way with one exception (event: 11-14.01.98). For the entire Nahal Zin catchment, a runoff event is simulated where discharge data of three gauging stations are available. The simulated hydrographs peaks of this downstream routing are relatively similar to the measured ones. But the simulated hydrograph at the last gauging station (Aqrabim) showed quite a time lack to the measured one. Further an additional slow runoff component occurred (interflow), a process that is not represented by the Zin-model

Three runoff events are chosen for the Kuiseb River according to the discharge and precondition attributes to validate the modified model. The simulation of the small event is satisfying whereas the simulated hydrographs of the two large events (with different preconditions) are less accurate. Both events lasted more than ten days so additional factors (tributary inflow or additional precipitation between the gauging stations) that influence the hydrographs cannot be excluded.

The next chapter discusses the modifications of the model and the results for these different runoff events.

VII Discussion and outlook

7.1 Modifications

The primary objective of this study was to improve the routing scheme of the ZIN-model with respect to transmission losses. Different modifications were performed to connect the modeling of the losses with the real processes that control transmission losses. Many of the flood and channel characteristics that influence transmission losses, as described in chapter II, were integrated into the ZIN-model. These modifications and more detailed descriptions for the infiltration achieved a temporal and spatial variability of the transmission losses. The precise description of the infiltration and the factors influencing the infiltration, resulted in an important role for the choice of the needed parameters. I.e. to achieve satisfying results the parameters have to characterize the catchment in adequate way.

The modified model was tested in several simulations and compared with measured hydrographs. The losses in the modified model are now temporal variable and connected to the flood and channel characteristics. Particularly the flood characteristics that affect the infiltration rates and the process of scour and fill have wide influence on the temporal behavior of the transmission losses while the channel characteristics provide more or less the initial and boundary conditions and therefore the total volume that is able to infiltrate. The results of these simulations were satisfying but some points still need to be discussed and some need further investigations.

The main cause for the transmission losses is infiltration into the alluvial channel fills. Therefore, the formerly constant loss-rate is substituted by temporally variable infiltration rates (more precisely with the Green-Ampt approach and a single linear storage approach), which consider, at least roughly, different factors influencing infiltration. The main advantage of a temporally variable loss rate compared to a constant rate is that an effective change of the simulated hydrograph is possible. The hydrograph shape that is modelled with a constant loss rate does not change substantially compared to the shape that is simulated without losses, but a time varying loss rate enables an alteration of the modelled hydrograph compared to a simulation without losses (or constant loss rate). This becomes apparent in the simulations of the lower Zin (chapter 6.3) where the hydrograph shapes differ clearly from the modelled shapes without losses.

This study describes infiltration with the physically based Green-Ampt approach for the inner channel reach and with a single linear storage approach for the additional flooded area. Both methods must be carefully discussed.

The Green-Ampt approach and the required parameters presuppose from a homogeneous soil, a condition that is not realized in the applications of the ZIN-model that simulates rainfall runoff events in large catchments. Besides this, the Green-Ampt approach does not consider processes like preferential flow (macro pores) and fingering (downward soil water movement instabilities), processes that are present in nature and strongly influence the procedure of infiltration. In the context of this study, the parameters used for the Green-Amt equation have to compensate these factors. They (should) approximate several soil characteristics that influence infiltration. Therefore, the different effective parameters, which the Green-Ampt equation requires, represent more or less averaged values for relatively large channel sections with changing conditions in the vertical and lateral extent and in the temporal progression as well. Consequently, the physical basis of the Green-Ampt approach weakens. Still, in comparison to other infiltration models, the Green-Ampt approach considers explicitly the surface water depth and the resultant increasing pressure head.

In contrast to the Green-Ampt approach, the single linear storage approach does not claim to reflect the various processes that happen on the additional flooded area. Yet, this empirical approach varies in time depending on the flooded area. The selection of the storage constants and the initial infiltration rate considers channel characteristics but this could be improved by additional field data (infiltration tests or directly by flood observations).

The previously addressed time varying infiltration rate is limited to a certain loss volume in the inner channel and to a certain time period for the additional flooded area. After the alluvium is saturated, a final constant loss rate is assumed. Originally, this final constant loss rate was thought to represent the infiltration into the underlying strata (if possible) but it can also be regarded as losses according to evaporation or according to new space in the alluvium as the soil water moves in the alluvium along the hydraulic gradient.

In discussing in to what extent the Green-Amt approach is adequate to model infiltration into the inner channel reach, the question arises how to compute the initial cumulative infiltration that is needed to calculate the infiltration rate. This study presents two methods, in particular a decomposition series and an iteration method. When the methods are applied, the results of both methods show no obvious differences. Nevertheless, the decomposition series requires a convergence criterion according to equation 3.3.14. According to Serrano (2003), this criterion is not satisfied when the absolute value of the pressure head at the wetting front is large. Due to incipient ponding conditions and the frequent steep rising hydrographs of arid rivers, the condition for convergence is rather not satisfied. This is caused in the swell of the water depth that increases the pressure head. As mentioned above the computed values yield acceptable and comparable results irrespective of the used method. Still, the Newton iteration method is preferred for further simulations with regard to the convergence criterion.

To simulate the process scour and fill two alternatives are put forward. One uses a critical flow velocity as criterion for the occurrence of erosion or sedimentation and the other uses a critical shear stress. The methods are compared with different literature values. Due to a certain range of possible critical values, the upper and lower boundary values were applied and tested achieving middling results. They achieve acceptable results when the critical values are calibrated. In this case, it is possible to adjust the beginning of infiltration so that the simulated and measured hydrograph shapes correlate. Nevertheless, both methods are imperfect. The attempt to describe these processes with a single critical value (flow velocity or shear stress) does not consider the various complex processes that occur on or happens to the channel bed surface. The different kinds of erosion such as particle-by-particle or block-by-block appear at different critical values and the erosion rates differ extremely depending on the type of erosion (Briaud et al., 2001). Consequently, the particle-by-particle erosion needs some time to erode a certain depth of a fine grained topping. Furthermore, the shear stress and the flow velocity vary locally in the channel and in addition to this, there are areas in the river with higher or lower turbulence resulting in shear stresses that fluctuate around a mean value. According to Dittrich (1996) in Lang (2001), the maximum stresses can reach eighteen times the mean value. Therefore, the attempt to simulate the process scour and fill in this study certainly has an influence on the modeled discharges but it is a strong simplification of the real processes that are complex it and needs further investigation.

The simple empirical functions to model the antecedent soil moisture content seem to produce acceptable results, at least when they are compared with soil moisture measurements from Schwartz (2001) and Schmitz (2004) (see Figure 3.6.2). Still the measured moisture data (Schwartz, 2001; Schmitz, 2004) do not fall to zero after 60 days (or longer periods) whereas the simulated soil moisture content reaches a value of zero after this period. The measured soil moisture content in the Kuiseb amounts less than 4 % of the porosity and in the lower Zin less then circa 10 % of the porosity. However, these residual amounts of soil moisture do not influence the process of infiltration noticeably as the assigning of concrete values for the porosity and the depth of the alluvium that include larger errors.

The calculation of the discharge is improved to avoid sudden crashs to a discharge of zero or an unnatural amplifying of the hydrograph (see chapter 3.8). This modification should only be used for large runoff events where the above-mentioned problems occur. In general, small runoff events did not show theses unwanted features. Further, this modification can lead to wrong results especially for small events as the method to calculate the current discharge is modified and this modification is chiefly effective for small discharges.

7.2 Parameter

The different parameters that are required to describe the process of infiltration with the Green-Ampt approach are the porosity, the hydraulic conductivity and the effective suction head. Actually, they are connected to each other through the alluvial and fluid characteristics but in this study they act as 'individual' parameters. The porosity and the extent of the alluvium determine the total volume of water that can be absorbed. The hydraulic conductivity and the suction head (also the surface water depth) are responsible for the time dependent infiltration behavior. Therefore, these three parameters have a strong influence on the shape of the simulated hydrograph for runoff events. As mentioned in chapter V, the literature values for these parameters vary within certain ranges. So here, it is important to choose values, which are represent the catchment characteristics or to use experimental data from the corresponding catchment.

In this study, experimental data are scarce. Still it was possible to calculate the hydraulic conductivity with the Green-Amt equation for the lower Zin reach in Israel and the reach near the research station Gobabeb in Namibia with soil moisture measurements (Schwartz, 2001; Schmitz, 2004). The calculated values in the lower Zin varied between circa 610 mm/h and 250 mm/h with a mean average of circa 400 mm/h. The high k values for the near surface depths could result out of channel degradation (an actual shorter flow length would lead to an actual slower advancing of the wetting front), but this could not be verified by analyzing data given by Schwartz (2001). Many other processes that have already been discussed (preferential flow, fingering, changing riverbed surface…) influence and adulterate the values for k. In the simulations of the lower Zin reach, k is chosen as 250 mm/h. This is reasonable as the influences of the mentioned processes are more prominent in near-surface depths and because this is the upper limit for the (Green-Ampt-) hydraulic conductivity in literature. Therefore, a calculated value for k with soil moisture data from the deepest sensor (depth: 1.22 m) is used. The value for the initial infiltration rate on the bars, banks and floodplains is chosen as 1000 mm/h. This is reasoned as according infiltration tests (Külls, 1994) the initial infiltration rates on a silty bank in the lower Zin reach values up 832 mm/h. Additionally, the floodplains often enclose dead end channels, reaches where large water volumes can be temporally stored as surface water. Indeed this water does not infiltrate immediately but it presents additional losses next to the infiltrated water. Both are represented by the linear storage approach and the related parameter and therefore the increase of the experimental value is justified.

The simulated events of the 'large' Nahal Zin catchment and the Kuiseb used values for the (Green-Ampt-) hydraulic conductivities between zero and 50 mm/h. These values correspond to literature values as well as to the calculated values from the Kuiseb (chapter 5.1). A conspicuous difference between the initial infiltration rates on the bars, banks and floodplains is noticeable (Kuiseb: 0-20 mm/h; Zin: 0-250 mm/h). This can be explained by the different catchment characteristics. Overall, the Kuiseb shows a lower channel gradient so here the possibility of fine-grained deposits on the floodplains is expected and therefore a smaller initial infiltration rate is assumed. To prove or disprove this assumption, additional infiltration data on these areas are required.

The differences in the hydraulic conductivity (inner channel) as well as in the initial infiltration rates (bars, banks and floodplains) between the 'lower Zin' reach and the 'large Zin' reach are striking. The two sites of application differ in size. According to Table 2.2.1, the lower Zin is classified as meso scale whereas the large Zin is classified as macro scale. Due to spatial and temporal heterogeneity of the systems, transferring data from one scale to another holds large uncertainties. This problem ahs already briefly been addressed in chapter 2.2. For ephemeral streams Parissopoulos et al. (1990) addresses the major difficulties in up-scaling profile measurement, which derive from the presence of silt lenses within the alluvium. Wheater (2002) states that it is impossible at present to infer hydraulic properties from in-situ point profile to transmission losses from wadi channels. However, the different channel properties such as alluvial deposits or the extension of the alluvial body (and consequently the different infiltration characteristics) of the 'lower Zin' and the 'large Zin' should not be ignored.

The use of a constant effective suction head is reasonable as the effect of a varying surface water depth (plus the corresponding calculation uncertainty) overlaps with the relatively small possible range of the effective suction head.

7.3 Applications

7.3.1 Lower Zin

The January `97 runoff event is used to evaluate different methods and parameters for the lower Zin reach. The methods and parameters are discussed above. The simulated hydrograph matches the measured hydrograph well, where the best results are obtained with fitted parameters for the scour and fill criterion. The obtained parameters from the January `97 event are applied unaltered for the three other runoff simulations. The simulated February `96 event (see Figure 6.3.1) shows a good correspondence compared with the measured data in the increasing part and with the peak value. One can clearly see that the process scouring in the different channel segments sets in more or less at the right point of time. Also, the point of time when the process of sealing the alluvial surface arrives, seems to be acceptable but the reduction of the infiltration rate is too high (steep incline at 3:50). Around 5:00 the measured values still increase whereas the simulated values start to decline again. So here, it looks like (in reality) the alluvial body is saturated and so the infiltration process is stopped or at least strongly limited. The model on the other side still infiltrates the incoming water so the choice of the porosity and / or the depth of the alluvium is probably too large.

This assumption seems to be confirmed in the November `96 event (see Figure 6.3.1). Around 1:30 a peak is measured which declines to a discharge of zero. After 9.5 hours, the Zin flows again at the gauging station Brg. The simulated graph matches the peak but not the rising part 9.5 hours later. In this simulation, the scouring seems to set in too late, as the simulated peak is overestimated. Furthermore, the simulated peak shows retardation in comparison to the measured one, indicating infiltration at the beginning of the event with low discharges and that the flood deposited enough fine material to seal the surface only after a while. Later (for the last channel segment the discharge was circa 5 m^3/s) the surface open up again.

7.3.2 October `79 large Zin

The simulated shapes of the two gauging stations (Masso, Aqrabim) of the October `79 event when compared with the measured shapes are satisfying, especially the peak discharges values are almost equal (see Figure 6.2.1). The problem in this simulation is the distinct time lack between the modeled and the measured hydrograph at the station Aqrabim.

The possibility of measurement problems cannot be excluded as the measurement instruments in arid regions are exposed to extreme conditions and the instruments used in 1979 did not meet today’s standards (personal communication with Dr. J. Lange). Another explanation is that the estimated value for the roughness coefficient (Manning n) for the section between Massos and Aqrabim is too low. In this section, 25.8 km of the total 33.8 km (circa 76%) channel length are classified as channel type three. Whereas in the reach between Mapal and Massos not a single segment is declared as channel type three and here the temporal correlation of the measured and simulated flood make an almost perfect fit. It is possible to move the temporal course of the simulation backwards by increasing the Manning n value (only for channel type three). For a good temporal fit of simulated and measured values of station Aqrabim, the roughness coefficient has to be increased from 0.045 to 0.13. Different factors like irregularities, variation in the cross sectional geometry, obstructions and vegetation allow a rising of the roughness coefficient. Base values for Manning n values vary between 0.011 and 0.07 according to Albridge (1973) and according to Chow (1959) irregularities like eroded and scalloped banks or exposed tree roots can enlarge the value by as much as 0.02. The influence of a varying cross sectional geometry is, according to Benson et al. (1967), relatively small with a maximal increase of 0.003. According to Chow (1959) the roughness value increases depending on of the percentage of cover of the obstructions (50 % obstruction cover + 0.05; 15 % obstruction cover + 0.015). Vegetation (dependent on foliage) can also noticeably enlarge the roughness coefficient by as much as 0.03 (Arcement et al., year unknown). All mentioned factors suit to the channel characteristics below the gauging station Massos. As mentioned in chapter 4.1.2, the channel broadens in this reach and due to a major tributary inflow, the dimensions of the alluvial deposits are large. Consequently, an enlargement of the Manning n roughness coefficient from 0.045 to 0.13 (difference is 0.085) is possible and the channel characteristics agree, at least roughly, with the conditions under which such an increase is possible. Yet, to justify such a raise of the roughness coefficient (almost threefold) further and more detailed information about the channel are recommended.

Another conspicuousness of the measured hydrographs is a second slow component that creates even a second peak at the gauging station Gobabeb. A possible way to simulate such a slow component is described in chapter 7.4.

7.3.3 Kuiseb

For the Kuiseb catchment three runoff events were simulated and compared to measured data. One was relatively small, one was relatively large with a long duration and the last had a preceeding flood with a time difference of approximately a week.

The small flood (February 1995, see Figure 6.4.1 or Figure 6.4.2) discharged maximum values of about 4.4 m^3/s and passed the Gobabeb gauging station within one day. The simulated hydrograph peak reaches the same order of magnitude with a maximum value of approximately 4.7 m^3/s (that is in the margin of the measurement error). Both of the other simulations did not yield such good results.

Especially the January `97 event (‘large event’) at the gauging station Gobabeb with duration of more than 13 days has to be considered as poor in comparison to all the other simulated runoff events. But here one can see that the influence of several modifications affects the hydrograph only for a certain time, more specifically until the alluvium is saturated. In this case the impact on the hydrograph shape is limited to the beginning of the event (first peak) and in addition to the high discharge periods where the floodplains are widely flooded. Between the peaks, the measured hydrograph (Figure 6.4.3) shows a kind of base flow. In principle, this is possible as the infiltrated water into the floodplain as well as the infiltrated water into the main channel can exfiltrate (return flow) as shown by Lange et al. (1997). Nevertheless, the periods between the peaks of the measured hydrograph show explicitly constant values indicating measurement failures, e.g. the floater stuck to something (personal communication with Dr. J. Lange).

As mentioned before, the last simulated runoff event (19.02. - 4.03.1985, see Figure 6.4.4) has been chosen as approximately one week before a flood took place and the influence of the antecedent moisture is observable. The shapes of the two modelled hydrographs are more or less similar but the simulation including transmission losses always shows a smaller discharge because infiltration is still diminished. The initial moisture content reduces the infiltration rates so that the otherwise obvious influences, chiefly at the start of runoff events, vanish. The influence of the antecedent moisture on the floodplains becomes also visible. The differences of the simulated (with and without losses) high peaks discharges are noticeably reduced compared to the January `97 event. For example, the measured discharges on January 18th 1997 (11:37) reached a value of approximately 59 m^3/s (see Figure 6.4.3). The difference of the simulations with and without losses amounts to circa 33.6 m^3/s. On February 2nd 1985 (21:36), the Gobabeb gauging station measured a comparable discharge of about 56 m^3/s. In this case, the difference between the simulation with and without losses is circa 3.9 m^3/s. The losses for these comparable discharges are reduced more than a tenfold due to the influence of the antecedent moisture index.

7.4 Outlook

Basically, all modifications leave room for improvement. However, the attempt to simulate the process scour and fill is rather in its infancy. An improvement could be made by correlating the critical values with channel (e.g. the thickness of silt layers) as well as flood (e.g. a turbulent flow index) characteristics. In this context, the scouring could be integrated into the model as a time dependent process for channels with a loose topping and as a more or less instant process for channels with a cohesive topping. This would also require different critical values as the particle by particle erosion occurs already at relatively low flow velocities or shear stresses in contrast to the block by block erosion that occurs at higher values. Another factor that has been not addressed so far is the sediment load, in particular the grain sizes that are factually responsible for the sealing of the alluvial surfaces. Here the time lag between two floods plays a role. When the no runoff period is long, the amount of accumulated fine grained material is large. Therefore, the concentrations of suspended sediment are especially high in the first event of the year (Alexandro, 2003). This fact could also be integrated into the model when regarding at the sealing of the surfaces.

Another feature with regard to scouring and filling the alluvial surface is the empirical factor 'l' that reduces the infiltration rate. In this study, the values for 'l' were chosen between zero and 0.1. This is interpretable in two ways. First, a special interpretation. i.e. that a percentage of the channel (dependent on l) just does not infiltrate anymore, or second the infiltration occurs in the entire channel but is reduced (dependent on l). The values of 'l' were chosen arbitrarily as no other informations were available. Therefore, this factor (l) needs further investigations with regard to the areal extent and to the limiting influence on the infiltration.

An enhancement of the simulation of the infiltration itself could consist in a more detailed spatial differentiation, especially for the flooded floodplains. This study divided the additional flooded area into just two sections and although the flooded width is considered in the calculation of the infiltration rate, a higher resolution would reflect the natural system in a better way. In addition, a more detailed differentiation of the channel into more channel types would probably yield better results.

This study disregarded the possibility of return flow from the main channel and exfiltration out of floodplains or banks and bars respectively. After the alluvium is saturated, the soil water moves along the hydraulic gradient. With regard to this, the alluvial body could be described as a storage with certain geometric characteristics (form and inclination). After this storage is saturated, the water could flow and according to the cross sectional geometry (e.g. narrowing) or the shape of the channel inclination (e.g. concave shape) the infiltrated water would have the possibility to create return flow. Likewise, a lateral inflow from the floodplains into the inner channel could be integrated into the model. To intergrate such a storage approach would lead to a slow discharge componet that is observable in some measured hydrographs (e.g. Figure 6.2.1).

In this study, the problem to assign and to determine the different parameters needed becomes obvious. The rare existing field data are used. In case that no data were available (mostly), literature values are used. Doing this, the model is afflicted with large uncertainties as the literature values allow more or less large variations. To prevent this, additional experimental data are necessary.

All the above-mentioned suggestions to improve the simulation of transmission losses are related to a more detailed knowledge about the catchment and the channel. Therefore, they require additional data witch again involve additional efforts and costs. Therefore, the question arises if the improvements would weight up the additional efforts.

VIII Literature

Adomian G. (1994); Solving frontier problems in physics - The decomposition method; Kluwer Academic, Boston

Ahnert F. (1996); Einführung in die Geomorphologie; Stuttgart 1996

Ahuja, L. R. & Ross J. D. (1983); Effect of subsoil conductivity and thickness on interflow pathways, rates and source areas for chemicals in a sloping layered soil with seepage face; Journal of Hydrology, 64; P: 189 – 204

Aldridge B. N. & Garrett J. M. (1973); Roughness coefficients for stream channels in Arizona; U.S. Geological Survey Open-File Report; P 87

Alexandrov Y., Laronne J. B. & Reid I. (2003); Suspended sediment transport in flash floods of the semiarid northern Negev, Israel; Hydrology of Mediterranean and Semiarid Regions, International Association of Hydrological Sciences, 278; P 346-352.

Arcement G. J. Jr. &. Schneider V. R. (year unknow); USGS Guide for Selecting Manning's Roughness Coefficients for Natural Channels and Flood Plains; United States Geological Survey Water-supply Paper 2339, Metric Version (from http: http://www.fhwa.dot.gov/bridge/wsp2339.pdf)

Barry D. A, Parlange J. -Y, Sander G. C., Li L., Jeng D.-S., Hogarth W.L. (2003); Discussion of "explicit solutions to Green and Ampt Infiltration equation by Sergio E. Serrano; Journal of Hydrological Engineering, May/June 2003; P 166-168

Benson M. A., & Dalrymple T, (1967); General field and office procedures for indirect discharge measurements; U.S. Geological Survey Techniques of Water-Resources Investigations book 3

Ben-Zvi A. and Shentsis I. (2001); Assessment of runoff as a component of water resources in the Negev and Arava; Israel Journal of Earth Science, 50, 2001; P 61-71

Bourke M. C., Childs A. & Stokes S. (2003); Optical age estimates for hyper-arid fluvial deposits at Homeb, Namibia; Quaternary Science Reviews 22; P 1099–1103

Breymann U. (1994); C++, eine Einführung; Carl Hanser Verlag München Wien

Briaud J. L., Ting F. C. K., Chen H. C., Cao Y., Han S. W., Kwak K. W. (2001); Erosion function apparatus for scour rate predictions; Journal of Geotechnical and Geoenvironmental Engineering, Feb. 2001; P 105-113

Chang H. H. (1988); Fluvial processes in river engineering; John Wiley & Sons, New York, Chichester, Brisbane, Toronto, Singapore

Childs E.C. (1969); An introduction to the physical basis of soil water phenomena; John Wiley & Sons Ltd., London, UK

Chow V. T. (1959); Open-channel hydraulics; New York, McGraw-Hill Book Co

Crerar S., Fry R. G., Slater P. M., van Langenhove G. & Wheeler D. (1988); An unexpected factor affecting Recharge from ephemeral river flows in SWA/ Namibia; in Simmers I. (1988), estimation of natural groundwater recharge; D. Reidel Publishing Company; P 11-28

Dick G. S. (1997); Controls on flash flood magnitude and hydrograph shape, upper Blue Hills badlands, Utah; Geology (boulder), 25, 1; Geological Society of America (GSA); P 45 – 48

Dong W. (2003); Simulations on soil water variation in arid regions; Journal of Hydrology, 275, 2003; P 152-181

Dooge J. C. I. (1988); Hydrology in perspective; Hydrological Science Journal, 33; P 61-85

Dunkerly D. & Brown K. (1999); Flow behavior, suspended sediment transport and transmission losses in a small (sub-bank-full) flow event in an desert stream. Hydrological Processes, 13; P 1219-1232

Dyer K. R. (1990); Coastal and Esuarine Sediment Dynamics; J. Wiley Chichester

Evenari M., Shanan L., & Tadmor N. (1971); The Negev, the challenge of a desert; Harvard University Press Cambridge, Massachusetts

Feddes R. A. (1995); Space and time scale variability and interdependencies in hydrological processes; International Hydrology Series, CUP; P 420

Freyberg D. L. (1981); Models of surface – subsurface flow interaction in an ephemeral channel; Dissertation submitted to the Department of Civil Engeneering, Stanford University to obtain the degree Doctor of Philosophy

Freyberg D. L., Reeder J.W., Franzini J.B. & Remson I. (1980); Application of the Green-Ampt Model to Infiltration Under Time-Dependent Surface Water Depths; Water Resource Research, Vol. 16, No. 1, Feb. 1980; P 517-528

Goldman D. M. (1989); Loss rate representation in the HEC-1 watershed model; in Morel-Seytoux (1989), Unsaturated flow in hydrologic modeling, theory and practice; Kluwer Academic Publisher, Boston, MA

Green W. H. & Ampt C. A. (1919); Studies on soil physics I. The flow of air and water through soils; Journal of Agriculture Science IV; P1-24

Guwang B. (2004); Hydrologische Prozesse im Stadtgebiet von Freiburg und deren adäquate Modellierung; Diplomarbeit am Institut für Hydrologie, Albert Ludwigs Universität Freiburg i. Br.

Hachum A. Y. & Alfaro J. F. (1980); A physically based model of water infiltration in soil; Utah Agriculture Experiment Station Bulletin 505; Logan,Utah, USA

Herrmann D. (1997); C++ für Naturwissenschaftler: Beispielorientierte Einführung; Bonn: Addison-Wesley-Longman Verlag

Indlekofer H. M. F. (2005); Zur Ermittlung der mittleren Schwebstoffkonzentration sowie zur Differenzierung von Schwebstoff- und Geschiebebewegung im offenen Gerinne; Wasserbau-Heft, FH Aachen, 2005, Heft 4; P 28-31

Jacobson P. (1997); An ephemeral perspective of fluvial ecosystems: Viewing ephemeral rivers in the context of current lotic ecology; Dissertation submitted to the Faculty of the Virginia Polytechnic Institute and State University in partial fulfillment of the requirements for the degree of Doctor of Philosophy in Biology

Jordan P. R. (1977); Streamflow transmission losses in western Kansas; Journal of the hydraulic division, Proc A.S.C.E., 103; P 905-919

Knighton A. D. & Nanson G. C (1994); Flow transmission along an arid zone anastomosing river, Cooper creek, Australia; Hydrological Processes, 8, 1994; P 137-154

Külls C. (1994); Transmission Losses from ephemeral floods in Nahal Zin, Israel; Diplomarbeit am Institut für Physische Geographie, Albert Ludwigs Universität Freiburg i. Br.

Külls C., Leibundgut Ch. Schwartz U. & Schick A. P. (1995); Channel infiltration study using dye tracer; IAHS Publication No. 232; P 429-436

Kyle R., Gimenez D., Rawls W. J., & Lauren J. G. (1999); Scaling properties of saturated hydraulic conductivity in soil; Geoderma, 88 No 3; P 205-220

Lado M., Ben-Hur M. & Shainberg I. (2004); Soil wetting and texture effects on aggregate stability, seal formation and erosion; Soil Science Society of American Journal 68, 6; Madison, WI, United States; P 1992-1999

Lane L. J.(1990); Transmission losses, flood peaks, and groundwater recharge; Hydrology of Arid Lands; Proc. Int. Symp., French R. H., ed., A.S.C.E., Reston, VA; P343-348

Lang C., De los Santos Ramos F. J. & Kühn G. (2001); Stabilität und Materialtransport bei Durch- und Überströmung der Sohle von Wasserstrassen; Institut für Hydrodynamik Universität Karlsruhe (TH)

Lange J. & Leibundgut C. (2003); Surface runoff and sediment dynamics in arid and semi-arid regions; in: Understanding water in a dry environment – hydrological processes in arid and semi-arid zones, International Association of Hydrologists, editor: Simmers I., AA Balkema Publishers; P115-150

Lange J. (1999); Anon-calibrated rainfall-runoff model for large arid catchments, Nahal Zin, Israel; Dissertation zur Erlangung des Doktorgrades der Geowissenschaftlichen Fakultät der Albert Ludwigs-Universität Freiburg i. Br.

Lange J. (2005); Dynamics of transmission losses in a large arid stream channel; Journal of Hydrology 306; P 112-126

Lange J., Leibundgut C., Grodek T., Lekach J. & Schick A. (1997); Using artificial tracer to study water losses of ephemeral floods in small arid streams; IAHS Publication 247, Karst Hydrology; P 31-41

Lee J. S. (1999), Experimental studies on the estimation of deposition and erosion parameters of silty mud; Costal Sediments’99; 3, 1999; P 1897-1911

Le Houérou H. N. (1996); Climate change, drought, and desertification; Journal of Arid Environments, 34; P 133 -85

Maniak U. (1997); Hydrologie und Wasserwirtschaft – Eine Einführung für Ingenieure, Springer Verlag, 4. Auflage

Martinez-Landa L. & Carrera J. (2005); An analysis of hydraulic conductivity scale effects in granite (Full-scale Engineered Barrier Experiment (FEBEX), Grimsel, Switzerland); Water Resources Research, Vol. 41, No 3 (from http: www.h2ogeo.upc.es/publicaciones/2005/Art.Mart%C3%ADnez-Carrera.pdf)

Moore I. D. (1981); Infiltration equation modified for subsurface effects; Journal of Irrigation and Drainage

Morel-Seytoux H. J. & Bilica J. A.(1985); A two phase numerical model for prediction of infiltration: applications to a semi-infinite soil column; Water Resource Research; Vol. 21; P 607-615

Moussa R. and Bocquillon C. (2000); Approximation zones of the Saint-Vernant equations for flood routing with overbank flow; Hydrology and Earth System Science, 4 (2), 2000; P 251-261

Nestmann F. & Ihringer J. (2002); Hydrologie, Kursbegleitendes Skript; Universität Karlsruhe (TH), Institut für Wasserwirtschaft und Kulturtechnik

Osterkamp W. R., Lane L. J. & Savard C. S. (1994); Recharge estimates using a geomorphic / distributed-parameter simulation approach, Amargosa river basin; Water Resource Bulletin, American Water Resource Association, 30,3; P 494-507

Parissopoulos G. A. & Wheater H. S. (1991); Effects of wadi flood hydrograph characteristic on infiltration; Journal of Hydrology, 126/127, 1991; P 247- 263

Parlange J. -Y, Barry D. A., Haverkamp R. (2002); Explicit infiltration equations and the Lambert W-function; Advances in Water Resources, 25, 2002; P 1119-1124

Peebles R. W., Smith R. E. & Yakowitz S. J. (1981); A leaky reservoir model for ephemeral flow recession, Water Resource Research, 17,3; P 628-636

Philip J. R. (1957); The theory of infiltration: 4. Sorptivity and algebraic infiltration equation; Soil Science, No 84; P 257-264

Ponce V. M., Lohani A. K. & Scheyhing C. (1996); Analytical verification of Muskingum-Cunge routing; Journal of Hydrology ,174; P 235-241

Raudkivi A. J. (1982); Grundlagen des Sedimenttransports; Springer-Verlag, Berlin, Heidelberg, New York

Ravi V. & Williams J. R. (1998); Estimation of infiltration rate in the vadose zone: Compilation of simple mathematical models, Volume I, U.S. Environmental Protection Agency

Rawls W. J. & Brakensiek D. L. (1983); A procedure to predict Green-Ampt infiltration parameters; Adv. Infiltration, American Society of Engineering; P 102-112

Rawls W. J.,Ahuja L. R., Brakensiek D. L. & Shirmohammadi A. (1992); Infiltration and soil water movement; in Handbook of Hydrology, Editor in Chief: Maidment D. R.; Chapter 5; McGraw-Hill, Inc., New York

Reed S. M. & Maidment D. (1998); Use of Digital Soil Maps in a Rainfall-Runoff Model; Center for Research in Water Resources, Bureau of Engineering Research; University of Texas, Austin

Reeder J. W., Freyberg D. L., Franzini J.B. & Remson I. (1980); Infiltration under rapidly varying water surface depths; Water Resource Research, Vol. 16, No. 1, Feb. 1980; P 97-104

Scanlon B. R. & Goldsmith R. S. (1997), Field study of spatial variability in unsaturetd flow beneath and adjacent to playas; Water Resource Research, vol. 33, no. 10, October 1997; P 2239-2252

Schmitz A. (2004); Transmission losses and soil moisture dynamics in the alluvial fill of the Kuiseb river, Namibia; Diplomarbeit am Institut für Hydrologie, Albert Ludwigs Universität Freiburg i. Br.

Schwartz U. (2001); Surface and Near Surface Responses to Floods in a Large Channel (Nahal Zin) in the Context of an Alluvial Aquifer in a Hyper-Arid Environment; Ph. D.-thesis, The Hebrew University of Jerusalem

Serrano S. E. (1997); Hydrology for engineers, geologists, and environmental professionals. An integrated treatment of surface, subsurface, and contaminant hydrology; Hydro Science Inc., Lexington, Kentucky

Serrano S. E. (1998); Analytical decomposition of the nonlinear unsaturated flow equation; water Resource Research, 34, 1998; P 397-407

Serrano S. E. (2001); Improved decomposition solution to Green and Ampt equation; Journal of Hydrologic Engineering, May/June 2003; P 158-160

Serrano S. E. (2003); Closure to “Explicit solutions to Green and Ampt Infiltration equation” by Sergio E. Serrano; Journal of Hydrologic Engineering, May/June 2003; P 168-170

Serrano S. E. (2003); Explicit solutions to Green and Ampt Infiltration equation; Journal of Hydrologic Engineering, July/ August 2001, Vol. 6 No.; P 336-340

Serrano S. E. (2004); Modeling infiltration with approximate solutions to Richard’s equation; Journal of Hydrologic Engineering, September/October 2004; P 421-432

Shentsis I. ,Meirovich L., Ben-zvi A., Rosenthal E., (2001); Assessment of transmission losses and groundwater recharge from runoff events in a reach of Nahal Paran, Israel; Israel Journal of Earth Science, 50, 2001; P 187-199

Shields A. (1936); Anwendung der Ähnlichkeitsmechanik und der Turbulenzforschung auf die Geschiebebewegung; Mitteilungen der Preußischen Versuchsanstalt für Wasserbau und Schiffbau, Berlin, Heft 26

Simon A., Langendoen E.J., Collison A., Layzell A. (2003); Incorporating bank-toe erosion by hydraulic shear into a bank-stability model: Missouri river, eastern Montana; Proceedings, Ewri-Asce, World Water & Environmental Resources Congress

Sorman A. U. & Abdulrazzak M. J. (1993); Infiltration-recharge through wadi beds in arid regions; Hydrological Sciences, 38; P 173-186

Sorman A. U., Abdulrazzak M. J.(1995); Estimation of Actual Evaporation Using Precipitation and Soil Moisture Records in Arid Climates; Hydrological Processes, 9; P 729 – 743

Sorman A. U., Abdulrazzak M. J.(1997); Estimation of wadi recharge from channel losses in Tabalah Basin, Saudi Arabia; in Simmers I.; Recharge of aquifers in (semi-) arid areas; IAH - ICH; Vol. 19; P 187-200

Stewart J. B., Engmann E. T., Feddes R. A. & Kerr Y. (1996); Scaling-up in Hydrology Using Remote Sensing; Wiley, Chichester

Stomph T. J., De Ridder N., Steenhuis T. S. & Van De Giesen N. C. (2002); Scale effects of Hortonian overland flow and rainfall-runoff dynamics: Laboratory validation of a process based model; Earth Surface Processes and Landforms, No 27; P 847-855

Talsma T. (1985), Prediction of hydraulic conductivity from soil water retention data; Soil Science volume 140, Wiliams &Wilkins Baltimore, Maryland 21202; P 184-188

Thormählen A. (2003); Hydrological modelling in a small hyperarid catchment - Nahal Yael, Israel runoff generation and transmission losses; Diplomarbeit am Institut für Hydrologie, Albert Ludwigs Universität Freiburg i. Br.

Uhlenbrook S. (1999); Untersuchung und Modellierung der Abflussbildung in einem mesoskaligen Einzugsgebiet; Freiburger Schriften zur Hydrologie, Band 10

Vivoni E. R. (2005); Distributed aquifer recharge enhancements in arid zones; web page: http://web.mit.edu/vivoni/www/aridzone.html; Page created and maintained by Enrique R. Vivoni; Last modified on: May 15, 2000; (contact: *vivoni@mit.edu*)

Vollmer S., Träbing K., & Dittrich A. (2000); Turbulence induced penetration of near bottom water into the porous media – experimental study; Proceedings of the international symposium on river flood defence, Kassel; P E17-E24

Ward J. P. (1987); The Cenozoic succession in the Kuiseb valley, central Namib Desert, Geological Survey of South West Africa, Namibia, 9; P 1-124

Ward R. C. & Robinson M. (2000); Principals of hydrology, 4th edition; McGraw-Hill International (UK) Limited

Wheater H. & Kirby C. (1998); Hydrology in a changing environment; Wiley, Chichester, 3 vols

Wheater H. (2002); Hydrology of wadi systems; IHP-V, Technical Documents in Hydrology, No. 55, UNESCO, Paris, 2002; P 5-23

Wiberg P. L. (1987); Calculations of the critical shear stress for motion of uniform and heterogeneous sediments; Water Resources Research; 8, 1987; P 1417-1480

Wyrwa J. (2003); Turbulenzmodellierung für stabil dichtegeschichtete Strömungen bei der Simulation des Transports von kohäsiven Sedimenten in Ästuaren; Dissertation zur Erlangung des akademischen Grades Doktor-Ingenieur der Fakultät V, Verkehrs- und Maschinensysteme, der Technischen Universität Berlin

Web-pages:

http://www.hydrology.uni-freiburg.de/forsch/zinmod/zinmod.htm

http: www.h2ogeo.upc.es/publicaciones/2005/Art.Mart%C3%ADnez-Carrera.pdf http: www.uni-koeln.de/inter-fak/sfb389/e/e1/download/atlas_namibia/e1_download_climate_e.htm#annual_rainfall

http://www.fhwa.dot.gov/bridge/wsp2339.pdf

IX Appendix

9.1 Tables

Tab. IX.1 Channel properties for the lower part of the Nahal Zin catchment

segment	length (m)	area alluvium (m²)	mean width area alluvium (m)	total area (m²)	total mean width (m)	% inner channel	channel type
1	1802.24	40919.37	22.70	54368.43	30.17	0.75	1
2	141.13	1163.18	8.24	3515.38	24.91	0.33	2
3	894.74	25373.84	28.36	110010.27	122.95	0.23	3
4	229.64	4486.45	19.54	14388.69	62.66	0.31	2
5	1500.00	86963.44	57.98	313948.57	209.30	0.28	3
6	225.00	7141.38	31.74	21711.38	96.50	0.33	3

Tab. IX.2 Percentage inner channel of total width, average value for each channel type (lower Zin)

channel type	mean % of inner channel
1	0.75
2	0.32
3	0.27

Tab. IX.3 Parameters for runoff simulation on 23.01.1997 (lower Zin)-comparisson iteration vs decomposition and for runoff simulations Feb. 9th 96, Nov 21st 96 and Feb. 98

	channel type 1	channel type 2	channel type 3
da	3	3.5	03. Mai
mn	0.03	0.025	0.02
v	0.75	0.35	0.27
Hf	1	3	3
ni	0.5	0.5	0.5
k	250	250	250
kb	1000	1000	1000
kf	10	3	3
he	0.35	0.35	0.4
I	0.1	0.1	0.1
Antec=	1-0.8T	1-0.85T	1-0.9T
T	6	6	6
To	0	0	0

Tab. IX.4 Parameters for runoff simulation on 23.01.1997 (lower Zin)-comparisson shear stress vs. flow velocity

	channel type 1	channel type 2	channel type 3
da	3	3.5	03. Mai
mn	0.03	0.025	0.02
v	0.75	0.35	0.27
Hf	1	3	3
ni	0.5	0.5	0.5
k	250	250	250
kb	1000	1000	1000
kf	10	3	3
he	0.35	0.35	0.4
I	0	0	0
Antec=	1-0.8T	1-0.85T	1-0.9T
T	6	6	6
To	0	0	0

Tab. IX.5 Parameters for runoff simulation October 1979 **(Nahal Zin)**

	channel type 1	channel type 2a	channel type 2b	channel type 3	channel type 4
da	2	2	2.5	2	0
mn	0.075	0.03	0.03	0.05	0.07
v	0.2	0.45	0.035	0.2	1
Hf	2	2	2	2	2
ni	0.3	0.48	0.48	0.45	0.3
k	20	50	50	40	0
kb	50	250	250	180	0
kf	1	5	5	5	0
he	0.3	0.25	0.4	0.3	0.3
vk	2.5	2	2	2	2.5
I	0.1	0.1	0.1	0.1	0.5
Antec=	$1-0.9^T$	$1-0.9^T$	$1-0.9^T$	$1-0.9^T$	$1-0.9^T$
T	100	100	100	100	100
To	0	0	0	0	0

Tab. IX.6 Parameters for runoff simulation on 18.02.1995 (Kuiseb)

	channel type 1	channel type 2	channel type 3
da	0	1	2
mn	0.05	0.04	0.04
v	1	0.1	0.05

Hf	2	3	3
ni	0	0.3	0.3
k	25	15	20
kb	0	10	5
kf	1	2	2
he	0.3	0.3	0.3
vk	0.2	1.7	1.3
l	0.5	0.1	0.1
Antec=	$1\text{-}0.8^T$	$1\text{-}0.85^T$	$1\text{-}0.9^T$
T	>60	>60	>60

Tab. IX.7 Parameter for the runoff simulation on 19.02.-2.03.1995 (Kuiseb)

	channel type 1	channel type 2	channel type 3
da	0	1	2
mn	0.05	0.04	0.04
v	1	0.1	0.05
Hf	2	3	3
ni	0	0.3	0.5
k	25	15	15
kb	0	7	5
kf	1	6	4
he	0.3	0.2	0.2
vk	0.2	1.9	1.4
l	0.5	0.01	0.01
Antec=	$1\text{-}0.8^T$	$1\text{-}0.85^T$	$1\text{-}0.9^T$
T	7	7	7

Tab. IX.8 Parameters for runoff simulation on 17.-30-01-1997 (Kuiseb)

	channel type 1	channel type 2	channel type 3
da	0	1	2
mn	0.05	0.05	0.05
v	1	0.1	0.05
Hf	2	3	3
ni	0	0.4	0.4
k	25	20	50
kb	0	20	10
kf	1	5	5
he	0.3	0.3	0.3
vk	0.2	1.7	2.2
l	0.5	0.01	0
Antec=	$1\text{-}0.8^T$	$1\text{-}0.85^T$	$1\text{-}0.9^T$
T	>60	>60	>60

Ehrenwörtliche Erklärung:

Hiermit erkläre ich, dass die Arbeit selbständig und nur unter Verwendung der angegebenen Hilfsmittel angefertigt wurde.

Ort, Datum Unterschrift